

Inaugural dissertation
for obtaining the doctoral degree
of the
Combined Faculty of Mathematics, Engineering and Natural Sciences
of the
Ruprecht - Karls - University Heidelberg

Presented by
M.Sc. Simge Kelekçi
born in: Ankara, Turkey
Oral examination: 04.12.2024

Epigenetic compound screening in AML with *MNX1* overexpression

Referees:

Prof. Dr. Karsten Rippe

Prof. Dr. Christoph Plass

Contributions

Unless mentioned otherwise, I performed the experimental work, analyzed, and interpreted it. The epigenetic compound library was obtained from Prof. Dr. Udo Oppermann's lab (Oxford University, United Kingdom), and the treatment protocol was established based on their protocol. GDM-1 cells expressing shRNAs were obtained from Dr. Mariam Hakobyan (DKFZ, Heidelberg). Fluorescence-activated cell sorting (FACS) for GFP and BFP-positive cells was performed with the help of the DKFZ Flow Cytometry core facility. Anna Riedel (DKFZ, Heidelberg) and I performed the epigenetic drug screening. Dr. Cindy Körner and Dr. Birgitta Michels (DKFZ, Heidelberg) guided me during the first library preparation of miRNA sequencing. I carried out the CTCF ACT-seq with close supervision from Marion Bähr (DKFZ, Heidelberg). Elena Everatt (DKFZ, Heidelberg) and Marion Bähr (DKFZ, Heidelberg) performed library preparation for 4C-seq. Dieter Weichenhan (DKFZ, Heidelberg) analyzed CTCF ACT-seq and 4C-seq, whereas Katherine Kelly (DKFZ, Heidelberg) analyzed RNA-seq and miRNA-seq. Michael Scherer (DKFZ, Heidelberg) analyzed the local deep bisulfite sequencing MiSeq data that I generated under the supervision of Dieter Weichenhan (DKFZ, Heidelberg). Library preparations of RNA-seq and Infinium Methylation EPIC array and sequencing of prepared libraries of miRNA-seq, ACT-seq, MiSeq, and 4C-seq were done by DKFZ NGS core facility. Binje Vick (Helmholtz Zentrum Munich, Germany) generated PDX models.

The results showing miRNA-dependent mechanisms that explain the global hypomethylation-mediated *MNX1* downregulation will be integrated into a publication of which I am the first author.

Summary

Acute myeloid leukemia (AML) is a form of blood cancer characterized by impaired differentiation and accelerated proliferation due to (epi)genetic dysregulation of hematopoietic stem cells (HSC). The European LeukemiaNet (ELN) classifies AML into three subtypes: favorable, intermediate, and unfavorable. In-house, we found that ~1.4% of AML subtypes (including deletion 7q or translocation (7;12) AML) express *motor neuron and transcription factor 1 (MNX1)*, a homeobox transcription factor (TF) known to be expressed during endoderm differentiation, in motor neurons and in pancreatic cells, but generally not in hematopoietic stem and progenitor cells (HSCs). *MNX1*-expressing AML typically belongs to the adverse subcategories of AML. *MNX1* drives leukemogenesis when overexpressed in human fetal HSCs, and these cells are transplanted into immunosuppressed mice. No therapeutic agent has been identified yet that directly targets *MNX1* or reduces *MNX1* expression. Therefore, finding a compound that either targets *MNX1* or reduces *MNX1* expression is essential for treating *MNX1*-expressing AML cases.

GDM-1 is the only AML cell line that expresses *MNX1*. In these cells, *MNX1* is expressed when a hijacked enhancer from the *AHI/MYB* region (chromosome 6) is juxtaposed with the *MNX1* promoter (chromosome 7). In my thesis, I hypothesized that epigenetic modifications could disrupt the enhancer-promoter interaction that drives *MNX1* expression. Thus, an epigenetic compound screen was performed, and compounds that affect GDM-1 cell viability were revealed. One compound that reduces *MNX1* expression was identified. In particular, decitabine (DAC), a hypomethylating agent, emerged as a promising candidate from this screen. DAC treatment resulted in global hypomethylation and significant downregulation of *MNX1* at both the RNA and protein levels. I found that a miRNA-dependent mechanism mediates *MNX1* downregulation, while I could rule out two miRNA-independent mechanisms, e.g. DAC mediated changes in TAD structures in which *MNX1* is embedded and the silencing via a long-noncoding RNA. miRNA-seq revealed that miR-200a-3p, predicted to bind to the *MNX1* 3'UTR, is upregulated upon DAC treatment. I validated DAC-mediated hypomethylation at the promoter region of this miRNA by local deep bisulfite sequencing and confirmed the interaction between miR-200a-3p and *MNX1* 3'UTR by luciferase assay. DAC treatment in patient-derived xenografts (PDX) expressing *MNX1* resulted in the same phenotype, indicating the reduction of *MNX1* levels through the same mechanism via upregulation of miR-200a-3p.

Epigenetic therapies promise a reversible therapeutic strategy for cancer treatment. In summary, this work focused on epigenetic-based therapies for *MNX1*-expressing AML and filled the gaps in the literature regarding potential therapeutics for *MNX1*-expressing AML. DAC treatment reduced *MNX1* via hypomethylation-mediated activation of miR-200a-3p, which targets the *MNX1* 3'UTR. Previous work showed the regulation of *MNX1* by miR-200a and miR-141-3p in motor neurons and pancreatic insulin-producing cells. This work demonstrated the upregulation of miR-200a-3p in an AML cell line and PDX models and investigated the upregulation of miR-

200a-3p upon DAC treatment in the context of AML. These results suggest the potential use of DAC or miR-200a-3p mimics against *MNX1*-expressing AML cases in a clinical setting.

Zusammenfassung

Die akute myeloische Leukämie (AML) ist eine Form von Blutkrebs, die durch eine Blockade der Differenzierung und eine (epi)genetische Dysregulation der hämatopoetischen Stammzellen (HSC) charakterisiert ist. Das European LeukemiaNet (ELN) hat die AML in drei Subtypen eingeteilt: günstig, mittel und ungünstig. Wir haben intern festgestellt, dass ~1,4 % der AML-Subtypen (z. B. Deletion 7q oder Translokation(7;12) AML) den *Motorneuronen- und Transkriptionsfaktor 1 (MNX1)* exprimieren; einen homeobox Transkriptionsfaktor (TF), der während der Endoderm-Differenzierung, in Motorneuronen und in Pankreaszellen exprimiert ist, im Allgemeinen aber nicht in hämatopoetischen Stamm- und Vorläuferzellen (HSC). MNX1-exprimierende AML gehört typischerweise zu den ungünstigen Unterkategorien der AML. MNX1 fördert die Leukämogenese, wenn es in menschlichen fötalen HSCs überexprimiert wird und diese Zellen in immunsupprimierte Mäuse transplantiert werden. Es gibt aktuell keinen therapeutischen Wirkstoff, der direkt auf MNX1 abzielt, oder die MNX1 Expression reduziert. Daher ist die Suche nach einem solchen Wirkstoff, der entweder auf MNX1 abzielt oder die MNX1-Expression reduziert, für AML Patient*innen mit *MNX1*-Expression von entscheidender Bedeutung.

GDM-1 ist die einzige AML-Zelllinie, die MNX1 exprimiert. In diesen Zellen wird MNX1 exprimiert, wenn ein ‚hijacked‘ Enhancer aus der *AHI/MYB*-Region (Chromosom 6) an den *MNX1*-Promotor (Chromosom 7) angekoppelt wird. In meiner Dissertation stellte ich die Hypothese auf, dass epigenetische Verbindungen die Enhancer-Promoter-Interaktion, die zur *MNX1* Expression führt, stören könnten. Daher wurde ein epigenetisches Wirkstoffscreening durchgeführt und Verbindungen gefunden, die die Lebensfähigkeit von GDM-1 beeinträchtigen, sowie eine Verbindung, die die *MNX1*-Expression reduziert. Eine vielversprechender Wirkstoffkandidat ist Decitabin (DAC), eine Substanz, die die DNA Methylierung reduziert. Die Behandlung mit DAC führte zu einer globalen Hypomethylierung und einer signifikanten Herunterregulierung von *MNX1* sowohl auf RNA- als auch auf Proteinebene. Ich fand heraus, dass ein miRNA-abhängiger Mechanismen die *MNX1*-Herunterregulation vermittelt, während ich zwei miRNA-unabhängige Mechanismen ausschließen konnte, z. B. DAC-vermittelte Veränderungen in den TAD-Strukturen, in die *MNX1* eingebettet ist, und das Silencing durch eine lange nicht-kodierende RNA. miRNA-Sequenzierung ergab, dass miR-200a-3p, die an die 3'UTR von MNX1 binden soll, bei DAC-Behandlung hochreguliert wird. Ich validierte die DAC-vermittelte Hypomethylierung in der Promotorregion dieser miRNA durch lokale tiefe Bisulfit-Sequenzierung und bestätigte die Interaktion zwischen miR-200a-3p und *MNX1* 3'UTR durch einen Luziferase-Assay. Die DAC-Behandlung in von Patienten stammenden Xenotransplantaten (PDX), die *MNX1* exprimieren, führte zum gleichen Phänotyp, d. h. zu einer Verringerung der MNX1-Spiegel durch Hochregulierung von miR-200a-3p.

Epigenetische Therapien versprechen eine reversible Therapiestrategie für die Krebsbekämpfung. Zusammenfassend konzentrierte sich diese Arbeit auf epigenetische Therapien für *MNX1*-exprimierende AML und konnte die Lücken in der Literatur in Bezug auf *MNX1* als

therapeutisches Ziel füllen. Die DAC-Behandlung reduzierte MNX1 über eine durch Hypomethylierung vermittelte Aktivierung von miR-200a-3p, die an die 3'UTR von *MNX1* bindet. Frühere Studien haben gezeigt, dass *MNX1* in Motoneuronen und insulinproduzierenden Zellen der Bauchspeicheldrüse über miR-200a und miR-141-3p reguliert wird. In dieser Arbeit wurde die Hochregulierung von miR-200a-3p in einer AML-Zelllinie und in PDX-Modellen nachgewiesen und die Hochregulierung von miR-200a-3p bei DAC-Behandlung im AML-Kontext untersucht. Zusammengefasst deuten diese Ergebnisse auf das Potenzial des Einsatzes von DAC oder miR-200a-3p-Mimics gegen *MNX1*-exprimierende AML-Fälle in der Klinik hin.

Table of Contents

Contributions.....	v
Summary.....	vi
Zusammenfassung.....	viii
Table of Contents.....	x
List of Tables.....	xiii
List of Figures.....	xiv
List of Abbreviations.....	xv
1. Introduction.....	1
1.1. Acute Myeloid Leukemia (AML).....	1
1.1.1. Genetic Mechanisms Driving AML.....	2
1.1.1.1. Cytogenetic Classification of AML.....	3
1.1.2. Epigenetic (Dys)regulations.....	3
1.1.2.1.1. DNA Methylation.....	5
1.1.2.1.2. Histone Modifications.....	7
1.1.2.1.3. 3-dimensional (3D) Genome and Topologically Associated Domains (TADs) Structures.....	7
1.1.3. Epigenetics of AML.....	8
1.1.3.1. Recurrent Mutations in Epigenetic Enzymes in AML.....	9
1.1.4. Hematopoiesis and Alterations during Hematopoiesis in AML Leukemogenesis.....	9
1.1.5. Current Treatment Options for AML.....	10
1.1.5.1. Venetoclax Treatment.....	11
1.1.5.2. Decitabine Treatment.....	11
1.2. Oncogenic Activation of <i>MNX1</i> in AML.....	12
1.3. Enhancer Hijacking Events in AML.....	13
1.4. microRNAs.....	14
1.4.1. Epigenetic Regulation of miRNA Expression.....	16
1.4.2. Role of miRNAs in AML Progression.....	17
1.4.3. The miR-200 Family and The Role of miR-200a-3p in Cancer.....	17
1.4.4. miRNAs Regulating <i>MNX1</i> Expression.....	18
2. Hypotheses and Aims.....	19
3. Materials and Methods.....	21
3.1. Cell culture.....	21
3.2. Epigenetic drug screening.....	21

3.3. Selection of the compounds from the screening and dose-response curve (DRC) analysis	21
3.4. Decitabine and MG132 treatment schedule	24
3.5. shRNA-mediated knockdown of <i>MNX1</i>	25
3.6. RNA isolation, cDNA synthesis, and quantitative polymerase chain reaction (qPCR).....	25
3.7. RNA-seq preparation and analysis.....	26
3.8. LB medium, LB-Agar preparation, and transformation of vectors.....	26
3.9. Agarose gel electrophoresis	27
3.10. Lentivirus production and collection.....	27
3.11. Transduction of GDM-1 cells	28
3.12. Generation of empty vector.....	28
3.13. miRNA isolation, cDNA synthesis, and qPCR.....	29
3.14. Overexpression of miRNA mimics and antagomirs	29
3.15. Luciferase assay	29
3.16. miRNA-seq sample preparation and analysis	30
3.17. Protein isolation, quantification, and western blot.....	31
3.18. Genomic DNA isolation and Infinium Methylation EPIC array.....	32
3.19. Patient-derived xenografts (PDX) <i>in vitro</i> culture and DAC treatment.....	33
3.20. Bisulfite treatment of genomic DNAs and local deep bisulfite sequencing via MiSeq...	33
3.21. CTCF Antibody-guided chromatin tagmentation followed by sequencing (ACT-seq) sample preparation and analysis.....	34
3.22. CTCF ACT-seq library PCR and purification of CTCF ACT-seq library.....	35
3.23. Bioinformatics analysis of CTCF ACT-seq.....	35
3.24. 4C-seq library preparation.....	36
3.25. 4C-seq analysis.....	37
3.26. Statistical Analysis	38
4. Results.....	39
4.1. Chapter 1: Epigenetic compound screening in GDM-1	39
4.1.1. Knockdown of <i>MNX1</i>	39
4.1.2. Epigenetic compound screening and dose-response curves of the selected compounds	40
4.1.3. Expression of <i>MNX1</i> upon the treatment of selected compounds.....	43
4.2. Chapter 2: Effect of DAC treatment in GDM-1 cells	44
4.2.1. Hypomethylation upon DAC treatment.....	44
4.2.2. Effect of DAC treatment on <i>MNX1</i> RNA and protein expression	46

4.3. Chapter 3: Possible miRNA-independent mechanisms downregulating <i>MNX1</i> upon DAC treatment.....	48
4.3.1. Hypothesis 1: By altering TADs, DAC treatment may disrupt the enhancer-promoter interaction, enabling oncogenic <i>MNX1</i> overexpression.	49
4.3.2. Hypothesis 2: CAT7 and PRC1 recruitment to the <i>MNX1</i> promoter region could explain the observed <i>MNX1</i> downregulation.	53
4.4. Chapter 4: miRNA-dependent mechanisms behind <i>MNX1</i> downregulation upon DAC treatment.....	54
4.4.1. miRNA-seq results	54
4.4.2. Overexpression of <i>MNX1</i> without 3'UTR.....	59
4.4.3. Validation experiments with PDX samples.....	61
5. Discussion.....	63
5.1. Epigenetic compound screening in GDM-1.....	63
5.2. Effect of DAC treatment in GDM-1 cells	64
5.3. miRNA-independent mechanisms behind <i>MNX1</i> downregulation upon DAC treatment .	64
5.4. miRNA-dependent mechanisms behind <i>MNX1</i> downregulation upon DAC treatment.....	65
5.5. Overexpression of <i>MNX1</i> without 3'UTR	66
6. Conclusion and Outlook	69
7. Supplementary Figures and Tables.....	70
7.1. Supplementary figures.....	70
7.2. Supplementary tables	71
8. References.....	102
9. Poster Presentations and Publications.....	129
9.1. Publications	129
9.2. Poster presentations.....	130
10. Acknowledgements.....	131

List of Tables

Table 1: The epigenetic compounds further used in the thesis and their targets and mechanisms of action as described in current literature.	22
Table 2: The two highest-ranked known results of HOMER motif enrichment.....	50
Table 3: The list of miRNAs predicted to target <i>MNX1</i> 3'UTR and get upregulated upon DAC treatment.	55
Supplementary Table 1: Authentication of cell lines.....	71
Supplementary Table 2: Cell culture media/reagents	71
Supplementary Table 3: Epigenetic compounds in the library.....	72
Supplementary Table 4: The IC ₈₀ concentrations of the epigenetic compounds tested.	79
Supplementary Table 5: Buffers	80
Supplementary Table 6: Kits	83
Supplementary Table 7: PCR reagents	84
Supplementary Table 8: Primers.....	85
Supplementary Table 9: qPCR conditions.....	92
Supplementary Table 10: Constructs used in the thesis.....	92
Supplementary Table 11: miRNA qPCR probes	93
Supplementary Table 12: miRNA mimics and qPCR conditions.....	93
Supplementary Table 13: Antibodies.....	94
Supplementary Table 14: Reagents used.	95
Supplementary Table 15: Consumables.....	98
Supplementary Table 16: Machines used.	98
Supplementary Table 17: Softwares used.....	100
Supplementary Table 18: 4C-seq experiment PCR conditions.....	100
Supplementary Table 19: The names and the number of the reads obtained after the second 4C-seq.	101

List of Figures

Figure 1: The representation of the 3D genome.	4
Figure 2: Representation of leukemic transformation and potential therapies.	12
Figure 3: Generation of miRNAs.....	15
Figure 4: Effects of <i>MNX1</i> knockdown in GDM-1.	40
Figure 5: Epigenetic compound screening and dose-response curves of the 10 epigenetic compounds.	43
Figure 6: Treatments with 10 selected epigenetic compounds.	44
Figure 7: Methylation changes upon DAC treatment.	46
Figure 8: Changes in transcriptomics upon DAC treatment.	47
Figure 9: The illustration of the first hypothesis tested.	49
Figure 10: Representation of CTCF ACT-seq results.....	51
Figure 11: Representation of 4C-seq results when <i>MNX1</i> viewpoint is used.....	52
Figure 12: The illustration of the second hypothesis tested.....	53
Figure 13: The illustration of the third hypothesis tested.	54
Figure 14: Changes in miRNA transcriptomics upon DAC treatment.	56
Figure 15: Elucidation of miR-200a-3p-dependent <i>MNX1</i> reduction.....	57
Figure 16: Generation of GDM-1 cells stably expressing MNX1-ORF fused with GFP and HA or EV with GFP and HA.	59
Figure 17: Changes in the expression of MNX1-ORF without 3'UTR upon DAC treatment.	60
Figure 18: Changes in the levels of MNX1-ORF without 3'UTR upon proteasomal inhibition.	61
Figure 19: Changes in PDX samples upon DAC treatment.....	62
Supplementary Figure 1: CAT7 qPCR results.....	70
Supplementary Figure 2: Methylation frequencies of each CpG on the amplicons represented in Figure 15.	70

List of Abbreviations

Abbreviation	Long-form
μM	Micro molar
4C-seq	Circular chromosome conformation capture sequencing
ab	antibody
ACT-seq	Antibody-guided chromatin tagmentation sequencing
AML	Acute myeloid leukemia
ATP	Adenosine triphosphate
CAT7	Chromatin-associated transcripts
cDNA	Complementary deoxyribonucleic acid
ChiPSC22	Human induced pluripotent stem cells
CpG	Cytosines followed by guanine residues
CRISPR/Cas9	Clustered regularly interspaced palindromic repeats/ CRISPR-associated protein 9
CTA	Cancer testis antigen
CTCF	CCCTC-binding factor
DAC	Decitabine
DMEM	Dulbecco's modified eagle medium
DMSO	Dimethyl sulfoxide
DNMT	DNA methyltransferase
dNTP	Deoxynucleotide triphosphate
DSMZ	Deutsche Sammlung von Mikroorganismen und Zellkulturen
FACS	Fluorescence-assisted cell sorting
FCS	Foetal calf serum
Figeno	Figure Generator for Genomics
gDNA	Genomic deoxyribonucleic acid
GFP	Green fluorescence protein
HA	Hemagglutinin
HDAC	Histone deacetylase
HEK293T	Human embryonic kidney 293T
HMA	Hypomethylating agents
HSCs	Hematopoietic stem cells
HSCPs	Hematopoietic stem and progenitor cells
IGV	Integrative Genomics Viewer
LINE1	Long interspersed nuclear element-1

lncRNA	Long noncoding RNA
MDS	Myelodysplastic syndromes
miRNA	Micro RNA
ml	milliliter
MNX1	Motor and neuron transcription factor 1
MNX1-AS1	MNX1-antisense 1
NGS	Next generation sequencing
ORF	Open reading frame
PDX	Patient-derived xenograft
qPCR	Quantitative polymerase chain reaction
SAM	S-adenosyl methionine
SDS	Sodium dodecyl sulfate
shRNA	Short hairpin RNA
TAD	Topologically associated domain
TBS-T	Tris-buffered saline with Tween
TSS	Transcription start site
UTR	Untranslated region
V2	Version 2
WB	Western blot

1. Introduction

1.1. Acute Myeloid Leukemia (AML)

Acute myeloid leukemia is a blood cancer that results from genomic alterations (Yang et al., 2017), mutations (Kayser & Levis, 2023), and epigenetic changes (Wouters & Delwel, 2016) in hematopoietic stem and progenitor cells (HSPC) (Pelcovits & Niroula, 2020). All these alterations lead to abnormalities in the proliferation and differentiation of myeloid blast cells (Pollyea et al., 2023). Transformed HSPCs accumulate mutations, chromosomal abnormalities, or epigenetic changes, leading to alterations in self-renewal and generation of leukemia stem cells (LSC). Additionally, the microenvironment in which LSCs (niche) reside can contribute to leukemogenesis via cytokine/chemokine signaling changes, aberrant immunosuppression, and cell adhesion (Wachter & Pikman, 2024).

AML has an age-adjusted rate of 4.3 cases per 100,000 people in the United States (Shallis et al., 2019). Many risk factors, such as exposure to chemotherapy or radiation, environmental factors like tobacco exposure, and, most importantly, having myelodysplastic syndrome (MDS), have been identified (Wachter & Pikman, 2024). Although AML can be seen in all ages, it is most frequently seen in patients who are older than 60 years of age. The main symptoms of the disease are shortness of breath, extreme fatigue, and frequent infections. If AML is left untreated, it leads to bone marrow failure and might be fatal within weeks of diagnosis (Khwaja et al., 2016). AML has poor outcomes among elderly patients. Only 2.4% of these patients who are unfit for stem cell transplantation survive, and they have, on average, 10 years of remission (Jonas & Pollyea, 2019). The Food and Drug Administration (FDA) approved the use of hypomethylating agents (HMA) plus venetoclax as a new standard of care for elderly or unfit patients for chemotherapy and allogeneic stem-cell transplantation (Abaza et al., 2024). Patients younger than 60 years old receive classic treatment regimens, for example, cytarabine-based chemotherapy and hypomethylating agents or allogeneic stem-cell transplantation, and 40% of them have around a 5-year overall survival rate (OS) (Yang & Wang, 2018). HMA treatment led to complete remission (CR) or complete remission with incomplete count recovery for roughly 20% of the patients who achieved OS of less than 12 months (Jonas & Pollyea, 2019). Patients with CR often can get relapsed, and an OS rate of more than 5 years is rarely achieved (Yang & Wang, 2018). However, childhood AML or pediatric AML patients have survival rates of about around 70% with intensive therapy and care. These patients usually get intensive anthracycline- and cytarabine-based therapies for allogeneic stem cell transplantation (Creutzig et al., 2012)

AML is usually diagnosed if the blast count is above 10% in the bone marrow or blood, along with common AML genetic abnormalities like fusions, translocations, and mutations. Flow cytometry is also used to identify cell surface and intracellular markers for AML. However, AML is a heterogeneous disease, so not all AML blasts express those markers (Dohner et al., 2022). Due to the heterogeneous phenotype of this disease and because of a stepwise acquisition of structural

variations, somatic mutations, disruption in the standard mechanism of self-renewal, and block in differentiation in hematopoietic cells, it is hard to choose potential therapeutics and predict the outcome of the disease (Desai et al., 2022).

1.1.1. Genetic Mechanisms Driving AML

Structural variations (SVs) in the genome, which include deletions, translocations, duplications, and inversions, can lead to cancer. Oncogenes are known to be activated upon an SV, particularly in hematopoietic malignancies, and can be inhibited via therapeutic agents (Dixon et al., 2018). Approximately 55% of AML patients carry one or more SVs, which the World Health Organization (WHO) describes as prognostic solid factors for AML (Lagunas-Rangel et al., 2017; Meyer & Levine, 2014). Some of the most common alterations are t(8;21), inv(16), t(15;17), trisomies (8 or 21), monosomal karyotypes (monosomy 5,5q, 7, 17), t(9;11), inv(3), and t(6;9) (Akhila Raj et al., 2022; Bullinger et al., 2017).

AML with t(8;21) and t(16;21) results in an in-frame fusion between parts of RUNX1 and ETO. The fusion protein is an oncoprotein responsible for genomic instability and the block in myeloid differentiation (Kellaway et al., 2020). Patients with t(8;21) appear to have more frequent del(5q) (Yamamoto et al., 2015). Del(5q) or monosomy 5 is one of the most common unbalanced chromosomal abnormalities observed in AML or myelodysplastic syndrome (MDS) (Venugopal et al., 2021), a disorder characterized by risk of progression to AML and ineffective hematopoiesis (H. Li et al., 2022).

Del(7q) or monosomy 7 is another common chromosomal abnormality observed in myeloid neoplasms (Inaba et al., 2018). Researchers investigated the presence of tumor suppressors in the deleted regions. *CUX1*, *SAMD9/SAMD9L*, *EZH2*, and *MLL3* genes are among the most deleted genes and may behave as tumor suppressors in -7/del(7q) AML patients (Inaba et al., 2018). In a recent publication, Mori et al. proposed haploinsufficiency rather than loss of TS activity of these genes and novel genes such as *KRIT1*, *RINT1*, *XRCC2*, and *NRF1* in -7/del(7q) patients (Mori et al., 2023).

Another common translocation among pediatric AML patients younger than 2 years old involving chromosome 7 is t(7;12). Translocation happens between chromosome 7 (7q36.3), proximal to *MNX1* (*motor neuron and pancreas transcription factor 1*) and chromosome 12 (12p13.2), on the 5' portion of *ETV6* gene (Ragusa, Ciciro, et al., 2022). Patients have both *MNX1* overexpression and deficient *ETV6*. Infant t(7;12) AML patients have poor clinical outcomes, and t(7;12) is classified as an adverse risk cytogenetic abnormality (Ragusa et al., 2023).

The abovementioned abnormalities can occur alone or with other abnormalities, like in the case of complex karyotype AML (ckAML) (Mori et al., 2023). ckAML patients carry more than or equal to 3 cytogenetically visible SVs (excluding the recurring deletions or inversions or translocations

such as *inv(3)/t(3;3)*, *t(8;21)*), and the majority have TP53 mutations (around 70% of *ckAML*) (Klever et al., 2023).

In addition to SVs, mutational signatures are essential for driving AML. Most MDS patients develop AML via accumulating specific mutations (Ogawa, 2019). Mutations in chromatin regulators such as *DNMT3A*, *EZH2*, *MLL*, *IDH1/2*, *TET2*, *CEBPA* transcription factors *ETV6*, *RUNX1*, *GATA2*, RNA splicing such as *SF3B1*, genes involved in the regulation of pathways like *KRAS*, *FLT3* and *JAK2* and in the nucleophosmin *NPM1* are known recurrent mutations in MDS/AML (Cook et al., 2022). Co-occurring mutations, such as the co-occurrence of *NPM1* mutations with *FLT3*, *ITD* or *DNMT3A* mutations, may influence the predictive value of a particular mutation in AML. Understanding the entire genomic landscape (e.g., mutations and SVs) of AML is essential for optimal personalized prognosis (DiNardo & Cortes, 2016).

1.1.1.1. Cytogenetic Classification of AML

The WHO and the International Consensus Classification (ICC) have subcategorized AML (Shimony et al., 2023). The ICC subdivided AML into AML with recurrent genetic abnormalities: AML not otherwise specified, AML with TP53 mutations, AML with MDS-related gene mutations, AML with MDS-related cytogenetic abnormalities, and AML with therapy-related myeloid neoplasms (Arber et al., 2022; Weinberg et al., 2023). Whereas in the 5th edition of the WHO classification, AML was divided into two groups, AML with defining genetic aberrations (such as AML with *PML::RARA* or *RUNX1::RUNX1T1* fusions, *MECOM* or *NPM1* or *CEBPA* rearrangements, etc.) and AML defined by differentiation (such as AML with minimal differentiation, maturation, and acute erythroid leukemia, etc.) (Chen et al., 2024; Khoury et al., 2022). However, AML is classified into three subgroups based on European LeukemiaNet (ELN) risk stratification. AML with *t(8;21)*, *inv(16)* or *t(16;16)*, *NPM1* mutations without *FLT3-ITD*, *CEBPA* mutations are classified as favorable risk. AML with *FLT-ITD* mutations, with *t(9;11)*, is classified as intermediate risk. Finally, AML with *t(6;9)*, *t(v;11)* (*v* means chromosomes with translocation to chromosome 11), *t(9;22)*, *t(8;6)*, *inv(3)*, *t(3q26.2;v)* (*v* means chromosomes with translocation to chromosome 3), monosomy 5 or *del(5q)*, monosomy 7 or *del(7q)*, monosomy of 17 or abnormalities in 17p, complex karyotype, mutations in *ASXL1*, *BCOR*, *EZH2*, *RUNX1*, *SF3B1*, *SRSF2*, *STAG2*, *U2AF1*, *ZRSR2* or *TP53* are classified as unfavorable risk (Dohner et al., 2022; Shimony et al., 2023).

1.1.2. Epigenetic (Dys)regulations

Genetic information is carried in the DNA, whereas epigenetics maintains the information beyond genomes (Tronick & Hunter, 2016). Waddington first described epigenetics in the epigenetic landscape as valleys where undifferentiated cells are on top and rolling downhill while altering their epigenomes and differentiating (Ferrell, 2012; Waddington, 1957). Epigenetic mechanisms include DNA methylation and histone post-translational modifications such as acetylation,

methylation, ubiquitylation, and sumoylation. Altered epigenetic mechanisms are essential during development (Skvortsova et al., 2018), in aging (la Torre et al., 2023), heart diseases (Akerberg & Pu, 2020), neurodevelopmental disorders (Berson et al., 2018), stroke (Morris-Blanco et al., 2022), and cancer (Herceg & Vaissiere, 2011).

Regulatory elements such as enhancers, silencers, and promoter regions are essential in epigenetic regulation. Promoters are the regions where RNA polymerase II is recruited and transcription is initiated with the help of TFs and cofactors (Thomas & Buecker, 2023). On the other hand, enhancers are several hundred base pair long DNA sequences that boost the level of transcription driven by promoters. Enhancers interact with promoters via short or long-distance interactions. On average, a promoter is regulated by 4-5 enhancers, whereas a single enhancer regulates 2 promoters (Mulet-Lazaro & Delwel, 2023) (Figure 1).

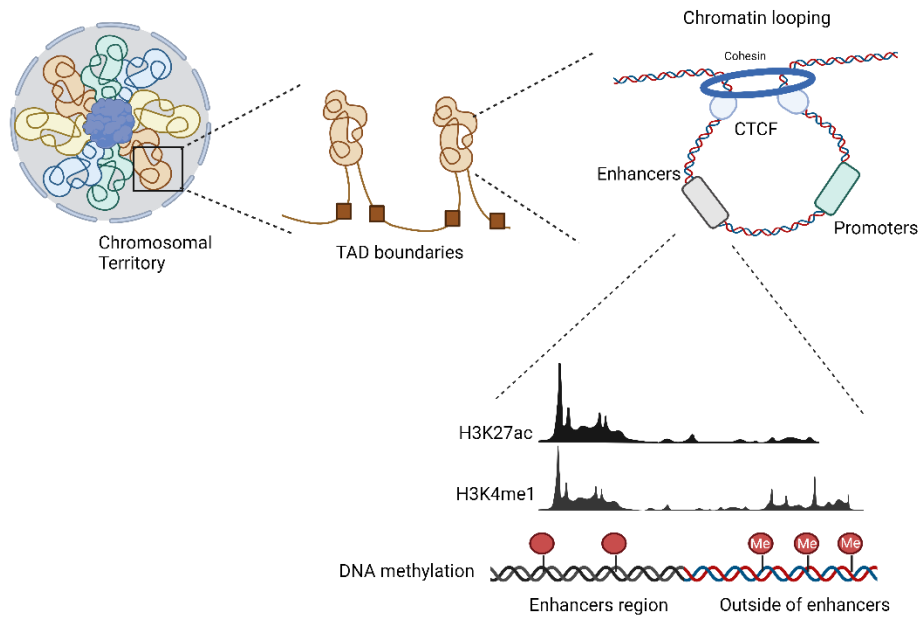


Figure 1: The representation of the 3D genome.

The architecture of the 3D genome is established in the chromosomal territories with two nucleosomal phases: A and B compartments. Whereas A compartments are euchromatin (open chromatin), B compartments include repressed regions with closed chromatin. TAD structures determine the chromatin looping, which drives enhancer and promoter interactions. Enhancers are regulatory elements of the genome, enriched in hypomethylation, H3K27ac, and H3K4me1 signals. This figure is modified according to a figure in Szabo et al. (Szabo et al., 2019) and was created with Biorender.

1.1.2.1.1. DNA Methylation

DNA methylation happens by adding a methyl group (-CH₃) at the 5-position of a cytosine residue, creating 5-methylcytosine (5-mC). This addition usually occurs in the cytosines, followed by a guanine in CpG dinucleotides (Herceg & Vaissiere, 2011; Spruijt & Vermeulen, 2014). However, studies show that there are methylated cytosines without the CpG configuration (Jang et al., 2017). In addition to the cytosines, adenosines are methylated in the genome (Li et al., 2019).

DNA methyltransferase enzymes are responsible for the establishment of DNA methylation. *De novo* DNA methyltransferases are DNMT3 family enzymes, and they are responsible for the addition of new methyl groups to the DNA. There are three known members of the family: DNMT3A, 3B, and 3L (Lu et al., 2024). In contrast to the DNMT3 family, DNMT1 maintains DNA methylation by copying the DNA methylation patterns from the parental strand to the daughter strand during DNA replication (Kikuchi et al., 2022). The last member of the DNMT family is DNMT2, which methylates tRNAs (Tuorto et al., 2012). DNA methylation follows these steps. Firstly, folates are converted to methyl-tetrahydrofolate (THF) via cofactors like vitamins B6 and B12, and then methyl-THF serves as an intermediate product for transforming homocysteine into methionine. Secondly, S-adenosylmethionine (SAM) is a universal methyl donor, and methionine is activated to SAM via methionine adenosyltransferase. The methyl group from SAM is added to a cytosine next to a guanine (CpG dinucleotide) to establish the DNA methylation pattern. Finally, converting SAM to S-adenosylhomocysteine (SAH) is essential during methylation, as SAH inhibits methylation (Fukumoto et al., 2022).

DNA demethylation happens either through a lack of functional DNA methyltransferases and, therefore, dilution of 5mC during DNA replication (passive) or via the activity of the Ten Eleven Translocation (TET) protein family (active) (Wu & Zhang, 2017). TET1, TET2, and TET3 are responsible for DNA hypomethylation through the oxidation of 5-mC to 5-hydroxymethyl cytosine (5-hmC), 5-carboxyl cytosine (5-caC) or 5-formyl cytosine and dilution of 5-mC through DNA replication. Therefore, 5-hmC is usually used as a marker for TET activity studies (Rasmussen & Helin, 2016).

The human genome has around 28 million CpGs, 60-80% of which are usually methylated (Smith & Meissner, 2013). Regions with a higher frequency of CpGs are called CpG islands (CGI), primarily located in the promoter regions of genes. Gardiner-Garden et al. described CGI as a region with at least 200 bp (usually around 1000 bp (Bird et al., 1985)) and more than 50% GCs (Gardiner-Garden & Frommer, 1987). Around 55-60% of genes contain CGIs in their promoters, but particularly housekeeping or developmental genes have CGIs in their promoters (Craig & Bickmore, 1994; Sarda et al., 2017). CpGs in the promoter or the first exon of the genes are generally unmethylated, and around 75% of annotated promoters have unmethylated CGI. Meanwhile, CGIs in the short and long interspersed retrotransposable elements (SINE, LINE) and long terminal repeats (LTR) regions are hypermethylated. The methylation of the remaining genome varies, and the effect of methylation on those regions, such as gene bodies, which include

many CGIs in the human genome, is debatable (Edwards et al., 2017). For example, gene body methylation upregulates the expression of genes in dividing cells, whereas it has the opposite effect in non-dividing or slowly dividing cells like neurons (Kikuchi et al., 2022).

Since methylation prevents interaction with transcription factors (TFs), hypermethylation on the promoter region is associated with the silencing of genes (Roman-Gomez et al., 2004). However, distal or orphan CGIs in the intragenic and intergenic regions also play essential roles in gene expression regulation. For example, Pachona et al. showed that those CGIs enhance the interaction of poised enhancers with the distally located regions (Pachano et al., 2021). As mentioned above, methylation of the CGIs prevents the binding of TFs such as ETS, Bzip, and the bHLH family of TFs. However, Yin et al. found that it facilitates binding some homeodomain TFs, such as POU and NFAT family of TFs, to the promoter or enhancer regions (Pachano et al., 2021). Kaluscha et al. deleted methyl-CpG-binding domain proteins (MBD) (Kaluscha et al., 2022), which are known to be recruited to the methylated CGIs and prevent the binding of TFs (Lewis et al., 1992). They showed the inhibition of TFs binding on the genic and repeat regions upon deletion and confirmed the presence of methylation-sensitive TFs (Kaluscha et al., 2022). Furthermore, methylation of CCCTC-binding factor (CTCF) binding regions rewires the chromatin structure (Monteagudo-Sanchez et al., 2024).

Retrotransposons are grouped as either long terminal repeats (LTRs), long interspersed nuclear elements (LINEs), or short interspersed nuclear elements (SINEs) (Banuelos-Sanchez et al., 2019). There are over 1 million copies of LINE-1 in the human genome. The full length of LINE-1 is usually 7kbp, but most are found in the genome as truncated versions with a typical 3' end. CGIs regulate the expression of LINE-1 on the internal promoter. Promoters of LINE-1 are silenced by both hypermethylation and recruitment of SETDB1, a H3K9 methyltransferase (Ardeljan et al., 2017; Smith & Meissner, 2013).

Bisulfite-converted DNA-based PCR products can be sequenced massively in parallel using NGS sequencing (e.g., Mi-seq), enabling the sequencing of DNA fragments and quantifying CpG methylation level resolution (Ravi et al., 2018). During bisulfite conversion, non-methylated cytosines are converted into uracils via reacting with sodium bisulfite, whereas methylated cytosine remains as cytosines. This allows for performing PCR afterward because, during the PCR, thymines replace uracils, and methylated cytosines remain as cytosines (Taryma-Lesniak et al., 2022). During the sequencing, 4-color fluorescently labeled nucleotides are used to synthesize the new DNA fragments via reversible terminator sequencing method, generating around 7.5-8.5 Gb data with 50 million paired-end reads if paired-end 300 bp DNA fragment is used (Han et al., 2024). Wang et al. used the MiSeq platform to assess methylation levels of promoter regions of genes involved in vitamin D metabolism (Wang et al., 2018). Another sequencing method is whole genome bisulfite sequencing (WGBS), allowing researchers to sequence CpG's entire genome. With tagmentation-based WGBS (T-WGBS), researchers can sequence precious samples with lower DNA concentrations (Wang et al., 2013; Weichenhan et al., 2018). However, WGBS or T-WGBS are expensive and require technical expertise. Therefore, researchers use methylation

arrays such as Illumina HumanMethylationEPIC BeadChip, which covers 850,000 CpGs probes enriched in enhancer and promoter regions of genes, including miRNAs (Moran et al., 2016; Noguera-Castells et al., 2023)

1.1.2.1.2. Histone Modifications

Histone post-translational modifications (PTMs) happen on the histone proteins (H2A, H2B, H3, H4). These histone proteins form the central histone octamer wrapped around 200bp of DNA to create a nucleosome core. PTMs include acetylation, methylation, phosphorylation, SUMOylation, and ubiquitination and regulate chromatin structure and, therefore, gene expression (Millan-Zambrano et al., 2022). Whereas H3K27ac (acetylation on the lysine residue at N-terminal position 27 of histone 3) and H3K4me1 or H3K4me3 are associated with active transcription, H3K9me2/3 or H3K27me3 are associated with silencing and heterochromatin formation (Zhang et al., 2021). Similarly, a typical enhancer region contains a gain of H3K27ac and H3K4me1 histone marks and p300 and Mediator complex, whereas an active promoter usually has reduced DNA methylation and gain of H3K4me3. H3K27me3 and H3K4me3 may be found in the poised enhancers or promoter regions. (Mulet-Lazaro & Delwel, 2023). Antibody-guided chromatin tagmentation (ACT-seq) can map the genome-wide histone modifications with low cell numbers and less background noise (Carter et al., 2020).

1.1.2.1.3. 3-dimensional (3D) Genome and Topologically Associated Domains (TADs) Structures

3D organization of the genome plays a vital role in the regulation of gene expression. Chromosomes are portioned in chromatin loop structures, topologically associating domains (TADs), and multi-megabase A and B compartments (da Costa-Nunes & Noordermeer, 2023; Mohanta et al., 2021). Enhancer-promoter contacts are determined by TADs, which generally are preserved in all human cell types. TADs create regulatory neighborhoods throughout the genome, which prevents the looping of enhancers and promoters in different TADs (Hnisz et al., 2016; Lupianez et al., 2015). However, Balasubramanian et al. observed that regulation of developmental genes in *Drosophila* embryos is pursued by intra and inter-TAD interactions, and genomic distances do not constrain the interaction between enhancers and promoters in different TAD structures (Balasubramanian et al., 2024).

Genetic structural variations are known to create new TADs (Xu et al., 2022). Hi-C is one method for studying the 3D genome (Gulino et al., 2021), whereas 4C (chromosome conformation capture-on-circular capture) is one for studying enhancer-promoter interactions (Miranda et al., 2022; Weichenhan et al., 2022).

TAD structures are usually determined by the binding of the CTCF, which, together with the ring-shaped cohesion complex, is responsible for genomic loops through loop extrusions. Knockout (KO) of CTCF is lethal in developing mice embryos (Monteagudo-Sanchez et al., 2024). In

contrast to bridging promoter-enhancer interactions, CTCF may isolate the contacts by acting as an insulator protein. The binding of CTCF is DNA methylation-sensitive. Whereas CTCF only binds to hypomethylated CpGs downstream of poly(A) sites, it also protects DNA from being methylated (Mujahed et al., 2020).

1.1.3. Epigenetics of AML

Epigenetic mechanisms drive cancer progression (Hanahan, 2022), regulate epigenetic/transcriptomic heterogeneity, and determine therapy responses (Hinohara et al., 2019). Therefore, insights into altered epigenetic mechanisms are essential in AML.

DNA methylation plays an essential role in AML. For example, hypermethylation on the promoter region of tumor suppressor genes such as *CDKN2B*, *APAF1*, and *E-cadherin (CDH1)* leads to silencing of these genes in AML (Furukawa et al., 2005; Shimamoto et al., 2005). Yamato et al. investigated genome-wide DNA methylation changes in 64 pediatric AML patients. They observed that patients can be classified into four clusters based on the DNA methylation profile associated with genetic alterations. They also showed that patients with high and low *MECOM* levels exhibit DNA methylation differences. For example, they observed hypomethylation on the *HOXB* genes, such as *MECOM* and *SCHIP1*, in patients with high *MECOM* expression (Yamato et al., 2022). Koldobskiy et al. compared the methylation profile of AML patients with MLL rearrangements with normal myeloid controls and showed genome-wide hypomethylation and dysregulation in the methylation of bivalent promoters or enhancers in the MLL rearranged AML patients. Additionally, they showed that differentially regulated genes in MLL rearranged AML have significant methylation changes (Koldobskiy et al., 2020).

DNA methylation profiles of AML patients can be used to predict the outcome of anti-cancer treatments. Achille et al. investigated DNA methylation changes of the promoters of 6 genes (*CDKN2A*, *APAF1*, *CDH1*, *CDKN2B*, *RARB*, and *HIC1*) during HMA treatment of AML patients. They found that global methylation changes are not associated with response to the treatment. However, early hypomethylation (3 days after the treatment) and (7 days after the treatment) on the *CDKN2A* promoter are associated with good prognosis, meaning patients with these DNA methylation changes during the therapy respond better to the treatment (Achille et al., 2016). Similarly, in a recent paper, the methylation pattern of *GATA3* and *WNT10A* genes are found to play a role in response to hypomethylating agent treatment (Schmutz et al., 2023).

Alterations in DNA methylation in cancer generally occur as hypomethylation in introns and repetitive regions like LINE and hypermethylation in the CpGs, usually located on the promoters (Schoofs & Muller-Tidow, 2011). Similarly, genome-wide DNA hypermethylation was observed in patients with MDS. The differentially methylated fragments were shown to be in or around CpG islands, playing an essential role in regulating transcription (Zhou et al., 2020). Genome-wide DNA methylation analysis in AML patients revealed three methylation-dependent subtypes of AML and different clinical outcomes within each subtype (Gao et al., 2020). In a different study,

unsupervised clustering of DNA methylation profiles of AML depicted different subtypes. Patients with *IDH1* and *IDH2* mutations had hypermethylation signatures, whereas patients with MLL rearrangements had hypomethylation signatures (Cancer Genome Atlas Research et al., 2013).

In addition to the abnormal DNA methylation, alterations in the CTCF binding and, therefore, changes in the 3D genome architecture are often observed in AML (Xu et al., 2022). Mujahed et al. found aberrant CTCF occupancy in AML patients, particularly with TET2 mutations. They showed enrichment of CTCF binding to the binding sites of critical myeloid TFs (Mujahed et al., 2020). Additionally, Luo et al. discovered that CTCF binds the site located between *HOXA7* and *HOXA9* genes in AML, leading to aberrant *HOXA9-HOXA13* gene expression. When they disrupted this binding, they observed the spreading of H3K27me3 and impairment of enhancer-promoter interactions, resulting in a reduction of *HOXA* genes, which are known to be putative oncogenes in AML (Luo et al., 2018).

1.1.3.1. Recurrent Mutations in Epigenetic Enzymes in AML

Around 50% of AML cases have normal karyotypes (nkAML). Targeted sequencing methods revealed recurrent mutations in genes essential for epigenetic mechanisms such as *DNMT3a*, *TET2*, *IDH1*, or *IDH2* (isocitrate dehydrogenase) or transcription factors such as *CEBP α* but also *FLT3*, *NPM1*, and *KIT* in the patients with nkAML (Cancer Genome Atlas Research et al., 2013). Mutations in *DNMT3A* usually occur as missense mutations due to the substitution of arginine to histidine in the exon 23 at arginine 882 (Khrabrova et al., 2021). This mutation induces focal DNA hypomethylation at the defined subtypes of retrotransposons, leading to the formation of double-stranded RNA (dsRNA) and the production of autonomous viral mimicry responses (Scheller et al., 2021). Mutations in *TET2* are usually loss-of-function mutations or somatic depletions, leading to global hypermethylation and dysregulation of the transcriptome (Huang et al., 2020). The percentage of AML patients with TET2 abnormalities is around 15-20%, whereas in MDS patients, the rate increases to 30% (Delhommeau et al., 2009). Treatment with vitamin C induces DNA hypomethylation *in vivo* by mimicking TET2 restoration since vitamin C is the main co-factor of Fe⁺² and α -KG-dependent dioxygenases, which are critical factors required for TET-mediated DNA hypomethylation. Restoration of TET2 prevents aberrant self-proliferation and leukemogenesis *in vivo* (Cimmino et al., 2017). MDS/AML patients with *TET2* mutations are classified as better responders to DNA hypomethylating agent treatment (Bejar et al., 2014; Itzykson et al., 2011). Mutations at arginine 132 of *IDH1* or arginine at 140/172 lead to oncogenic activation of IDH and generation of (R)-2-hydroxyglutarate ((R)-2HG) (Dang et al., 2009). (R)-2HG inhibits TET2 and KDM5 demethylases (Gunn et al., 2023).

1.1.4. Hematopoiesis and Alterations during Hematopoiesis in AML Leukemogenesis

Hematopoiesis is a fundamental process of self-renewal in which hematopoietic stem cells (HSCs) are renewed to produce blood and immune cells in the bone marrow (Hofer & Rodewald, 2018). HSCs are divided into two categories: long and short-term HSCs. Depending on the cytokines and intrinsic or extrinsic signals, short-term HSCs differentiate into hematopoietic progenitor cells, committed to be either a common lymphoid progenitor (CLP) or a common myeloid progenitor (CMP). Then, CMP cells differentiate into megakaryocyte-erythrocyte progenitor cells (MEP) and granulocyte-macrophage progenitor cells (GMP). CLP cells transform into B, T, and natural killer cells. On the other hand, GMP cells produce monocytes, granulocytes, and dendritic cells. Moreover, MEP cells form megakaryocytes and erythrocytes (Mann et al., 2022).

Changes in the HSC environment are essential for AML progression. For example, knockout of the *Lama4* gene increases AML induction *in vivo*, leading to impaired hematopoietic recovery after irradiation therapy (Cai et al., 2022). Similarly, dysregulation of the *SETBP1* expression leads to the transformation of hematopoietic cells (Tanaka et al., 2023).

Clonal hematopoiesis (CH) is a process in which clonally selected HSPCs expand by accumulating specific mutations or SVs. Those mutations can initiate transformation into hematologic malignancies or cardiovascular diseases (Desai et al., 2018). However, most individuals with clonal hematopoiesis of intermediate potential (CHIP) do not develop leukemia. Mutations in the epigenetic modifiers *TET2*, *ASXL1*, *DNMT3A*, RNA spliceosome components *SF3B1*, *SRSF2*, and DNA repair genes *TP53* and *PPM1D* are seen in around 80% of CHIP patients (Marnell et al., 2021). Scheller et al. found that CH or AML cells with *DNMT3A* mutations, one of the most frequently found mutations in CH and AML, are selectively responsive towards hypomethylating agent treatment and show viral mimicry responses upon the treatment (Scheller et al., 2021).

1.1.5. Current Treatment Options for AML

Since 2017, 12 new FDA-approved treatment opportunities for AML have been introduced into the clinics. Clinicians decide on the treatment based on the patient's fitness (age, physical fitness, medical history). Patients who are fit for intensive chemotherapy may get treatments following 7+3 (anthracycline and cytarabine or CPX-351) or high doses of cytarabine induction regimens (Forsberg & Konopleva, 2024; Mohamed Jiffry et al., 2023). Cytarabine is a chemotherapeutic agent that inhibits DNA synthesis by being an analog of deoxycytidine (Shabashvili et al., 2022). Following intensive therapy or patients unfit for intensive treatment may get allogeneic hematopoietic stem cell transplantation (Allo-SCT) (Forsberg & Konopleva, 2024; Mohamed Jiffry et al., 2023). Patients with CD33+ AML get gemtuzumab ozogamicin, an anti-CD33 monoclonal antibody coupled with a cytotoxic antibiotic (Kayser & Levis, 2022). In addition, with the advances in NGS techniques, patients may get targeted therapies such as FLT3 inhibitors (midostaurin) if they have *FLT3* mutations. AML patients with *IDH1* mutations (which is around 33% of AML) have been administered with *IDH1/2* inhibitors (ivosidenib, enasidenib), or novel

KMT2A (Menin) inhibitors have been investigated recently for patients with Menin rearrangements with *NPM1* mutations (Mohamed Jiffry et al., 2023).

1.1.5.1. Venetoclax Treatment

Patients who are newly diagnosed with AML and not fit for intensive chemotherapy follow venetoclax (VEN) and hypomethylating agents (HMA) combination therapy (Short et al., 2024). VEN is a BCL-2 inhibitor, a protein involved in intrinsic or mitochondrial apoptosis pathways. BCL-2 binds to BAX or BAK proteins, which disrupt the mitochondrial membrane upon activation and enable the release of cytochrome C. This induces caspase activation, which damages cellular organelles and nuclear structures (Roberts, 2020). AML patients under the VIALE-A trial were administered VEN (400 mg/daily) and azacytidine (75mg/m²) from day 1 to day 7 in 28-day cycles. They showed better survival rates and the incidence of remission than patients administered with azacitidine only (DiNardo et al., 2020; Kayser & Levis, 2022). Recently, researchers developed MAC-Score (Mediators of apoptosis combinatorial score), which links the ratio of BCL-2, XL, and MCL1 protein in leukemic stem cells and predicts the initial response against VEN and HMA treatment (e.g., 5-azacytidine) (Waclawiczek et al., 2023).

1.1.5.2. Decitabine Treatment

Since its identification in 1970, Azacitidine has been extensively studied (Forsberg & Konopleva, 2024). Azacitidine or 5-azacytidine (5AZA) or its deoxy derivative decitabine (5-aza-2'-deoxycytidine, DAC) inhibits DNA methylation. While 5AZA is also involved in RNA methylation, DAC is only involved in DNA methylation. DAC is transported by HCNT1 or HENT nucleoside transporter and converted to its biologically active form DAC-dCTP via several pathways involving kinases. Later, cytosines are replaced by DAC-dCTP during the S phase. DNMT1 binds to DNA and forms a covalent bond with DAC, and since DAC has nitrogen in its carbon at position 5, it can not be methylated. Therefore, DAC treatment disrupts DNMT function, leading to hypomethylation (Seelan et al., 2018). DAC is administered to patients as 15 mg/m² for 8h during 3 3-day periods, and this regimen is repeated every 6 weeks or for 5 days in 20mg/m² in 28-day cycles (Stomper et al., 2021).

5AZA or DAC has several effects against AML. First, HMA treatments induce the activation of differentiation-related genes and cause terminal differentiation of the leukemic cells (Hofer & Rodewald, 2018). Klobuch et al. found that combining HMA, all-trans retinoic acid (ATRA), and Pioglitazone (PGZ) triggers myeloid differentiation and inhibits cell growth (Klobuch et al., 2018). HMA treatments also decrease methylation on the promoter regions of tumor suppressor genes, which are known to be hypermethylated in cancer (Hackanson & Daskalakis, 2014). Furthermore, HMA treatment induces expression of cancer-testis antigen (CTA) genes such as the MAGEA family of genes, *NY-ESO-1*, *TAG-2a/2b/2c*. This induction represents antigens at sufficient levels to CD8+ T cells, leading to immune responses (Srivastava et al., 2016; Zhong et al., 2022). Finally, DAC treatment, especially in combination with HDAC inhibitors, activates human endogenous

retroviral elements, exclusively long terminal repeat (LTR) member *LTR12C* (Goyal et al., 2023) (Figure 2).

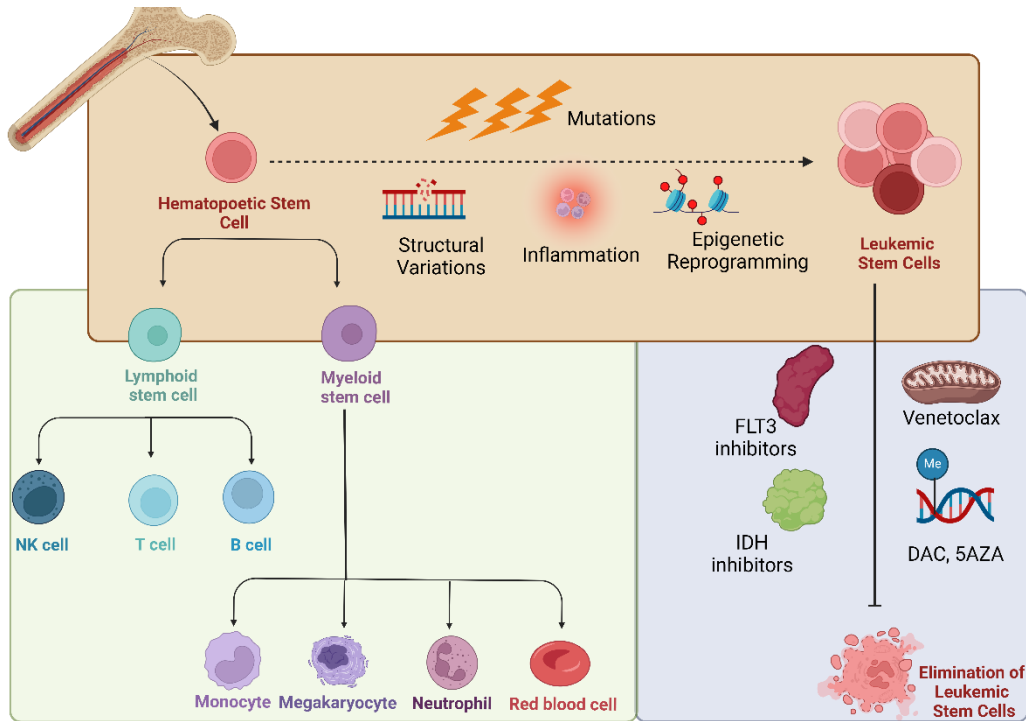


Figure 2: Representation of leukemic transformation and potential therapies.

HSPCs differentiate into lymphoid or myeloid progenitors, differentiating into NK, T, and B cells or monocytes, megakaryocytes, neutrophils, and red blood cells, respectively. However, SVs, inflammations in the stem cell niche, aberrant epigenetic changes, and mutations may drive AML. AML can be treated by eliminating leukemic stem cells with HMAs, venetoclax, or targeted therapies against the mutations. This figure is modified according to a figure in Nagel et al. (Nagel, 2021), and was created using BioRender.

1.2. Oncogenic Activation of *MNX1* in AML

Motor neuron and pancreas homeobox 1 (MNX1) is located on chromosome 7q36 and codes for a homeobox TF. *MNX1* is expressed during pancreatic (Harrison et al., 1999) and motor neuronal development (Thaler et al., 1999). Whereas heterozygous loss of function mutations in *MNX1* cause Currarino syndrome, which is a rare hereditary sacral agenesis disorder (El Amrani et al., 2024), homozygous recessive missense *MNX1* mutations lead to permanent neonatal diabetes mellitus (Aly et al., 2023). CAT7, a lncRNA, recruits members of polycomb repressive complex 1 to the promoter region of *MNX1* and regulates the expression of *MNX1* during neuronal differentiation (Ray et al., 2016).

MNX1 has oncogenic roles in several cancers, such as lung adenocarcinoma via regulation of *CCDC34* expression (Wu et al., 2023), colorectal cancer (Li et al., 2023), and human epidermal growth factor receptor 2 (HER2)-positive breast cancer (Chi et al., 2023). Additionally, *MNX1* is abnormally expressed in AML with t(7;12) in children under 2 years old or in del(7q) AML patients (Federico et al., 2019). Around 30% of infant AML patients have t(7;12) and show poor prognosis. The translocation involves breakpoints between exons 1 and 3 of *ETV6* (chr12q13) and breakpoints at 7q36. Whereas all t(7;12) cases express *MNX1*, around 50% express *ETV6::MNX1* fusion, first identified by Beverloo et al. in 2001 (Ragusa et al., 2023). Espersen et al. showed co-occurrence of t(7;12) with trisomy 19 (Espersen et al., 2018). T(7;12), created via CRISPR/Cas9 editing in K562 and human CD34+ HSPCs, led to increased self-renewal with myeloid bias and block in the erythroid compartment during differentiation (Ragusa, Ciciro, et al., 2022). Additionally, when Nilsson et al. generated induced pluripotent stem cells (iPSCs) with t(7;12) and differentiated these cells into HSPCs for modeling the disease, they observed alleviated proliferation and blocked myeloid and erythroid differentiation. They showed that whereas megakaryocyte genes are significantly decreased in the t(7;12) iPSCs-derived HSPCs, genes involved in myeloid pathways are upregulated considerably (Nilsson et al., 2022).

MNX1 has 3 exons coding for a 403-amino-acid long protein (Gulino et al., 2021), whose function is still under investigation. Zhu et al. showed that *MNX1* downregulates p21 and increases cervical carcinogenesis (Zhu et al., 2020). When Ingenhag et al. overexpressed *MNX1* in human and murine cells, they showed that overexpression leads to the induction of the p53-p21 tumor suppressor network and premature senescence. Additionally, they found that *MNX1*-overexpressed murine HSPCs resulted in differentiation arrest and accumulation of megakaryocytic and erythropoietic progenitor cells (Ingenhag et al., 2019). Finally, Waraky et al. proved that *MNX1* acts as an oncogene in AML as they observed induction of leukemogenesis, such as an increase in spleen size, infiltration of the liver with leukemia, severe anemia, and leukocytosis, in immune incompetent mice upon transplantation of fetal HSPCs expressing *MNX1*. They also showed increased H3K4me1/me2/me3 marks with a reduction in H3K27me3 upon expression of *MNX1*, suggesting that *MNX1* might act as an epigenetic regulator. They found that treating *MNX1*-expressing cells with sinefungin, a nucleoside analog of SAM, reversed the alterations observed after *MNX1* expression (Waraky et al., 2024).

1.3. Enhancer Hijacking Events in AML

SVs such as deletions, translocations, or inversions can lead to hijacking of enhancers. Hijacked enhancers, which generally regulate the expression of a different gene, are responsible for aberrant gene expression in tumorigenesis (Zhang et al., 2024). The first example of enhancer hijacking is the relocation of *IGH* enhancer to *MYC* locus in Burkitt and B-cell lymphoma and multiple myeloma through t(8;14) (Banerji et al., 1983; Gillies et al., 1983; Hayday et al., 1984). Additionally, *BCL11B* activation in T-cell acute leukemia was found to be due to the hijacking of enhancers (Montefiori et al., 2021). Another particular example is an activation of the oncogene

EVII via hijacking of *GATA2* in *inv(3)* and *t(3;3)* AML. For *inv(3)* and *t(3;3)*, a selective requirement of *MYB* binding was found to be necessary (Smeenck et al., 2021), whereas for *t(3;8)*, a *de novo* CTCF loop was found to be generated upon the translocation driving the oncogenic activation of *EVII* via *MYC* super-enhancer activity (Ottema et al., 2021).

In *t(7;12)* AML, *ETV6* enhancers are translocated to the proximity of *MNX1*. Due to this translocation, the *MNX1* gene is activated. Deleting the juxtaposed *ETV6* enhancers spanning a 200kb region significantly reduced *MNX1* expression (Weichenhan et al., 2024). In the GDM-1 cell line, different enhancers are responsible for activating *MNX1*. Enhancers from the *AH11/MYB* region are hijacked and responsible for creating new interactions with the *MNX1* promoter, validated via 4C-seq and ACT-seq experiments. The translocated enhancers are found to be active enhancers via luciferase assays (Weichenhan et al., 2023).

1.4. microRNAs

Non-coding RNAs include microRNAs (miRNAs), long non-coding RNAs (lncRNAs), small interfering RNAs (siRNAs), or PIWI-interacting RNAs (piRNAs) (Skvortsova et al., 2018). microRNAs are short 18-26 nucleotides non-coding RNA structures that play an essential role in silencing genes. miRNAs are first synthesized as long primary miRNA hairpins (pri-miRNA) from generally intronic regions of the genome. The generation of miRNAs can be divided into canonical or noncanonical pathways. Most miRNAs are produced via canonical pathways. First, the hairpin structure of the pri-miRNA is cleaved by the binding of Drosha, which is a 200 kDa RNase III protein, and two copies of DGCR8 (Svobodova et al., 2016). After this cleavage, precursor miRNA (pre-miRNA), around 55-70 nucleotide long, is released and exported to the cytoplasm via exportin 5. In the cytoplasm, another RNase III, DICER, cleaves the terminal loop of pre-miRNA. The ends of miRNAs are determined by DICER and Drosha complexes, and miRNA isoforms may be generated via alternative cutting. If the alterations are on the 5', then the resulting miRNA is called with 5p addition; if it is on the 3', it is called 3p (Bofill-De Ros et al., 2022). After the cleavage by DICER, a miRNA duplex is generated and interacts with the Argonaute (AGO) complex. AGO complex removes the passenger strand of miRNA and leaves only the miRNA sequence, which has specificity against the mRNAs. The resulting mature miRNA, AGO, and RISC complexes are directed to mRNA. Whereas miRNA in the complex is responsible for binding the specific sites, the AGO complex recruits proteins essential for translational repression, deadenylation, and decay (Figure 3). Noncanonical miRNA generation can be via Drosha or DICER-independent, meaning instead of RNase III, other RNases such as RNaseZ are involved (Ha & Kim, 2014; Shang et al., 2023).

miRNAs can be regulated via post-translational mechanisms, which alter the generation of miRNA and the loading of miRNAs to the RNA via the RISC complex. For instance, *LIN28A* is a pluripotency factor, which binds to the transcripts of pre-let-7 miRNAs and recruits terminal uridylyl transferases (TUT) that add uridylyl and inhibit DICER processing of the let-7 family of miRNAs.

Let-7 binds and degrades *LIN28* and *MYC* mRNAs. Additionally, many RNA binding proteins (RBPs) can inhibit or promote the generation of mature miRNA. For instance, heterogeneous nuclear ribonucleoprotein A1 (hnRNPA1) changes the structure of pri-miR18a and enables interaction with DROSHA. In contrast to miR18a, hnRNPA1 inhibits the generation of let-7a-1 miRNAs (Treiber et al., 2019). Lastly, adenosine deaminases (ADARs) can catalyze the editing of the binding region of miRNA to the DROSHA or RNA methylation by BCDIN3D can interfere with the interaction of miRNAs with DICER via methylation (Ha & Kim, 2014).

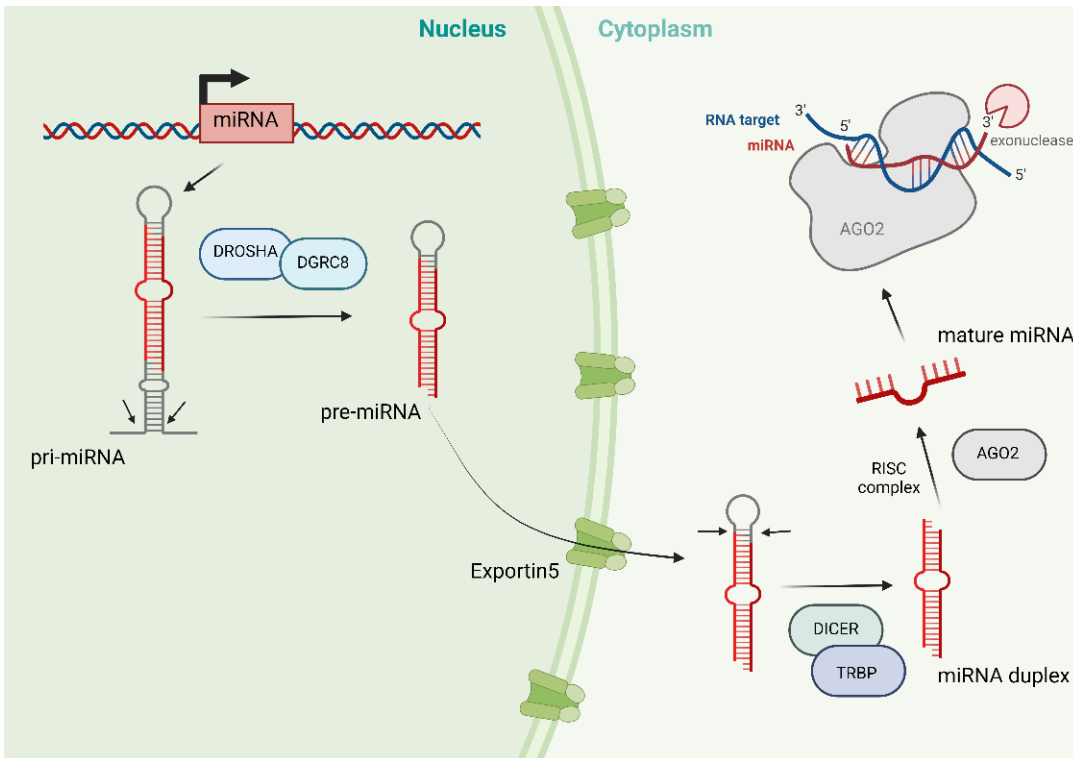


Figure 3: Generation of miRNAs.

MiRNAs are first coded as pri-miRNAs, which are cleaved with DROSHA and DGRC8 complexes and later exported from the nucleus to the cytoplasm. Later, pre-miRNAs are further cleaved with DICER and TRBP complexes. Finally, AGO forms mature miRNAs, and together with RISC and AGO complexes, miRNAs bind and degrade their target mRNAs. This figure was modified according to a figure in Peng et al. (Peng & Croce, 2016), and was created using Biorender.

miRNAs usually function by binding to the 3' untranslated regions (UTR) of the mRNAs. They have 'seed' regions on positions 2-7 of the 5' end, responsible for strict Watson-Crick pairing between the mRNA and miRNA (Rani & Sengar, 2022). The miRNA and RISC complex (miRISC) recruits the GW182 family of proteins. GW182 acts as a scaffolding protein for complexes such as deadenylases to deadenylate the mRNA, leading to 5'-to-3' mRNA decay through degradation. GW182 or RISC also recruits decapping complexes such as DDX6 to remove

the 5' m⁷ G-cap structure. Then, the final step is the mRNA degradation by XPN1 via 5'-to-3' exonucleolytic decay. (Iwakawa & Tomari, 2015). miRISC complex can compete with the eIF4E, the translation initiation factor. Another mechanism by which miRISC inhibits translation is by stimulating ribosomal dropoff or blocking the circularization of mRNAs. Finally, miRISC induces blocking of the association of 40S preinitiation complexes with 60S ribosomal subunits (Carthew & Sontheimer, 2009).

Silencing via miRNAs can also be via the binding of miRNAs to the 5' end or coding sequences (CDS) of mRNAs (Nemeth et al., 2024). Tay et al. published a paper in Nature showing that miR-134, miR-470, and miR-296 bind to CDS regions of pluripotency factors and regulate embryonic stem cell differentiation (Tay et al., 2008). Although miRNAs silence the expression of genes, there are some instances where miRNAs may boost the translation. For example, let-7 miRNA family members promote the translation of mRNAs that they bind to during the cell cycle arrest. Additionally, other miRNAs are activating the genes through binding to CDS or 5'UTR (Nemeth et al., 2024).

Although the characterization of the action of miRNAs on the target mRNA is complex, there are multiple prediction tools. TargetScan is one of them, which predicts the presence of 6mer, 7mer, and 8mer seed regions and uses 14 features, such as 3' UTR target site abundance, ORF length, 3' UTR length, number of offset-6 or 7 or 8mer sites in the ORF or 3'UTR, minimum distance of seed region of miRNAs to stop codon and polyadenylation sites, structural accessibility of miRNAs to the seed regions etc (McGeary et al., 2019; Riffo-Campos et al., 2016). miRTarBase is another prediction tool that combines experimentally verified miRNA-target interactions (MTIs) and information on SNPs nearby or on the seed region of the miRNA together with the information from curated publications (Huang et al., 2022). Lastly, miRDB is another prediction tool that uses machine learning methods to predict miRNA targets and combine them with MTIs from high-throughout NGS experiments (Chen & Wang, 2020).

1.4.1. Epigenetic Regulation of miRNA Expression

In addition to the post-transcriptional regulations of miRNAs mentioned above, miRNA expression can also be regulated via epigenetic mechanisms. Hypomethylation on the promoter region of miRNA increases its expression. Some epigenetically regulated miRNAs can either directly act as oncomirs (oncogenic miRNAs) or indirectly by degrading tumor suppressors in leukemogenesis (Agirre et al., 2012). Lu et al. found that hypomethylation on the CpG-rich region of 200bp upstream of miR-21 upregulated its expression in 8 different cancer types (Lu et al., 2020). In contrast, epigenetic silencing of miRNAs via hypermethylation can lead to cancer because there are miRNAs that downregulate oncogenes (Agirre et al., 2012). For instance, Cao et al. showed that DAC treatment alone or in combination with ATRA led to hypomethylation in the promoter region of miR-34a and activation of it and thereby reduction in *MYCN* expression because miR-34a binds and degrades *MYCN* mRNA (Cao et al., 2020). Epigenetic drugs that

induce re-expression of these epigenetically silenced miRNAs alone or combined with chemotherapy hold therapeutic potential in AML.

1.4.2. Role of miRNAs in AML Progression

Several studies show the importance of regulating miRNA expression in AML. For instance, epigenetic silencing of the miR-124a family via hypermethylation or by *EVII* led to the progression of AML. The same miRNA family binds to *CEBPA* and negatively regulates its expression, and loss of *CEBPA* leads to AML transformation via blocking the granulocyte differentiation (Agirre et al., 2012). Similarly, the silencing of miR-233 caused a blockage in differentiation in AML. miR-223 is expressed during myeloid lineage differentiation but not in AML. Competition between the binding of TFs on the promoter of miR-223 is vital for AML progression (Peng & Croce, 2016). Moreover, miRNAs can regulate the expression of tumor suppressor proteins in AML. miR-33 and miR-142-3p are known regulators of p53, which is a crucial tumor suppressor protein regulating cell division, senescence, DNA repair, and leading to apoptosis (Mann et al., 2022; Mao & Jiang, 2023). In contrast, miRNAs can behave as tumor suppressors by downregulating known oncogenes. For instance, mimics against miR-193b-3p are in the preclinical testing against AML as it is a tumor suppressor (Issa et al., 2023). Lastly, miRNAs can promote AML by regulating cytokines in the bone marrow niche. For example, miR-155 regulates the expression of IL-3 in AML (Sadras et al., 2017).

1.4.3. The miR-200 Family and The Role of miR-200a-3p in Cancer

The miR-200 family includes 5 miRNAs (miR-200a, miR-200b, miR-200c, miR-141 and miR-429). Whereas miR-200a, 200b, and 429 are located on chromosome 1 (chr1p36), miR-200c and miR-141 are located on chromosome 12 (chr12p13). miR-200a and miR-141 have a common seed sequence, 'AACACUG'; the rest share a different seed sequence (Choi et al., 2020; Fontana et al., 2021).

miR-200 regulates epithelial-to-mesenchymal (EMT) transition by inhibiting master regulators like *E-cadherin*, *ZEB1* and *ZEB2*. Overexpression of miR-200 inhibits the formation of distant metastasis of lung cancer (Choi et al., 2020; Pecot et al., 2013). Yu et al. found that miR-200a downregulates Yes-associated protein 1 (YAP1), leading to resistance to anoikis in breast cancer cells (Yu et al., 2013). Additionally, the miR-200 family is characterized as blood biomarkers for ovarian cancer diagnosis and prognosis (Choi et al., 2020). The miR-200 family plays a vital role in diabetes. Beta cell-specific expression of them leads to apoptosis and lethality in type 2 diabetic mice (Belgardt et al., 2015).

miR-200a-3p is a member of the miR-200 family and is known to decrease the proliferation of renal cell carcinoma via the downregulation of E3 ubiquitin-protein ligase CBL protein (Ding et

al., 2018) or promote esophageal cancer via inhibition of collapsing response mediator protein 1 (Zang et al., 2016). Li et al. showed that miR-200a-3p promotes gastric cancer tumorigenesis via binding and degrading *DLC-1*, a tumor suppressor gene (Z. Li et al., 2022). The expression of miR-200a, miR-200b, and miR-429 decreased in AML compared to healthy donors. Whereas miR-200b and miR-429 expression are associated with complete remission, miR-200b expression can be used as a prognostic biomarker for the overall survival of early-diagnosed AML patients (J. D. Zhou et al., 2018). Whereas there is no study for the function of miR-200a-3p in leukemias, miR-141-3p, which has the same seed sequence with miR-200a-3p but is expressed from different chromosomes, acts as a tumor suppressor in T-cell acute lymphoblastic leukemia by decreasing cell proliferation and promoting apoptosis (Klicka et al., 2022; Zhou et al., 2019).

1.4.4. miRNAs and lncRNAs Regulating *MNX1* Expression

Three publications show alterations in *MNX1* levels via miRs or lncRNAs. One of these publications showed that a long non-coding RNA (lncSHANK3) competes with miR-4530 to bind to *MNX1* 3'UTR in gastric cancer cells (Zhao et al., 2024). Another publication found that the expression of miR-200a and miR-141 is reciprocal with *MNX1* expression in insulin-producing cells, as these miRNAs are the prominent regulatory miRNAs of *MNX1*. When these miRNAs were overexpressed, they observed significant downregulation of *MNX1* and the pancreatic cell marker PDX1 (Mu et al., 2016). In another publication, the authors showed the binding of miR-141-3p to *MNX1* 3'UTR and the reduction of *MNX1* and increased inflammation response upon overexpression of miR-141-3p in necrotizing enterocolitis samples and IEC-6 cells (Chen et al., 2020). All these miRNA-related publications and the fact that overexpression of miR-200 led to the induction of beta cell apoptosis, which is known to express *MNX1*, show the importance of miRNA in regulating *MNX1* expression.

2. Hypotheses and Aims

AML with t(7;12)(q36;p13) are seen in infants under 2 years old and have a 3-year survival rate of 24%. *MNX1* is highly expressed in all t(7;12) (Weichenhan et al., 2024). Furthermore, some del(7q) AML cases express *MNX1* (Federico et al., 2019; Etienne Sollier et al., 2024). Overexpression of *MNX1* in fetal HSPCs and transplantation to immune-deficient mice resulted in leukemogenesis with accumulation of damaged DNA and differentiation blockage (Waraky et al., 2024). Considering that *MNX1* has oncogenic roles in AML and is highly expressed in subtypes of AML, defining a compound that demonstrates the ability to downregulate *MNX1* and, therefore, inhibit the growth of *MNX1*-dependent AML cells is essential. However, no small molecules inhibit *MNX1* expression. In this thesis, performing a high throughput epigenetic compound screening aimed to find an epigenetic compound that reduces *MNX1* expression and provides a clinically meaningful therapeutic opportunity to target *MNX1* in clinics against *MNX1*-expressing AML cases.

Since *MNX1* is activated via an enhancer-hijacking event in both pediatric and adult AML, I developed the following hypothesis:

MNX1 expression, mediated by enhancer-hijacking events in AML, can be reduced by epigenetic compounds that disrupt the enhancer-hijacking event.

Aim 1: To perform an epigenetic compound screen in GDM-1 cells to find drugs that reduce cell viability and *MNX1* expression.

Aim 2: To investigate the mechanisms behind DAC-treatment-induced reduction of *MNX1*. Here, I established several sub-hypotheses:

Aim 2.1: To test whether DAC-mediated upregulation of CAT7, a previously described *MNX1* targeting lncRNA known to recruit PRC1 complexes to the *MNX1* promoter (Ray et al., 2016), could be induced by DAC treatment.

Aim 2.2: To test the possible generation of demethylated CTCF boundaries and alteration of TAD boundaries upon global hypomethylation, which may help explain why *MNX1* expression is reduced upon DAC treatment.

Aim 2.3: To test the proposed activation of *MNX1*-targeting miRNA(s) upon hypomethylation of their promoter, which could explain the observed reduction of *MNX1*.

Aim 3: to develop and validate the phenotypes observed in AML cell lines using *MNX1*-expressing PDX models.

3. Materials and Methods

3.1. Cell culture

All the cell lines were authenticated with Multiplexion and checked for mycoplasma contamination on the dates specified in [Supplementary Table 1](#).

K562, OCIAML3, MOLM13, and HL60 cells were cultured in RPMI Medium 1640 + L-glutamine with 10% FCS and 1% Penicillin/streptomycin (P/S). GDM-1 cells were cultured in RPMI Medium 1640 + L-glutamine with 20% FCS and 1% Penicillin/streptomycin (P/S). All cell lines were subcultured at a 500.000 cells/ml density every second day. HEK293T cells were cultured in DMEM (1X) medium with 4.5 g/L D-glucose and L-glutamine without pyruvate and supplemented with 10% FCS and 1% P/S. After washing with DPBS without magnesium and calcium, HEK293T cells were trypsinized with Trypsin-EDTA (0.25%) with phenol red ([Supplementary Table 2](#)) and subcultured in a 1:10 ratio every three days.

3.2. Epigenetic drug screening

4 hours before the treatment, 35,000 GDM-1 cells in 90 μ l of growth medium were seeded in 96-well plates. The epigenetic compound library was obtained from Prof. Dr. Udo Oppermann's lab, and the treatment protocol was as per Cottone et al. (Cottone et al., 2020). Each epigenetic compound in the library was diluted 1:100 using the growth medium. GDM-1 cells were treated with either vehicle control (DMSO) ([Supplementary Table 14](#)) or 10 μ l of the diluted compounds ([Supplementary Table 3](#)). 5 days after the treatment, 20 μ l of cell titer blue was added, and viability was measured. Signals from the treated wells and DMSO-treated cells were subtracted from the only medium with DMSO control. The treatment was performed in 3 technical replicates within 2 biological replicates.

3.3. Selection of the compounds from the screening and dose-response curve (DRC) analysis

A485, SGC-CBP30, GSK-J4, ACBI1, JQ1, MZ1, GSK591, GSKLSD1, and IBRD9 are the compounds that were chosen from the library screening and used in this thesis. [Table 1](#) summarises the mechanism of action of each compound and its effects on diseases.

These 10 different epigenetic compounds ([Table 1](#)) were selected based on their commercial availability, viability results, and suggestions from Prof. Dr. Udo Oppermann. For dose-response analysis, 35,000 GDM-1 cells were treated with varying concentrations of the compounds in 96-well plates in 3 technical replicates within 3 biological replicates. 5 days after the treatment, 20 μ l of cell titer blue was added, and viability was measured using the plate reader. Signals from the

treated wells and DMSO-treated cells were subtracted from the only medium with DMSO control. Calculation of IC₅₀ was performed using the 4-parameter log-logistic model with the formula below in GraphPad Prism 10.1.2. IC₈₀ concentrations were calculated using the formula below.

$$Y = Bottom + \frac{(Top - Bottom)}{(1 + 10^{((LogIC_{50} - X) * HillSlope)})}$$

$$IC_p = IC_{50} \times \left(\frac{100}{100 - p} - 1 \right)^{\frac{1}{HillSlope}}$$

After calculating the IC₈₀ concentrations, 350.000 GDM-1 cells/ml were seeded in a 6-well plate format treated with the epigenetic compounds selected ([Supplementary Table 4](#)) and pelleted for DNA, RNA, or protein isolation after washing with DPBS without magnesium and calcium.

Table 1: The epigenetic compounds further used in the thesis and their targets and mechanisms of action as described in current literature.

Compound name	Function	Mechanism of action	Ordering details
A485	a catalytic inhibitor of p300-CBP (Lasko et al., 2017)	<ul style="list-style-type: none"> reduce the proliferation rate of 124 different cancers, including hematological malignancies, prostate cancer, triple-negative breast cancer, and small cell lung cancer (SCLC) (Lasko et al., 2017) reduce the expression of miR-34a-5p, which plays an essential role in hepatic gluconeogenesis (Y. Wang et al., 2022) 	Merck, Catalog number: SML2192
SGC-CBP30	an inhibitor of the bromodomain of HAT EP300 (Hammitzsch et al., 2015)	<ul style="list-style-type: none"> decreases H3K27ac and H3K9ac levels (X. Wang et al., 2022) reduces the proliferation of multiple myeloma cells (Conery et al., 2016) The combination of SGC-CBP30 with cisplatin shows an increased 	Sigma Aldrich, Catalog number: SML1133-5MG

		anticancer effect on chordoma samples, and this highlights the importance of the idea of a combination of epigenetic drugs with chemotherapeutic agents in clinics (Wen et al., 2024).	
GSK-J4	an inhibitor of histone demethylase jumonji domain containing protein-3 (KDM6B) (JMJD3/Lysine demethylase 6B) or ubiquitously transcribed tetratricopeptide repeat, X chromosome (UTX/Lysine demethylase 6A) (KDM6A) enzymes (Cottone et al., 2020)	<ul style="list-style-type: none"> • demethylases H3K27 di or trimethylation and GSK-J4 treatment, resulting in increased levels of H3K27me3 (Dalpatraj et al., 2023) • Another potent inhibitor of KDM6A/B led to the effective inhibition of H3K27 demethylases and specific reduction in the expression of Brachyury (Cottone et al., 2020), which is an oncogene important for chordoma (Sharifnia et al., 2019). Due to reduced <i>Brachurh (TBXT)</i> expression, chordoma viability decreased significantly upon the treatment (Cottone et al., 2020). 	Merck, Catalog number: 420205
ACBI1	proteolysis targeting chimeras (PROTACs) of the SWI/SNF complex subunits SMARCA4, SMARCA2, and PBRM1. SWI/SNF subunits are involved in ATP-dependent chromatin remodeling (Farnaby et al., 2019)	<ul style="list-style-type: none"> • Xiao et al. showed that enhancer-binding TF-addicted cancers are sensitive to SWI/SNF inhibition. They found that the treatment results in less binding of TF at the enhancer elements and reduced enhancer-driven oncogenic activities (Xiao et al., 2022) 	MedChemExpress, Catalog number: HY-128359
JQ1	a BET inhibitor via degradation of BRD4, which is a reader of H3K27ac (Loven et al., 2013)	<ul style="list-style-type: none"> • reduce the activity of the super-enhancer driving <i>MYC</i> oncogenic expression (Loven et al., 2013) 	Merck, Catalog number: SML1524

		<ul style="list-style-type: none"> overcomes the therapy resistance in AML and acute lymphocytic leukemia (ALL) cell lines (Bauer et al., 2024) 	
MZ1	a PROTAC of BET (Ma et al., 2022)	<ul style="list-style-type: none"> inhibits AML cell growth via induction of apoptosis in cell lines but also decreases proliferation of leukemic cells in vivo (Ma et al., 2022). 	MedChemExpress, Catalog number: HY-107425
GSK591	a selective inhibitor of PRMT5, the protein arginine methyltransferases responsible for demethylating H4 or H3 and silencing transcription (Brown-Burke et al., 2023; Brown et al., 2024)	<ul style="list-style-type: none"> anti-tumoral activity in MLL-rearranged AML <i>in vivo</i> models (Kaushik et al., 2018). 	MedChemExpress, Catalog number: HY-100235
GSKLSD1	an irreversible inhibitor of LSD1 that demethylates H3K4me1/2 and H3K9me1/2 (Cusan et al., 2018)	<ul style="list-style-type: none"> Treatment of MLL fusion AML mouse models with GSKLSD1 resulted in high lethality and the induction of myeloid differentiation (Cusan et al., 2018). 	MedChemExpress, Catalog number: HY-100546A
I-BRD9	a selective chemical probe against BRD9, a SWI/SNF ATPase complex subunit (Zhou et al., 2021)	<ul style="list-style-type: none"> reduces cell proliferation, ferroptosis induction, and apoptosis in AML (Zhou et al., 2021). 	Sigma Aldrich, Catalog number: SML1534
Decitabine (DAC)	A hypomethylating agent inhibiting DNMT1 (Pappalardi et al., 2021)	<ul style="list-style-type: none"> Low-dose decitabine treatment has been used in clinics against AML, which also synergistically worked with venetoclax (Briski et al., 2023). 	Sigma Aldrich, Catalog number: A3656-5MG

3.4. Decitabine and MG132 treatment schedule

Unless otherwise stated, the following treatment schedule was used. 350.000 GDM-1 cells/ml or PDX cells were seeded in a 6-well plate format, and the next day, 500 nM Decitabine (DAC) was added to the media. The cells were collected, centrifuged, and resuspended in freshly prepared growth media containing 500 nM DAC for 5 days. After the treatment, the cells were pelleted for further experiments after washing with DPBS without magnesium and calcium. For proteasomal inhibition, 10 μ M of MG-132 was used to treat the cells for 24 hours.

3.5. shRNA-mediated knockdown of *MNX1*

GDM-1 cells expressing shRNAs were obtained from Dr. Mariam Hakobyan at DKFZ. Upon Hydroxytamoxifen treatment, the Cre-ER system is activated, and the mCherry construct is silenced; BFP (blue fluorescence protein) is constitutively expressed, whereas GFP (green fluorescence protein) and shRNAs are upon 4-Hydroxytamoxifen (TAM) treatment. sh76 targets the second exon of *MNX1* (chr7: 156799237-156799258), and sh82 also targets the second exon of *MNX1* (chr7: 156799231-156799252), whereas GDM-1 expressing shScramble targets no human gene, was used as a control.

Aliquots of 10 mg/ml 4-Hydroxytamoxifen were thawed at 37°C in a water bath and then at 56°C for 3 minutes. The aliquots were vortexed, and the procedure was repeated until the solution became clear. Meanwhile, 400.000 GDM-1 cells stably transduced with shScramble, sh76, and sh86 were washed with DPBS and then seeded in one of the 6-well plates by resuspending them in 2ml of growth media containing 1 μ g/ml of 5-Hydroxytamoxifen. 48 hours after the treatment, cells were collected for sorting. Cells were washed twice with DPBS supplemented with 2%FCS and resuspended in 300 μ l of DPBS with 2%FCS. Assistant-directed fluorescence-activated cell sorting for GFP and BFP-positive cells was performed at the DKFZ Flow Cytometry core facility with the help of a technical assistant. Following sorting, 200.000 cells were pelleted for protein isolation and 100.000 cells for RNA isolation. The rest of the cells were seeded in one well of 24-well plates for recovery for cell viability assay. After one week of recovery, 35.000 sorted cells were seeded in one well of a 96-well plate. Cell viability was measured two days later using a Cell Titer Blue assay and a plate reader ([Supplementary Table 16](#)).

3.6. RNA isolation, cDNA synthesis, and quantitative polymerase chain reaction (qPCR)

RNA was isolated using an RNeasy Plus kit according to manufacturer instructions ([Supplementary Table 6](#)), including performing elimination with DNase columns. RNA was eluted in 30 μ l of RNase-free water twice. Total RNA concentrations were measured using the Qubit RNA BR kit. 500 ng of RNA was diluted with water, so the total volume was 9 μ l. Protocols for cDNA conversion and qPCR were adapted Goyal et al. (Goyal et al., 2023). For further DNase treatment, 1 μ l of 10x DNase buffer and 0.5 μ l of DNase I were added. Next, the samples were

incubated at room temperature for 10 minutes. 1 μ l of 12.5mM EDTA was added to each sample and incubated at 65°C for 10 minutes. 1 μ l of 10mM dNTP mix and 1 μ l of 200 ng/ μ l random hexamer were added to the samples and incubated at 65°C for 5 minutes. They were immediately put onto ice. 4 μ l of 5x First Strand buffer, 1 μ l of 0.1M DTT, 0.5 μ l of Ribolock, 0.2 μ l of Superscript III (200 Unit/ μ l), and 0.8 μ l of RNase-free water were added to each sample. Next, the samples were incubated at 25°C for 5 minutes, at 50°C for 60 minutes, and at 70°C for 15 minutes. 80 μ l of RNase-free water was added to each sample to reach 1:10 dilution.

The 384-well format was used for qPCR. 1,1 μ l of RNase-free water, 3,5 μ l of 2X SYBR Green Master Mix (primaQuant) buffer, and 0,4 μ l of 10 μ M forward and reverse primer mix listed in [Supplementary Table 8](#) were added to 2 μ l of 1:10 diluted cDNA. For each sample, 3 technical replicates were used, and the PCR setup described in [Supplementary Table 9](#) was used to carry out the qPCR. Expression of GAPDH was used to normalize the expression of genes after calculating average $2^{-\Delta(\text{Ct})}$.

3.7. RNA-seq preparation and analysis

RNA isolation was performed as described in [section 3.6](#). The quality of the RNAs was assessed using an RNA TapeStation kit and a TapeStation machine according to the manufacturer's instructions. Libraries of 13 samples were prepared in the DKFZ Next Generation Sequencing core facility, multiplexed, and sequenced using a NovaSeq 6K paired-end 100bp S1 machine.

Katherine Kelly (DKFZ, Heidelberg) analyzed RNA-seq data. RNA-seq analysis was performed by preprocessing with the nf-core RNA-seq pipeline, which included unique molecular identifiers (UMI) barcode extraction with UMI tools, quality control with the fastqc tool and adapter, quality trimming with the TrimGalore tool, alignment using the hg19 reference genome, and quantification using Salmon/STAR. Differential gene expression upon DAC treatment was identified using the DESeq2 package in R version 4.1.0. Genes whose false discovery rate (FDR)-adjusted p-value is less than 0.05 and whose absolute($\log_2(\text{Fold Change})$) is more than 1 were considered significant.

3.8. LB medium, LB-Agar preparation, and transformation of vectors

10g of agarose, 10g of bacterial peptone, 5g of yeast extract, and 5g of NaCl were used to prepare LB-medium, and for LB-agar medium, 13 g of agar was sterilized by autoclaving.

The constructs listed in Table 4 (1ng/ μ l) were transformed to 20 μ l of Stab13 E.coli (kindly provided by Oliver Mücke) using electroporation with 1600V and 5ms setting, and 200 μ l of LB medium without antibiotics was added. 70 μ l of transformed bacteria were spread on LB-agar plates containing 100 μ g/ml of Ampicillin. The next day, colonies were picked and inoculated in

5ml of LB-medium with 100 µg/ml of Ampicillin. Plasmids were extracted with 3ml of LB medium with inoculated bacteria using the mini-prep isolation kit. Later, the constructs were verified via sequencing by Microsynth. 1 ml of the rest of the LB medium with inoculated bacteria was mixed with 1 ml of 15% LB medium with glycerol to prepare glycerol stocks of each construct. The remaining 1 ml of the LB medium with inoculated bacteria was inoculated to 100 ml of LB medium with 100 µg/ml of Ampicillin. The next day, plasmids were extracted using a maxi-prep isolation kit.

3.9. Agarose gel electrophoresis

1xTBE buffer (Tris-borate-EDTA) ([Supplementary Table 5](#)) was prepared by diluting 10X stock with water. 1.2 grams of agarose was dissolved in 100 ml of 1xTBE buffer, and 4 µl of ethidium bromide was added. The solution was heated up in a microwave and, after cooling down, poured into a chamber. Next, 1.2% agarose gel was put inside 1xTBE solution with 4µl of ethidium bromide per 100 ml. 5 µl of either phage Lambda HindIII or DNA 100bp ladder were loaded to the corresponding combs of the gel. Next, plasmid DNAs or PCR products were mixed with Purple gel loading dye (6X) and were loaded to the combs. They were separated with 90 volts (V), and the duration of the separation was adjusted based on the size of the sample fragments and the percentage of agarose gel. Later, the sample fragments were visualized, and the pictures were saved using the UV machine ([Supplementary Table 16](#)) under UV light.

3.10. Lentivirus production and collection

The lentiviral generation protocol was adopted by Mancarella et al. (Mancarella et al., 2024). 800,000 HEK293T cells were seeded in one well of 6-well plates with 2 ml of growth medium. The next day, if the confluency of the cells reached 80%, the medium was refreshed with 1.5 ml of growth medium. 8.4 µl of TransIT-LT1 was added to 100 µl of RPMI Medium 1640 + L-glutamine and incubated for 10 minutes at room temperature. In a separate Eppendorf tube, 1 µg of pRCDEMP-EF1-GFP-HA-MNX1, 667 ng of psPAX2, and 333 ng of pMD2.G ([Supplementary Table 10](#)) were added to 300 µl of RPMI Medium 1640 + L-glutamine and incubated for 10 minutes at room temperature. 8.4 µl of TransIT-LT1 was added to 100 µl of RPMI Medium 1640 + L-glutamine and incubated for 10 minutes at room temperature. In a separate tube, 1 µg of pLVX-GFP, 667 ng of psPAX2, and 333 ng of pMD2.G were added to 300 µl of RPMI Medium 1640 + L-glutamine and incubated for 10 minutes at room temperature. Next, plasmid and TransIT-LT1 mixes were mixed and set for 30 minutes at room temperature. The cells were transferred to the S2 laboratory facility, and the mixture was added to HEK293T cells dropwise.

The next day after the transfection, 1.5 ml of fresh growth medium was added. GFP percentage was checked, and the virus-containing medium was collected and filtered the following day using a 0.45 µm filter and stored at -80⁰C in cryovials.

3.11. Transduction of GDM-1 cells

The transduction protocol was adopted from Anna Riedel and Mariam Hakabyon's protocol. Two times, 7×10^6 GDM-1 cells were seeded in 10 ml of growth medium in T75 flasks. One of the flasks will be used as a control during puromycin selection. 4 ml of lentiviruses and 5 $\mu\text{g/ml}$ of polybrene were added on the other flask. The following day, cells were collected, centrifuged, washed with DPBS two times, and resuspended in 15 ml of growth medium. The next day, cells were collected, centrifuged, washed with DPBS two times, and resuspended in 15 ml of growth medium containing 1 $\mu\text{g/ml}$ puromycin. The cells were transferred back to the S1 lab, and the GFP percentage was assessed under a fluorescence microscope. Puromycin selection was continued until 10% of the remaining control cells were left alive.

3.12. Generation of empty vector

pRCDEMP-MNX1-GFP-HA plasmid was digested to remove MNX1 using *EcoRI* HF at 37°C using Cut Smart Buffer, and then 1 μl of *BstBI* was added and incubated at 65°C. The cut plasmid was run on a 0.8% gel. The 7.8 kb long band (meaning the digested plasmid part without MNX1) was cut out and purified from the gel. 2 μl of 100 μM oligo stock, 2 μl of 10X T4 ligase buffer with ATP, 14 μl of RNase-free water, 1 μl of T4 Polynucleotide kinase, 100 μM Forward or Reverse primer were mixed and incubated at 37°C for 1 hour and at 65°C for 20 minutes. 1 μl of forward primer mix, 1 μl of reverse primer mix, and 8 μl of RNase-free water were mixed and incubated at 95°C for 5 minutes and slowly cooled down for 30 minutes. The annealed primer mix was diluted in a ratio of 1:10. Next, 1 μl of annealed primers were ligated with 33 ng digested plasmid DNA, 1.5 μl of 10X T4 ligation buffer with ATP, 1.0 μl of T4 ligase and 10 μl of RNase-free water. The mix was incubated at 25°C for 2 hours. 15 μl of ligation mix was mixed with 7.5 μl of Ammonium Acetate (kindly provided by Marion Bähr), 1 μl of glycogen (kindly supplied by Marion Bähr), and 59 μl of 100% ethanol and incubated on ice for 15 minutes. The sample was centrifuged at maximum speed for 3 minutes, and the supernatant was removed. The pellet was washed once with 80% ethanol, dried for 10 minutes at room temperature, and dissolved in 5 μl of RNase-free water. 20 μl of Stab13 electrocompetent bacteria were electroporated with 1 μl of the ligation mix under 1.6 kV for a 5 milliseconds setting, and 200 μl of LB medium without antibiotics was added. 70 μl of transformed bacteria were spread on LB-agar plates containing 100 $\mu\text{g/ml}$ of Ampicillin. The next day, colonies were picked and inoculated in 5ml of LB-medium with 100 $\mu\text{g/ml}$ of Ampicillin. Plasmids were extracted with 3ml of LB medium with inoculated bacteria using the mini-prep isolation kit. Later, the constructs were verified via sequencing from Microsynth company, and digestion with restriction enzymes was followed by agarose gel electrophoresis. 1 ml of the rest of the LB medium with inoculated bacteria was mixed with 1 ml of 15% LB medium with glycerol to prepare glycerol stocks of each construct. The remaining 1 ml of the LB medium with inoculated bacteria was inoculated to 100 ml of LB medium with 100 $\mu\text{g/ml}$ of Ampicillin. The next day, plasmids were extracted using a maxi-prep isolation kit.

3.13. miRNA isolation, cDNA synthesis, and qPCR

500,000 cells were lysed with 700 μ l of Qiazol buffer and incubated for 5 mins at room temperature. 140 μ l of chloroform was added, mixed thoroughly for 15s, and incubated for 2 mins at room temperature. Next, the mix was centrifuged at 12000g at +4°C for 15 mins. Three phases can be distinguished by color and cloudiness. The upper phase was transferred into a collection tube, and 525 μ l of 100% ethanol was added, mixed thoroughly, and transferred into RNeasy mini spin pink columns and centrifuged at 8000g at room temperature for 1 min. The columns were washed with RWT buffer (Catalog number: 1067933, Qiagen) and 500 μ l of RPE buffer twice from the RNeasy kit. The miRNAs were eluted with 25 μ l of RNase-free water. Total RNAs were quantified using a Qubit RNA BR kit. cDNAs were synthesized following the manufacturer's protocol (miRCURY LNA RT kit, catalog number 339340, Qiagen) using 200 ng of total RNA. cDNAs were diluted in a 1:5 ratio with RNase-free water. qPCR reaction was performed according to the manufacturer's protocol (miRCURY LNA SYBR Green PCR Kits, catalog number 339346, Qiagen), and the settings described in [Supplementary Table 12](#) were used. The probes described in [Supplementary Table 11](#) were dissolved in 220 μ l of RNase-free water. For analysis, the expression of each miRNA was calculated with $2^{-\Delta Ct}$ formulation and was normalized to SNORD44 or U6.

3.14. Overexpression of miRNA mimics and antagomirs

5 nmol of miRNA-381-3p, miRNA-410-3p, miRNA-200a-3p, and miRNA-NC mimics listed in [Supplementary Table 12](#) were dissolved in 250 μ l of RNase-free water by mixing thoroughly. Later, 20 μ M miRNA mimics were aliquoted in PCR tubes for further experiments.

5 nM, 10 nM, and 15 nM of miRNA mimics were nucleofected to 100,000 GDM-1 cells using the Neon transfection system using a 1500V 20ms 1pulse setting. Next, the cells were seeded in 24 wells in 600 μ l of growth media. 72h after the transfection, the cells were collected, counted, and nucleofected again with 5nM, 10nM, and 15nM of miRNA mimics. 72h after the second transfection, the cells were pelleted for qPCR and western blot analysis.

100 nM of negative control or miR-200a-3p antagomirs were nucleofected to 100,000 GDM-1 cells using the Neon transfection system using a 1500V 20ms 1pulse setting. Next, the cells were seeded in 6 wells. The next day, the cells were treated with DAC (500 nM). The media was refreshed with newly prepared DAC (500 nM) every day. 72h after the transfection, the cells were collected, counted, and nucleofected again with 100 nM of antagomirs and seeded in DAC-containing media. 72h after the second transfection, the cells were pelleted for qPCR and western blot analysis.

3.15. Luciferase assay

Dual-luciferase assays validate the interaction between miRNAs and their predicted target. In dual-luciferase assays, the predicted targets are fused with the firefly luciferase (LUC) expression cassette, whereas the renilla LUC expression cassette serves as an internal control. In the end, LUC is measured via a luminometer, and the firefly LUC signal is expected to decrease upon degradation of the predicted target via miRNAs (Clement et al., 2015; Moyle et al., 2017). miRNA-200a-3p and miRNA-NC (negative control) mimics were diluted 1:10 in RNase-free water to achieve a 2 μ M concentration. 3.4 μ l of DharmaFect transfection reagent was mixed with 336.6 μ l of RPMI medium without FCS and incubated at room temperature for 10 minutes. Meanwhile, 5.1 μ l of 2 μ M mimics were added to 164.9 μ l RNase-free water for a 5nM concentration. 170 μ l of DharmaFect mixture was added to each miRNA mimic, and the mixtures were incubated at room temperature for 30 minutes. Meanwhile, 630.000 HEK293T cells were pelleted and resuspended in 1 ml of growth medium. After the incubation, 170 μ l of miRNA mimic-DharmaFect mix was distributed to one well of 12 wells, and 630.000 HEK293T cells were seeded on top.

24 hours after miRNA transfection, 1100 ng of plasmids containing 3'UTR or mutated 3'UTR or pLVX-GFP were incubated for 30 minutes at room temperature with 2.2 μ l of TransIT-LT1 transfection reagent in a 100 μ l of OPTIMEM media. Later, the mix was added to the cells dropwise.

48 hours after plasmid transfection, the cells were trypsinized and counted. 80,000 cells were seeded after resuspending in 160 μ l of growth media into 8 wells of the 384-well plate as 8 technical replicates. Later, the cells were centrifuged at 300g for 5 minutes. 1 hour after seeding the cells, 20 μ l of luciferase buffer was added and incubated at room temperature for 15 minutes. Firefly luciferase signals were measured following plate reader settings for Cell-Glo Dual luciferase by only changing the plate setup to 384-well opaque. Next, 20 μ l of stop luciferase buffer was added and incubated at room temperature for 15 minutes. Renilla luciferase signals were measured. Renilla signals were divided into firefly signals and multiplied by 1000 for all the samples for calculation.

3.16. miRNA-seq sample preparation and analysis

miRNA was isolated following the protocol described in [section 3.13](#). 5 μ M cel-miR-65-5p and cel-miR-36-3p ([Supplementary Table 12](#)) were kindly provided by Dr. Birgitta Michels and used to spike in 1 μ g total RNA. The library was prepared following the NEBNext Small RNA Library Prep Set for Illumina Kit. First of all, 3' adaptor ligation was performed. And then, reverse transcription primers were hybridized. Next, 5' adaptor sequences were ligated. After the reverse transcription step, index primers from the same kit were ligated. A PCR was performed with the following conditions: initial denaturation at 94°C for 30 seconds, 13 cycles of denaturation at 94°C for 15 seconds and at 62°C for 30 seconds and at 70°C for 15 seconds, and final extension at 70°C for 5 minutes. The PCR products were purified using Monarch PCR and a DNA cleanup kit by diluting the PCR products with binding buffer using a 7:1 ratio. After the elution in 27.5 μ l of

RNase-free water, 32.5 μ l of AMPure XP beads were added and incubated at room temperature for 5 minutes. The samples were placed on a magnetic stand, and after the solution was clear, the supernatant was removed. 92.5 μ l of AMPure XP beads was added. The samples were placed on a magnetic stand, and after the solution was clear, the supernatant was removed. The beads were washed with 200 μ l of 80% ethanol for 30 seconds and dried for 10 minutes at room temperature. Next, the fragments were eluted in 15 μ l of RNase-free water. 1 μ l of the eluted samples was used to measure concentration using a Qubit DNA HS kit, and 1 μ l of some samples was used to check the size of the library prepared using a High Sensitivity D1000 tape station kit and 4150 tape station machine according to the sample's instruction. Equal molar (44 fmol/ μ l) of library samples from the identical amplicons were pooled and sequenced on the NextSeq 550 single read 75 bp high throughput platform at the DKFZ Next Generation Sequencing core facility.

Katherine Kelly (DKFZ, Heidelberg) analyzed miRNA-seq data. The sRNAmapper tool's bowtie aligner was used to align the reads to the hg38 human reference genome and to perform 3' adapter trimming via the Heidelberg Unix Sequence Analysis Resources (HUSAR) GUI. The resulting bam files were used to index via the samtools. Next, using the Bedtools multicov tool, the sequences overlapping with miRbasev22.1 isomiR annotation were counted. miRNA primary transcripts, sequences transcribed from more than one genomic sequence, and lowly expressed sequences with less than 5 median raw read counts in all samples were filtered. Counts from miRNA-level and arm-level were used for differential expression analysis upon DAC treatment via DESeq2 in R version 4.1.0. miRNAs whose false discovery rate (FDR)-adjusted p-value is less than 0.05 and whose absolute(\log_2 (Fold Change)) is more than 1 were considered significant. miRDB, TargetScan, and miRTarbase prediction tools retrieved miRNAs predicted to bind *MNX1* 3'UTR. miRNAs predicted to bind *MNX1* 3'UTR by at least two prediction tools were considered to have a high probability of predicting.

3.17. Protein isolation, quantification, and western blot

Hot lysis buffer was prepared according to [Supplementary Table 5](#). 1 μ l of Benzonase (250 Units/ μ l) was added to 1 ml of hot lysis buffer. A cell pellet containing 1 million frozen GDM-1 cells was resuspended in 20 μ l of hot lysis buffer and incubated on ice for 20 minutes. Next, the samples were transferred into 8-well strips, incubated at 97°C for 10 minutes, and centrifuged at 4000 rpm for 5 minutes. Around 18 μ l of the supernatants were transferred into new 8-well strips and used for quantification.

For quantification, a plate-based bicinchoninic acid (BCA) assay was used. 1.5 μ l of each protein sample was diluted to a final volume of 50 μ l of RNase-free water. Dilutions containing 0, 2.5, 5.0, 10, 15, and 20 grams of bovine serum albumin (BSA) were diluted in 50 μ l of RNase-free water as standards. CuSO₄ was added to BCA solutions in 1:50 dilution, and 200 μ l of this mix was added to each protein or standard sample. Next, the plate was incubated at 32°C for 40

minutes. After the incubation, the absorbance of each protein and the standard sample was measured using a 562 nm wavelength in the plate reader.

4 μ l of 4xloading buffer, 0.4 μ l of 1M DTT, and 0-30 μ g of each protein sample were mixed, and water was added until the final volume was 16 μ l. Next, protein samples were denatured for 10 minutes at 95°C. Samples were loaded in 4-20% TGX gels with 15 combs ([Supplementary Table 15](#)) and run with 80V for 60 minutes using around 1L of running buffer. 1X transfer buffer was used during the transfer buffer. Proteins were transferred using 4 layers of sponges and 2 layers of Whatman filter papers into a polyvinylidene difluoride membrane (PVDF) using 1X transfer buffer after the membrane was activated with 100% methanol for 30 seconds. The transfer took place with 200V for 2 hours in a cold room. After the transfer, the membrane with the proteins was blocked in 15 ml of blocking buffer with 1X TBST and 5% milk powder for 1 hour at room temperature. Primary antibodies ([Supplementary Table 13](#)) were diluted in a blocking buffer prepared with 1X TBST in 1:1000 dilution and then used to incubate the membrane overnight in a cold room. The next day, the membrane was washed 5 times with 1X TBST for 8 minutes and was incubated with a blocking buffer containing the secondary antibodies in 1:500 dilution. ECL buffer was prepared in a 1:1 ratio according to the manufacturer's instructions. After the secondary antibody incubation, the membrane was washed 5 times with 1X TBST for 8 minutes. Then, it was incubated with 1.5 ml of ECL buffer and visualized with an Amersham Imager 680.

The protein bands were quantified using Image Studio 5.2 software. The signals from protein bands incubated with a horseradish peroxidase-coupled antibody against β -actin ([Supplementary Table 13](#)) were used to normalize the signals from bands incubated with other antibodies. β -actin was used as a loading control. Signals from at least 3 biological replicates were used to quantify Western blots.

3.18. Genomic DNA isolation and Infinium Methylation EPIC array

According to the manufacturer's instructions, genomic DNAs (gDNAs) were isolated using a Qiagen Blood and Tissue Extraction kit. Elution was performed using RNase-free water. 1000 ng of gDNA was diluted with RNase-free water until 40 μ l volume. The samples were sequenced using the Infinium Methylation EPIC array at the Genomics and Proteomics Core Facility of DKFZ. IDAT files were downloaded and preprocessed using the RnBeads package in R version 4.1.0 (Muller et al., 2019). SNPs were removed, and normalization was performed using *bmiq* (Teschendorff et al., 2013) and *SeSesame* subtraction methods (W. Zhou et al., 2018). Probes on the X and Y chromosomes were preserved, whereas cross-reactive probes were filtered. The remaining number of CpG probes was 702882. To identify methylation changes on the LINE1 elements, probes located in those regions were filtered and averaged for each replicate. To determine the methylation levels on the *MNX1* gene, Katherine Kelly (DKFZ, Heidelberg) shared the list of CpGs on the *MNX1* gene. I filtered the probes in those regions and averaged for each replicate. A

box plot was drawn, and a t-test was performed using the `ggplot2` package in R version 4.1.0. Figeno was used to show the genes and chromosomal location.

3.19. Patient-derived xenografts (PDX) *in vitro* culture and DAC treatment

10 million PDX cells were thawed in 5 ml of growth media ([Supplementary Table 2](#)), so there are 2 million cells per ml. 2-3 days after thawing, 350,000 PDX cells/ml were seeded, and one day after that, the cells were treated with 500 nM of DAC for 5 days. At the end of the treatment, the cells were washed with 1X DPBS, pelleted, and frozen.

3.20. Bisulfite treatment of genomic DNAs and local deep bisulfite sequencing via MiSeq

Genomic DNAs (gDNAs) extracted from DAC or DMSO-treated GDM-1 cells were treated with bisulfite using an EZ DNA methylation kit per manufacturer instructions, including removing excess M-wash buffer via empty centrifugation. The samples were eluted using 40 μ l of RNase-free water, and the first PCR was performed. 0.7 μ l of 10X Taq polymerase buffer, 0.056 μ l of 10 mM dNTP, 0.056 μ l of Hot Start Taq Polymerase, 1 μ l of 1 μ M reverse and forward primer mix, 3.7 μ l of H₂O ([Supplementary Table 7](#)) and 1.5 μ l of each gDNA samples were mixed. The samples were incubated at 94°C for 15 minutes, in 45 cycles at 95°C for 30 seconds, at 62°C, at 72°C for 60 seconds, and lastly at 72°C for 5 minutes. The concentrations of the PCR products were measured with a Qubit DNA HS kit, and samples were run in agarose gel electrophoresis after 1:4 dilution with RNase-free water. Next, a second PCR with index primers was performed. gDNAs were diluted with RNase-free water to reach 0.5 ng/ μ l and mixed with 12.5 μ l of 2X Kappa 2G Robust Hotstart Readymix, 0.75 μ l of 10 μ M Tn5mCP1n (Forward primer), 0.75 μ l of 10 μ M Tn5mCP1n (either index 6, 8, 10, 16, 19, 20 primers), 0.25 μ l of 10X SYBR green and 9.75 μ l of RNase-free water and put into a 96-well plate. Later, the samples were incubated at 95°C for 3 minutes and 8 cycles at 95°C for 20 seconds, 62°C for 15 seconds, 72°C for 30 seconds, and finally at 72°C for 10 seconds. Later, the samples were collected from the wells and purified with AMPure beads. 330 μ l of 10X Ampure buffer (10 μ l per sample) was mixed with 825 μ l of AMPure beads (25 μ l per sample). 35 μ l of bead mix was added to each sample (25 μ l) in a 1:1,4 ratio, mixed thoroughly, and incubated at room temperature for 10 minutes. Next, the samples were put onto magnetic rocks, and the supernatant was removed after 3-5 minutes. The samples were rinsed with 100 μ l of 80% ethanol 5 times. The lids of the samples were left open and incubated at room temperature for 10 minutes to remove all the ethanol altogether. The PCR products attached to the beads were eluted using 12 μ l of EB buffer. 1 μ l of the eluted samples was used to measure concentration using a Qubit DNA HS kit, and 1 μ l of some samples was used to check the size of the library prepared using a High Sensitivity D1000 tape station kit and machine according to the sample's instruction. Equal molar (50 fmol/ μ l) of library samples from the different amplicons

were pooled and sequenced on the MiSeq Nano V2 (4-color) platform at the DKFZ Next Generation Sequencing core facility.

MiSeq samples were analyzed using tabsat (Pabinger et al., 2016). Raw data was aligned using reference genome hg19 with the Bismark tool (Krueger & Andrews, 2011). The number of methylated and unmethylated cytosines from each amplicon was identified. The methylation frequencies of each amplicon for each of the CpGs were visualized using Figeno (E. Sollier et al., 2024).

3.21. CTCF Antibody-guided chromatin tagmentation followed by sequencing (ACT-seq) sample preparation and analysis

The CTCF ACT-seq protocol was adopted from Dieter Weichenhan's protocol (Mulet-Lazaro et al., 2021; Weichenhan et al., 2023). 3 biological replicates of DAC or DMSO-treated samples were used (n=6). 4.5 μ l of 2X CB buffer (kindly provided by Marion Bähr, DKFZ), 2.5 μ l of pA-Tn5ase.2.3, 0.6 μ l of 50 μ M Tn5ME-A+B load adaptor mix, and 1.4 μ l of H₂O were mixed to prepare pA-Tn5 transposome mix for each sample (OMC mix). OMC mix was prepared for 12 CTCF and 6 IgG ACT-seq samples and incubated at room temperature for 10 minutes. For IgG, 4.8 μ l of 1XCB buffer, 9.6 μ l of 1:10 diluted IgG antibody (1 mg/ml), and 6 μ l of OMC mix were mixed and incubated at room temperature for 30 minutes. For CTCF, 9.6 μ l of 1XCB buffer, 19.2 μ l of anti-CCF antibody, and 12 μ l of OMC mix were mixed and incubated at room temperature for 30 minutes. After that, 250,000 GDM-1 cells were pelleted, resuspended in 100 μ l of ice-cold 1XCB buffer, and incubated on ice for 10 minutes. Next, the samples were centrifuged at 1000g for 5 minutes at 4°C. The supernatant was removed, and the pellet was resuspended in 50 μ l of PBS and 3.1 μ l of 1.6% Formaldehyde (prepared by adding 9 μ l of formaldehyde to 81 μ l of DPBS) ([Supplementary Table 14](#)) and incubated at room temperature for 2 minutes. Permeabilization was stopped by adding 1.5 μ l of 2.5 M glycine. After the centrifugation, the pellet was washed with 100 μ l of 1XCB buffer and resuspended in 100 μ l of 1XCB buffer. Permeabilization was assessed by mixing 5 μ l of permeabilized cells with 5 μ l of trypan blue. After that, 30 μ l of 1XCB buffer was added to the permeabilized cells. 3.2 μ l of IgG pA-TnpOme ab mix and 6.5 μ l of CTCF pA-TnpOme ab mix were added into the Eppendorf tubes. For IgG samples, 25 μ l of permeabilized cells were mixed with 25 μ l of 1XCB buffer and were added to the tubes containing IgG pA-TnpOme ab mix. For CTCF samples, 100 μ l of permeabilized cells were added to the tubes containing the CTCF pA-TnpOme ab mix. The samples were incubated at room temperature for 1 hour. To remove excess transposomes, the samples were washed once with 350 μ l of wash buffer (kindly provided by Marion Bähr, DKFZ). After the centrifugation at 600g for 5 minutes at room temperature, the supernatant was removed. Next, the samples were resuspended in 350 μ l of wash buffer, rotated for 5 minutes at room temperature, and centrifuged at 600g for 5 minutes at room temperature. These steps were repeated 3 times. Next, the samples

were resuspended in 1XCB buffer until their volumes were 100 μ l. 1 μ l of 1M MgCl₂ was added and incubated at 37°C for 30 minutes. Then, 4 μ l of 0.5 M EDTA (pH 8.2), 2 μ l of 10% SDS, and 1 μ l of proteinase K were added and incubated at 55°C for 30 minutes. After that, 550 μ l of PB buffer from the MinElute kit was added, and the samples were transferred to columns and centrifuged at 12000rpm for 1 minute. Next, they were washed with 730 μ l of PE buffer and centrifuged at 12000rpm for 1 minute. After empty centrifugation at 13000rpm for 3 minutes, they were eluted in 24 μ l of elution buffer (EB), which is pre-heated at 65°C.

3.22. CTCF ACT-seq library PCR and purification of CTCF ACT-seq library

The library PCR reaction was performed under real-time conditions, with an addition of 25 μ l of High Fidelity NEB buffer, 2.5 μ l of 10 μ M Tn5mCP1n (Forward primer), 2.5 μ l of 10 μ M Tn5mCP1n index primers ([Supplementary Table 8](#)) and 0.5 μ l of 100X SYBR. The samples were incubated at 72°C for 5 minutes for gap repair, 98°C for 30 seconds for initial melting, and cycles of 98°C for 10 seconds, 63°C for 10 seconds, and 72°C for 10 seconds. Cycling was stopped when the difference between the initial and final fluorescence units was 1-2 for CTCF samples (around 21 cycles) and 5 for IgG (around 12 cycles) samples.

The samples were purified using AMPure beads, diluted 1:1 in AMPure buffer (kindly provided by Marion Bähr, DKFZ) (2.5 M NaCl and 20% PEG 8000). 70 μ l of bead mix was added to each sample (50 μ l) in a 1:1.4 ratio, mixed thoroughly, and incubated at room temperature for 10 minutes. Next, the samples were put onto magnetic rocks, and the supernatant was removed after 3-5 minutes. The samples were rinsed with 100 μ l of 80% ethanol 5 times. The lids of the samples were left open and incubated at room temperature for 10 minutes to remove all the ethanol altogether. The fragments attached to the beads were eluted using 12 μ l of EB buffer. 1 μ l of the eluted samples was used to measure concentration using a Qubit DNA HS kit, and 1 μ l of some samples was used to check the size of the library prepared using a High Sensitivity D1000 tapestation kit and 4150 tapestation machine according to the sample's instruction. Equal molar (16 fmol/ μ l) of library samples from the identical amplicons were pooled and sequenced on the NextSeq 550 paired-end read 75 bp high throughput platform at the DKFZ Next Generation Sequencing core facility.

3.23. Bioinformatics analysis of CTCF ACT-seq

Analysis of the CTCF ACT-seq data was performed by Dieter Weichenhan (Cancer Epigenomics division, DKFZ) as per (Weichenhan et al., 2023). In summary, Adapter and quality were performed via TrimGalore v. 0.4.4 together with Cutadapt v. 1.14 using the non-default parameters "--paired", "--nextera", "--length_1 35", and "--length_2 35". Trimmed reads were mapped against the GRCh37/hg19 reference genome using Bowtie2 v. 2.2.6 with the "--very-sensitive" flag and a maximum insertion length of 2500 bp (Langmead & Salzberg, 2012). SAMtools merge v. 1.5 was

used to merge Aligned reads belonging to the same lane-multiplexed library. Mismatched mappings and alignments with a Phred score of less than 20 were filtered via the SAMtools view. Additionally, Alignments with fragment sizes below 38 bp were removed. The ends of the reads were adjusted to represent the center of the transposition event. Common Workflow Language v. 1.0 implemented fully containerized workflows. During Peak Calling, from MACS v.2.2.6, IgG control was subtracted for input subtraction, and a wrapper script called “callpeaks” provided by Encode was also used.

‘call peaks-derived bed files were used for differential analysis to find the CTCF peaks between the breakpoint in chr6 and the *AH11* region (chr6:135505080-135644755). For downstream analysis, HOMER motif analysis was used using the default parameters to find the motifs binding to the area of interest. Figeno was used to show the results and the genes and chromosomal location.

3.24. 4C-seq library preparation

The first batch of 4C experiments was carried out by Elena Everatt (DFKZ, Heidelberg) using one replicate of DAC, DMSO-treated, and untreated GDM-1 samples. The second batch of 4C experiments, using 3 replicates of DAC or DMSO-treated GDM-1 samples, was performed by Marion Bähr (DFKZ, Heidelberg). In both batches, cells were resuspended in 3ml of DPBS without magnesium and calcium and centrifuged at 600g for 5 minutes at +4°C. The supernatant was removed, dissolved in 5 ml DPBS without magnesium and calcium with 10%FCS, and shaken for 10 minutes at room temperature. Next, 1.42 ml of 1M ice-cold glycine was added, and the samples were incubated on ice and centrifuged at 600g for 12 minutes at +4°C. After removing the supernatant, they were resuspended and incubated in 1 ml of 4C lysis buffer for 5 minutes at room temperature, followed by shaking for 30 minutes at 65°C at 650rpm. The lysis was checked under a light microscope and stopped after 20 minutes of incubation at 65°C. Samples were centrifuged at 1000g at +4°C and washed with 400 µl of DPBS without magnesium and calcium. The pellets were dissolved in 440 µl of H₂O and 60 µl of NEB3.1 buffer and incubated at 55°C. After the addition of 7.5 µl of 20%SDS, the temperature was increased to 60°C and the samples were incubated at 60°C for 3 minutes, followed by shaking at 37°C for 55 minutes at 750rpm. Next, 75 µl of 20% Triton X-100 was added, and the samples were incubated at 37°C for 1 hour. 10 µl of *BgIII* enzyme (100U) was added and incubated with 7 µl of spike-in control overnight at 37°C, which is around 80 ng of BACe3.6 vector (a kind gift from Dieter Weichenhan). 10 µl of *BgIII* enzyme (100U) was added and incubated with 7 µl of spike-in control for 2.5 hours at 37°C. Next, 3 µl of Proteinase-K was added to the samples, and they were shaken for 45 minutes at 65°C at 750 rpm. Next, 1.2% agarose gel was run to check the digestion. After that, 550 µl of the restriction enzyme digested samples were mixed with 5.7 ml of H₂O, 700 µl of 10X ligase buffer, and 15 µl T4 ligase enzyme (400.000U/ml) and incubated overnight at room temperature. 1 µl of *EcoRI* cut BlueScript construct, which has around 100 ng vector per µl, was added to the 50 µl samples. Later, the samples were incubated with 3 µl of Proteinase-K for 45 minutes at 65°C and

run in an agarose gel. In a water bath, 20 μ l of Proteinase K was added to the samples and incubated for 2.5 hours at 65°C for decross-linking. Later, the samples were cool-downed at room temperature for 10 minutes, and 5 μ l of RNase A was added and incubated at 37°C for 30 minutes in a water bath. 770 μ l of 3M sodium acetate pH 5.2 and 7.5 ml of Isoamylalcohol/Phenol/Chloroform with 0.1% 8-Hydroxyquinolin were added. Then, the samples were centrifuged at 6000 rpm for 10 minutes at room temperature. The supernatant was taken, and 2 μ l of glycogen was added with 20 ml of 100% EtOH and incubated on ice for 15 minutes. Later, the samples were centrifuged for 10 minutes at 10°C with 10.000 rpm. The supernatant was removed, and the pellet was dissolved in 3 ml of 80% EtOH and air-dried for 20 minutes at room temperature after the removal of EtOH. The pellet was dissolved in 200 μ l of H₂O. The concentration of DNA was measured with a Qubit HS kit and Qubit 2.0 fluorometer. 200 μ l of the samples (all of the volume) was digested with the addition of 25 μ l of 10X CutSmart buffer, 5 μ l of NlaIII enzyme, and 20 μ l of H₂O. 6 μ l of the mix was mixed with 1 μ l of BlueScript vector, and all samples were incubated overnight at 37°C. Digestion was stopped via incubation at 65°C for 20 minutes. Next, 150 μ l of 10X ligation buffer and 7.5 μ l of T4 ligase were added to the samples, and the volumes were completed until 1.5 ml with H₂O. To 10 μ l of the samples, 0.5 μ l of *Eco*RI digested blue script construct (whose concentration is around 50ng per μ l) was added and run in an agarose gel. Later, 1 μ l of glycogen and 168 μ l of 3M sodium acetate were added, and the mix was distributed to 3 Eppendorf tubes in equal amounts (around 556 μ l). To each 556 μ l, 1.4 ml of 100% EtOH was added, incubated on ice for 30 minutes, and centrifuged for 15 minutes at 10°C with maximum speed. After washing the pellet with 150 μ l of 80% EtOH, removing the EtOH, and airdrying for 10 minutes, three aliquots were pooled in 75 μ l of H₂O. The first PCR was performed using 32.5 μ l of H₂O, 10 μ l of 5X buffer, 1.0 μ l of 10mM dNTP, 2.5 μ l of either *MNX1* or *MYB* viewpoint primers (listed in [Supplementary Table 8](#)), 0.5 μ l of Q5 DNA polymerase and 10 μ l of GC enhancer. The PCR conditions in [Supplementary Table 18](#) were used. Bead purification using HighPrep beads was performed using a 1:5 (60 μ l of beads: 40 μ l of PCR product) ratio. Next, library PCR was carried out using index primers listed in [Supplementary Table 8](#). For the PCR, 12.5 μ l of 2xKapa buffer, 0.75 μ l of forward universal index and reverse index primers with 8, 9, 10, 11, 17, 18, 13, 14, 15, 16, 19, 20, 2.0 μ l of SYBR green and 1 μ l of DNA were mixed. After the PCR, the products were purified using a 1.4:1 ratio and were eluted in 14 μ l of elution buffer. The concentrations were measured using a Qubit HS kit, and the quality of the libraries was assessed using a High Sensitivity D1000 tape station kit and a 4150 tape station machine according to the sample's instructions. Equal molar (25 fmol/ μ l) of library samples from the identical amplicons were pooled and sequenced on the NextSeq 550 paired-end read 75 bp high throughput platform at the DKFZ Next Generation Sequencing core facility.

3.25. 4C-seq analysis

Read files with *Bg*III or *Nla*III restriction enzyme sequences were analyzed using the Pipe4C pipeline (Krijger et al., 2020). The generated bigwig files were used to visualize the interaction via Figeno (E. Sollier et al., 2024).

3.26. Statistical Analysis

GraphPad Prism Software ([Supplementary Table 17](#)) was used to draw the graphs and calculate p values. Unless otherwise stated, all replicates represented in the graphs of this thesis are biological replicates. Unless otherwise noted, a one-tailed paired t-test was used to analyze the data in this thesis from at least 3 different biological replicates, and a p-value of 0.05 was considered significant according to the test results (*p-value \leq 0.05, ** p-value \leq 0.01, *** p-value \leq 0.001). While means are used in the bar graphs, each dot representing the mean of 3 technical replicates from one biological replicate, error bars represent \pm standard deviation (s.d.).

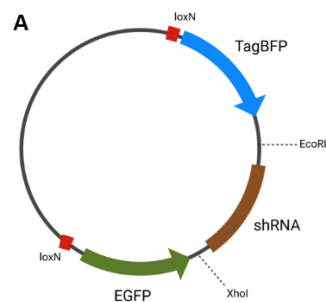
4. Results

4.1. Chapter 1: Epigenetic compound screening in GDM-1

4.1.1. Knockdown of *MNX1*

Premature senescence was observed upon overexpression of potent oncogenes like *BRAF*, *RAS*, *MEK*, and *RAF* (Michaloglou et al., 2005; Serrano et al., 1997; Zhu et al., 1998). In previous studies, *MNX1* was demonstrated to be an oncogene in AML (Waraky et al., 2024), and overexpression of *MNX1* was found to induce a DNA damage response and premature senescence in HSPCs (Ingenhag et al., 2019). Therefore, I hypothesized that the downregulation of *MNX1* would reduce the cell viability of GDM-1, the only AML cell line with *MNX1* expression (Nagel et al., 2005).

To demonstrate this, I used GDM-1 cells transduced with negative control shRNA (shRenilla) or shRNAs targeting different exons of *MNX1* (sh76 and sh82). A blue fluorescent protein (BFP), shRNAs, and green fluorescent protein (GFP) were surrounded by loxN sites, which flip the sequences via Cre activation. Upon 4-Hydroxytamoxifen (TAM)-mediated Cre activation, the BFP signal should disappear, and GFP and shRNA expression should be induced (Figure 4A). I treated the cells with TAM for 48 hours and prepared them for fluorescence-activated cell sorting (FACS). I observed that there are still BFP-positive (BFP+) cells after TAM induction, so I sorted BFP(+) and GFP (+) GDM-1 cells (Figure 4B). Western blot analysis using the proteins isolated from the sorted cells revealed a statistically significant downregulation of *MNX1* protein levels (Figure 4C) (p-value = 0.0062 for sh76 and p-value <0.0001 for sh82). The knockdown of *MNX1* resulted in statistically significant reduced viability of GDM-1 (p-value = 0.0021 for sh76 and p-value = 0.0135 for sh82) (Figure 4D).



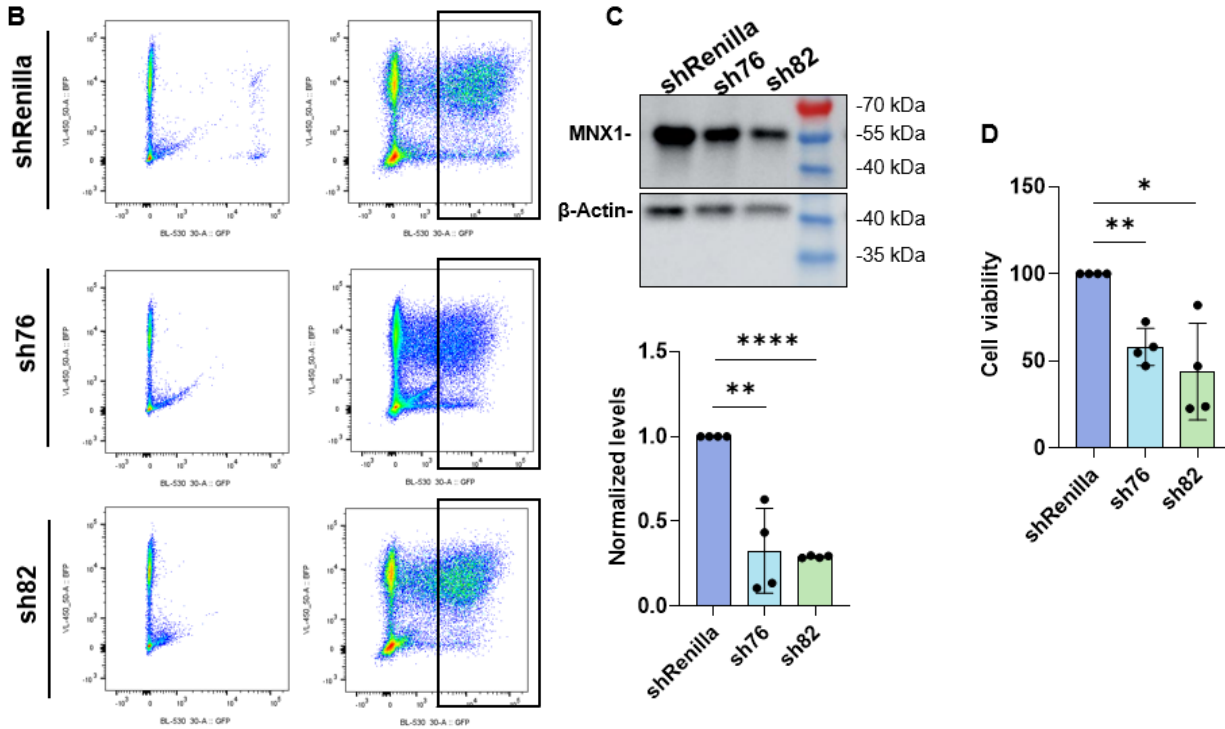


Figure 4: Effects of *MNX1* knockdown in GDM-1.

A. Representation of the vectors used to knockdown *MNX1*. **B.** FACS sorted GFP and BFP positive GDM-1 cells after 48 hours of TAM induction, shown in the black squares. The graphs on the left show the signals before TAM induction, and those on the right show the signals after TAM induction. **C.** A representative image of a Western blot analysis was performed on the sorted cells in Figure 1B. The bottom bar graph shows the quantification of knockdown in the sorted cells. **D.** Cell viability after 168 hours of TAM induction was measured and normalized to shScramble. A one-tailed t-test was used to analyze the data, and a p-value less than or equal to 0.05 was considered significant according to the test results. (* p-value \leq 0.05, **p-value \leq 0.01, *** p-value \leq 0.001).

From these experiments, I concluded that the viability of GDM-1 depends on *MNX1* expression. The next step was to treat GDM-1 cells with epigenetic compounds and measure cell viability. The hypothesis was that the compound that induces cell death could achieve this via downregulation of *MNX1*.

4.1.2. Epigenetic compound screening and dose-response curves of the selected compounds

Hijacked enhancers from the *AH11/MYB* region drive the expression of *MNX1* in GDM-1 (Weichenhan et al., 2023). Treatment with sinefungin, a SAM inhibitor, an epigenetic compound,

prevented MNX1-driven AML leukemogenesis (Waraky et al., 2024). These findings highlighted the fact that epigenetic mechanisms might regulate *MNX1* expression. Therefore, it was hypothesized that *MNX1* expression might be downregulated using the treatment of GDM-1 with epigenetic compounds.

To investigate this, I performed an epigenetic compound screening using a library of 174 different epigenetic compounds in the GDM-1 cell line (Supplementary Table 3). I used signals from media-only wells as negative controls and those from DMSO-treated wells for normalization. I identified the top 50 epigenetic compounds that decreased cell viability by more than 33% (Figure 5A). I selected 10 of these compounds for further analysis based on the viability results, commercial availability, and different mechanisms of action. Using a non-linear fitting formula (3.3 Selection of the compounds from the screening and dose-response curve (DRC) analysis) in GDM-1 (Figure 5B), I calculated the IC₅₀ and IC₈₀ concentrations of these 10 epigenetic compounds.

I showed that the cells seem resistant to higher concentrations than the IC₅₀ of GSK591 and GSK-LSD1. The IC₅₀ concentration for both compounds is 1.5 μM (Figure 5B). I observed that the IC₅₀ concentrations of DAC and ACBI-1 are lower than those of the other compounds (Figure 5B).

I concluded that epigenetic compound screening revealed valuable hits. Those hits can be further studied to assess the effect on *MNX1* expression. Therefore, I treated GDM-1 cells with IC₈₀ concentrations of those compounds for 48 hours and then evaluated *MNX1* expression via qPCR (Figure 6C, Supplementary Table 4).

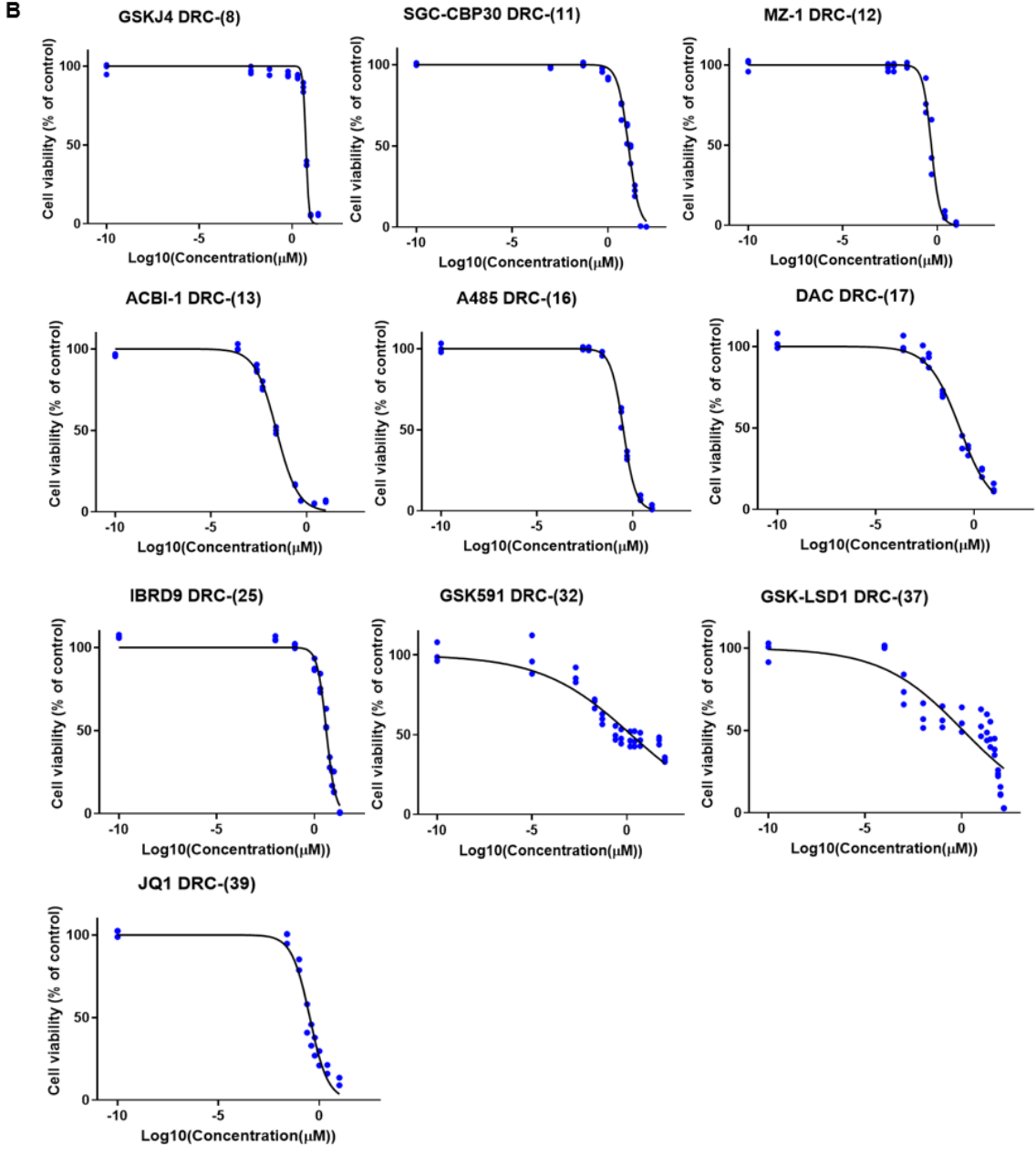
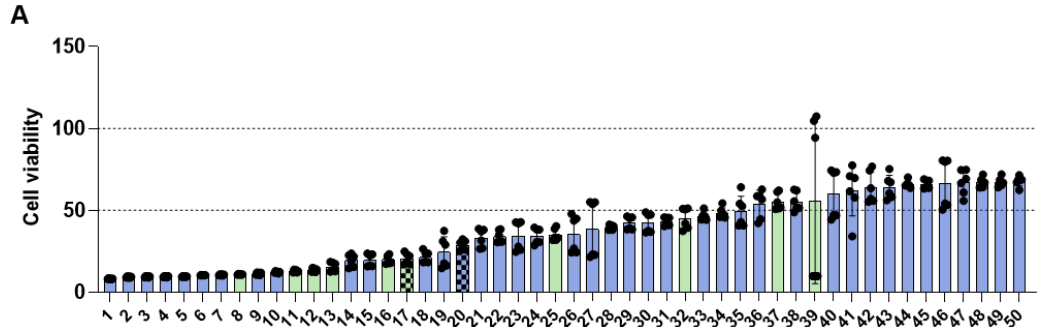


Figure 5: Epigenetic compound screening and dose-response curves of the 10 epigenetic compounds.

A. Bar graph shows the mean cell viability of the samples treated with the top 50 compounds. The results were normalized to DMSO control and showed as a single point. Green bars indicate the compounds selected for further analysis, and checkered bars indicate the treatments with HMAs (n=6, 2 biological replicates with three technical replicates in each). Numbers 1-50 represent the compounds in the list ([Supplementary Table 3](#)). **B.** The A485, MZ-1, ACBI-1, GSK591, GSK-J4, GSK-LSD1, IBRD9, JQ1, SGC-CBP30, DAC dose-response curves (DRCs). Numbers next to the compound's name represent their positions in the viability result.

4.1.3. Expression of *MNX1* upon the treatment of selected compounds

The questions left from the previous findings are whether *MNX1* expression influences the treatment response against these compounds and whether the treatments with 10 epigenetic compounds change *MNX1* expression. Therefore, I treated GDM-1 cells mainly with IC₈₀ concentrations of 10 epigenetic compounds ([Supplementary Table 4](#)) except for GSK-LSD1 and GSK-591. The cells seem resistant to higher concentrations than the IC₅₀ of GSK591 and GSK-LSD1, so the IC₅₀ concentration was used.

Upon the treatment with 9 epigenetic compounds, the viabilities of three *MNX1*(-) cell lines, HL60, OCIAML3, and MOLM13, which do not express *MNX1*, revealed that MOLM13 is sensitive to all epigenetic compound treatments. In contrast, the viability of HL60 was less affected than that of GDM-1 except for MZ-1 treatment ([Figure 6A](#)). The data indicated nearly half as much cell death in the *MNX1*(-) cell lines as in GDM-1 following DAC treatment ([Figure 6B](#)). This led me to speculate that DAC might affect *MNX1* expression.

I examined by qRT-PCR the effect of 10 compounds on *MNX1* expression in GDM-1 ([Supplementary Table 4, Figure 6C](#)). Only DAC treatment resulted in a statistically significant reduction (p-value = 0.0308) ([Figure 6C, D](#)). The drug that resulted in the second most robust reduction of *MNX1* expression was the BET inhibitor JQ1; however, this effect was not statistically significant (p-value = 0.3811), even with an increased number of replicates (i.e., in 6 biological replicates) (p-value = 0.1218) ([Figure 6E](#)).

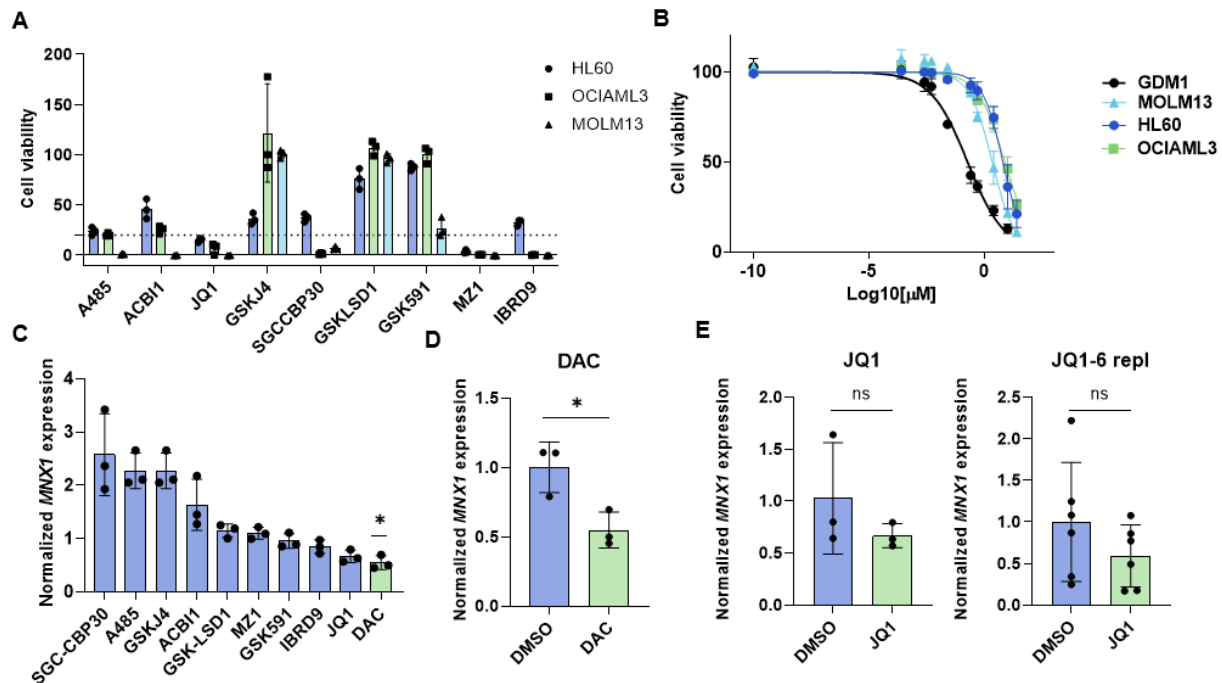


Figure 6: Treatments with 10 selected epigenetic compounds.

A. Mean viability results of MNX1 (-) AML cell lines treated with epigenetic compounds except for DAC using the concentrations listed in [Supplementary Table 4](#). The dashed line represents the viability results obtained from GDM-1 treatments. **B.** The DAC dose-response curve of GDM-1, HL60, MOLM13, and OCIAML3. **C.** Mean of *MNX1* mRNA expression levels of GDM-1 upon the treatment with the 10 epigenetic compounds. **D.** Mean of *MNX1* mRNA expression levels of GDM-1 upon the treatment with DAC. **E.** Mean of *MNX1* mRNA expression levels of GDM-1 upon the treatment with JQ1 on the two graphs with different biological replicate numbers.

A two-tailed t-test was used to analyze the data in Figures 6C, D, and E, and a p-value less than or equal to 0.05 was considered significant according to the test results. (* p-value ≤ 0.05 , **p-value ≤ 0.01 , *** p-value ≤ 0.001).

In summary, DAC is the only compound that induced a sharp decrease in GDM-1 cell viability, which the downregulation of *MNX1* RNA could explain. However, further validations were needed to prove that the DAC treatment worked.

4.2. Chapter 2: Effect of DAC treatment in GDM-1 cells

4.2.1. Hypomethylation upon DAC treatment

It is estimated that around 25% of DNA hypermethylation in the human genome happens in LINE-1 elements, which comprise around 17% of the human genome (Ewing et al., 2020; Yang et al., 2004). Therefore, analysis of LINE-1 methylation levels is commonly used to indicate global DNA methylation levels (Baba et al., 2018; Yang et al., 2004). I assessed the effect of DAC treatment by examining the methylation of LINE-1 elements using the Infinium Methylation EPIC array (Moran et al., 2016; Noguera-Castells et al., 2023). Upon treatment, the array showed a statistically significant hypomethylation of LINE-1 elements (p -value = 0.0005), confirming that DAC treatment results in the expected genome-wide hypomethylation (Figure 7A). RNA-seq data revealed upregulation of the genes previously described to be upregulated upon hypomethylating agent (HMA) treatment in the NCI-H1299 cell line (Goyal et al., 2023). Those genes were enriched among upregulated genes upon 120h long DAC treatment (Figure 7B). EPIC array analysis also showed that the *MNX1* 3'UTR regions (chr7: 156801419–156803578) and the rest of the *MNX1* region (chr7: 156797257–156801700) became hypomethylated upon DAC treatment (Figure 7C, D).

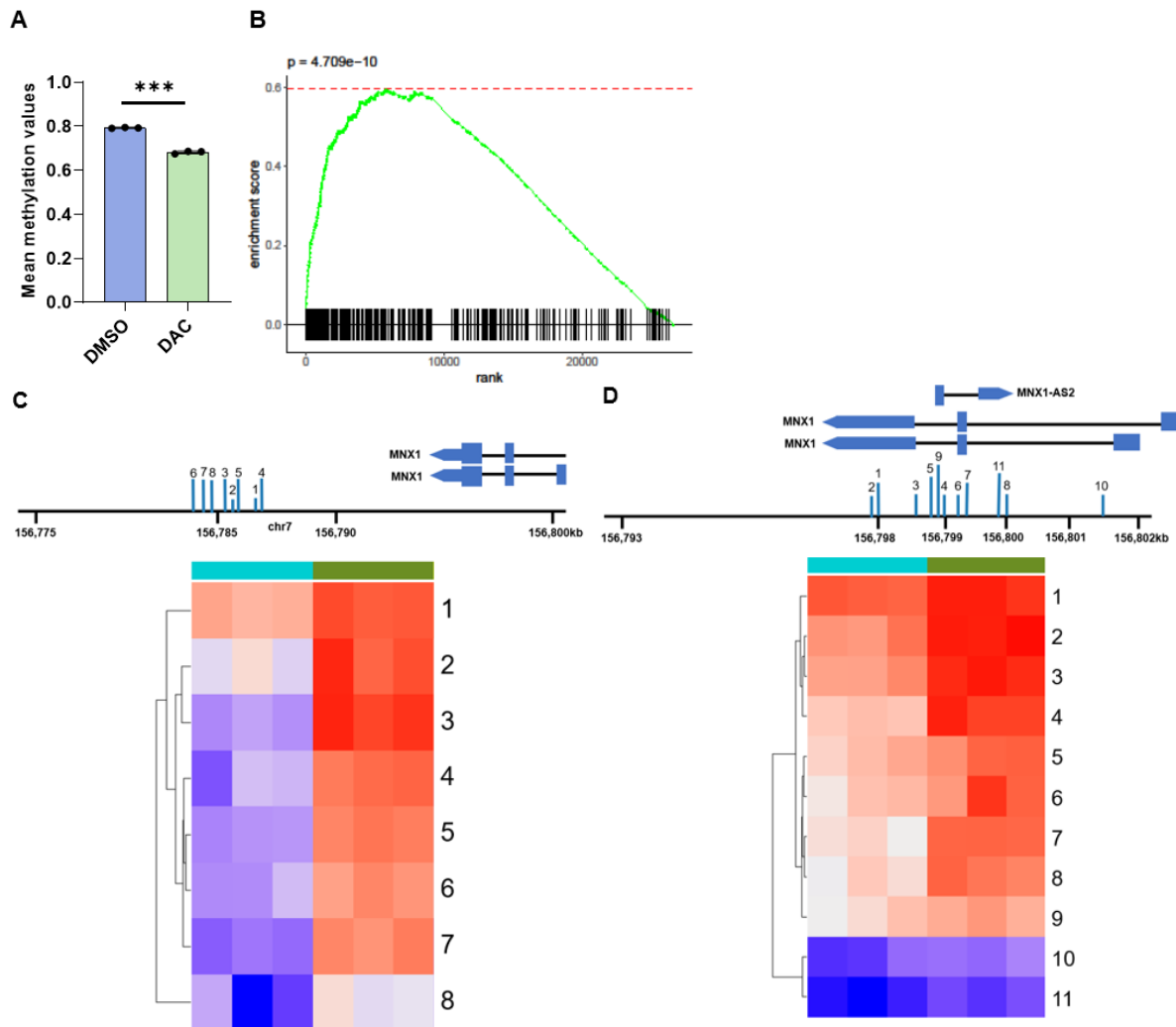


Figure 7: Methylation changes upon DAC treatment.

A. Mean methylation levels of each CpG overlapping with LINE-1 regions. **B.** Gene set enrichment analysis of GDM-1 RNA-seq data using the genes known to be upregulated upon HMA treatment in the NCI-H1299 cell line (Goyal et al., 2023). **C.** Heatmap showing the methylation difference between DAC and DMSO treated samples on the promoter region and around the 3'UTR of *MNX1*. **D.** Heatmap showing the methylation difference between DAC and DMSO treated samples on the promoter region and around the gene body region of *MNX1*. Each row represents the mean methylation of each CpG from one biological replicate. Light blue and green columns show the mean methylation of each CpG after 120 hours of either DAC or DMSO treatment. A one-tailed t-test was used to analyze the data in Figure 7A, and a p-value less than or equal to 0.05 was considered significant according to the test results. (* p-value \leq 0.05, **p-value \leq 0.01, *** p-value \leq 0.001).

I concluded that DAC treatment led to genome-wide hypomethylation, as expected.

4.2.2. Effect of DAC treatment on *MNX1* RNA and protein expression

Inhibition of BRD/BET complexes has been shown to disrupt the hijacked enhancer-promoter interactions generated upon t(8;12), which drives the *A2M* gene expression in gliomas (Wang et al., 2021). Furthermore, HMA treatment or triple knockdown of DNMT3A, 3B, and DNMT1 weakened AML-specific loops, altering 3D genome organization and changing the expression of AML-specific genes (Xu et al., 2022). By demonstrating the effects of epigenetic inhibitors on enhancer-promoter interactions and 3D genome organization, these studies highlight the potential utility of epigenetic compounds in cancer therapy.

Enhancers from the *AHI/MYB* region juxtaposed to the *MNX1* promoter drive *MNX1* expression in GDM-1. To study the effect of DAC treatment on the expression of *MNX1*, I isolated RNAs from 120-hour DAC or DMSO-treated GDM-1 cells. The DKFZ NGS core facility performed the library preparation and sequencing. As expected, I observed a significant downregulation of *MNX1* upon DAC treatment (Figure 8A). Upon DAC treatment, cancer-testis antigens (CTAs) are known to be activated (Srivastava et al., 2016; Zhong et al., 2022). RNA-seq analysis on DAC-treated GDM-1 cells showed that CTAs such as *MAEL*, *MAGEB2*, *PAGE2B*, *MAGEA3*, *MAGEB1*, and *FMR1NB* are activated upon DAC treatment, as expected (Figure 8A). I observed significant downregulation of *MNX1* expression after as early as 48 hours of treatment (p-value = 0.0096) (Figure 8B).

MNX1-AS1 is a lncRNA, an antisense RNA to *MNX1*, but its expression is known to be positively correlated with *MNX1* expression (Li et al., 2020). Although its expression is lower than that of *MNX1* in GDM-1, I found that *MNX1-AS1* expression is also reduced upon DAC treatment (p-

value = 0.0056 for 48 h treatment and p-value = 0.0151 for 120 h treatment) (Figure 8C). I could not detect any *MNX1-AS2* and *MNX1* variant 2 (*MNX1V2*) expression via qPCR (Figure not shown). However, RNA-seq analysis showed increased expression of *MNX1V2* after 48h treatment (p-value = 0.0085), no change after 120h treatment (p-value = 0.4642), and only very low expression of *MNX1-AS2* (transcript per million [TPM] is less than 10 for DMSO and DAC treated samples) (Figure 8D). Upon DAC treatment, the reduction in *MNX1* RNA levels was accompanied by a statistically significant decrease in *MNX1* protein levels (Figure 8E).

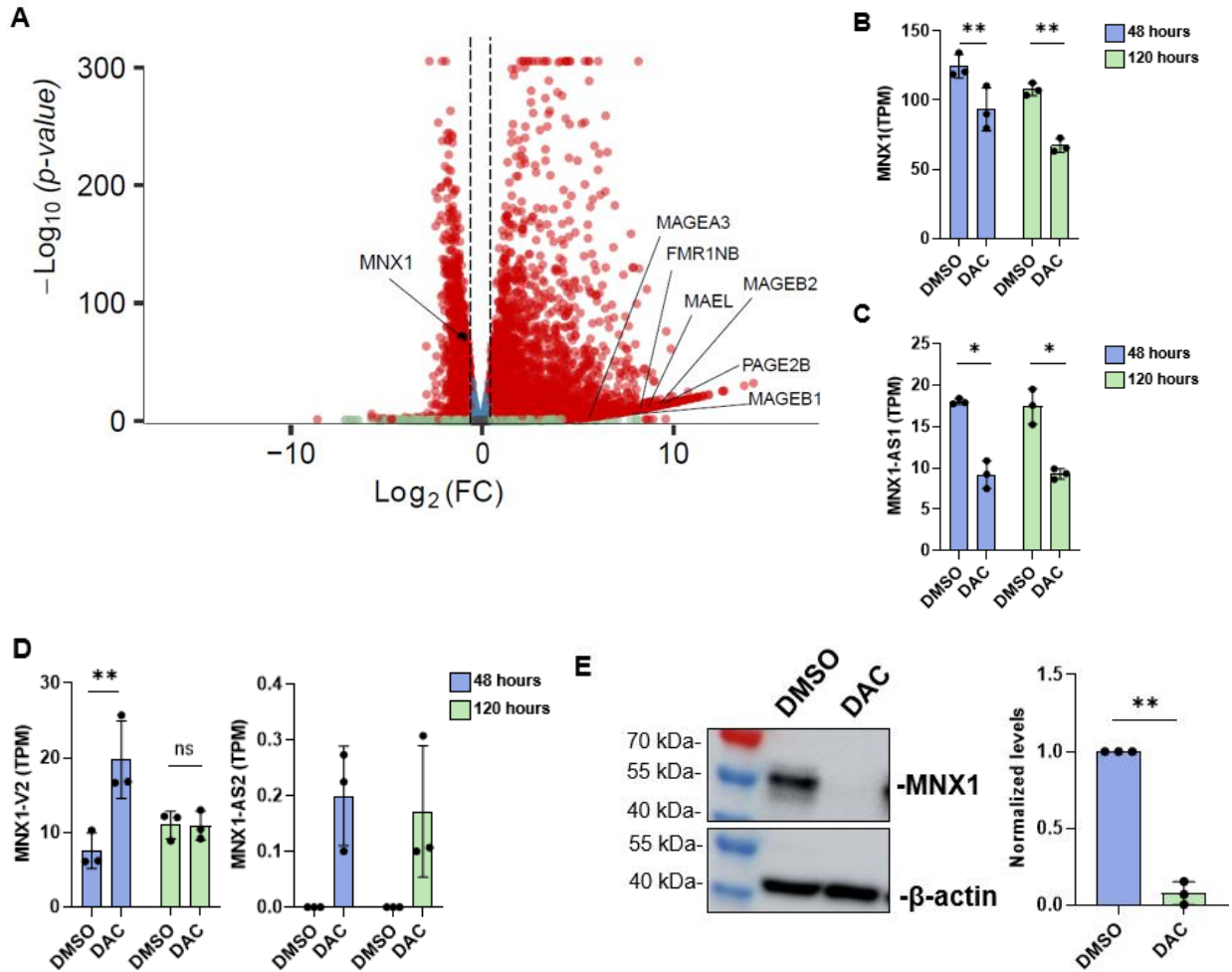


Figure 8: Changes in transcriptomics upon DAC treatment.

A. Volcano plot showing the differentially expressed genes during DAC treatment. Red dots represent the expression of genes whose FDR-adjusted p-value is less than 0.05 and whose absolute($\log_2(\text{Fold change})$) is more than 1. **B.** Bar graph shows *MNX1* TPM from 48 or 120 hours of DAC vs. DMSO-treated samples. **C.** Bar graph shows *MNX1-AS1* TPM from 48 or 120 hours of DAC vs. DMSO-treated samples. **D.** Bar graphs show *MNX1-V2* TPM (on the left) and *MNX1-AS2* (on the right) from 48 or 120 hours of DAC vs. DMSO-treated samples. **E.** A representative image of a Western blot analysis was performed on 120 h DAC vs DMSO-treated GDM-1 cells. The bar plot on the right shows the quantification of the treatments in 3 biological replicates. A one-tailed t-test was used to analyze the data, and a p-value less than or equal to 0.05 was considered significant according to the test results. (* p-value \leq 0.05, **p-value \leq 0.01, *** p-value \leq 0.001).

All these results validated that DAC treatment resulted in significant downregulation of *MNX1*. The question remains: What are the mechanisms behind DAC-mediated *MNX1* downregulation?

4.3. Chapter 3: Possible miRNA-independent mechanisms downregulating *MNX1* upon DAC treatment

DAC treatment reduced *MNX1* protein expression in GDM-1 by more than 70%. A number of hypotheses were put forward to elucidate the mechanisms underlying this reduction. The first hypothesis suggests that by modifying topologically associating domains (TADs), DAC treatment may alter TADs by demethylating not-accessible CTCF sites and disrupting the enhancer-promoter interaction, thereby reducing oncogenic *MNX1* overexpression. The second hypothesis posits that CAT7 and PRC1 recruitment to the *MNX1* promoter region could explain *MNX1* downregulation. The third hypothesis proposes that epigenetically silenced miRNAs predicted to target *MNX1* RNA may be upregulated by DAC treatment.

4.3.1. Hypothesis 1: By altering TADs, DAC treatment may disrupt the enhancer-promoter interaction, enabling oncogenic *MNX1* overexpression.

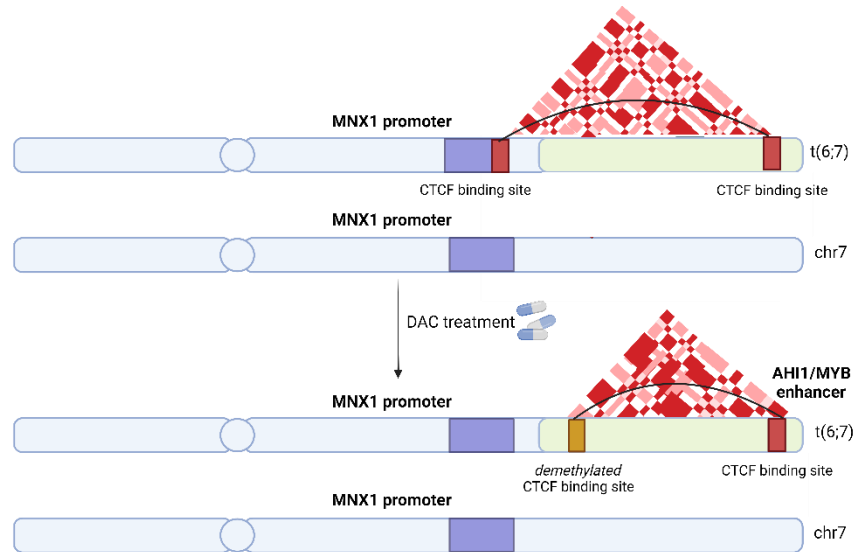


Figure 9: The illustration of the first hypothesis tested.



Translocation (6;7) leads to a TAD structure with CTCF boundaries on the *MNX1* promoter and another TAD in the translocated part of chromosome 6. However, this TAD structure might be disrupted after DAC treatment upon demethylation-mediated accessible CTCF boundaries.

Hypomethylation, for example, upon 5-AZA treatment, affected the CTCF-binding pattern in AML (Mujahed et al., 2020). Additionally, inhibition of DNA methylation increased the expression of genes regulated by CTCF (Damaschke et al., 2020). These studies highlight the interplay between DNA methylation and CTCF binding. This led us to hypothesize that DAC treatment may alter TADs by demethylation of previously blocked CTCF binding sites, disrupting the enhancer-promoter interaction driving *MNX1* expression (Figure 9).

To test this, I performed CTCF antibody-guided chromatin tagmentation (ACT-seq) and submitted the library for sequencing to the DKFZ NGS core facility. CTCF ACT-seq data uncovered a higher number of CTCF peaks genome-wide after DAC treatment; however, their peak intensities were lower than those in DMSO-treated samples.

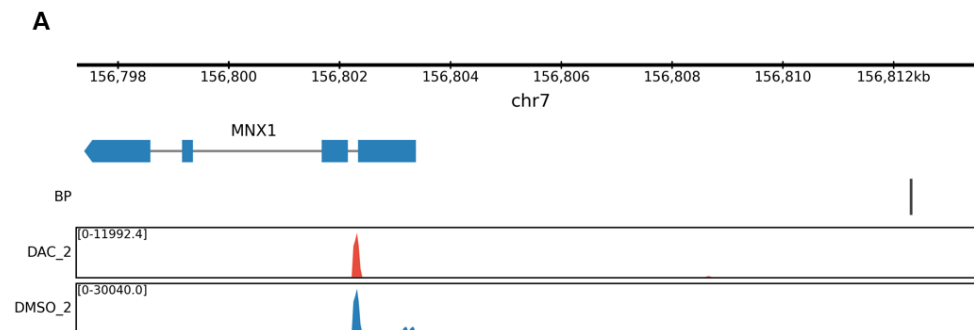
Table 2: The two highest-ranked known results of HOMER motif enrichment.

The first column represents the known motif, the second shows the motif's name, and the rest shows the p-values of replicates.

Motif	Motif's name	DMSO replicate 1 (p-value)	DAC replicate 1 (p-value)	DMSO replicate 2 (p-value)	DAC replicate 2 (p-value)
	CTCF(Zf)/CD4+-CTCF-ChIP-seq(Barski_et_al.)/Homer	1e-288	1e-218	1e-194	1e-546
	BORIS(Zf)/K562-CTCFL-ChIP-Seq(GSE32465)/Homer	1e-204	1e-149	1e-148	1e-371

The motif enrichments were analyzed using HOMER software from 2 biological replicates of DAC and DMSO-treated ACT-seq results (Table 2). These HOMER analysis results confirmed that the CTCF peaks indicate the enrichment for CTCF binding.

Consistent with previous in-house CTCF ACT-seq results, an expected CTCF peak appeared on the promoter region of *MNX1* in all replicates of DAC and DMSO-treated samples, proving that CTCF ACT-seq worked (Figure 10A). After differential peak calling, 5 CTCF peaks appeared in all DAC samples between the breakpoint of t(6;7) and the putative *AH11/MYB* enhancers, which drive *MNX1* expression. However, no CTCF motif enrichment was found overlapping with these peaks using HOMER software (Figure 10B).



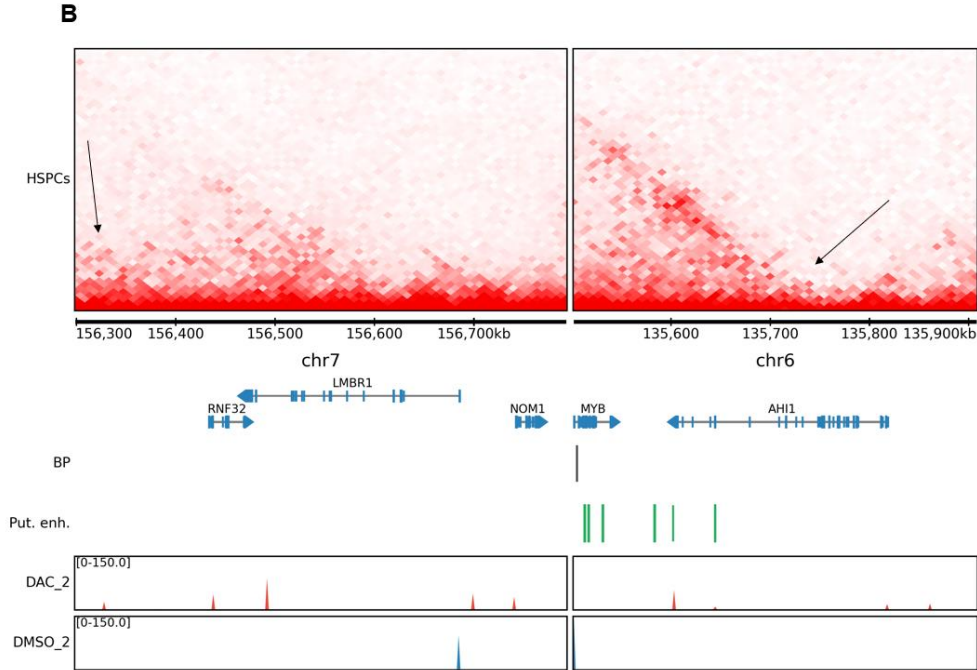


Figure 10: Representation of CTCF ACT-seq results.

A. Each lane represents the second replicate of CTCF ACT-seq peaks on the *MNX1* gene. **B.** The graph at the top depicts HSPCs HiC data (Weichenhan et al., 2024). Arrows demonstrate a possible TAD structure, including the *AHI/MYB* enhancers and *MNX1* promoter, responsible for *MNX1* expression in GDM-1. Below, each lane represents the second replicate of CTCF ACT-seq peaks around the *MNX1* gene and *AHI/MYB* region. BP depicts the breakpoint of t(6;7).

TAD structures are highly conserved among mammalian species and allow enhancer-promoter interactions within the same TAD structure (Okhovat et al., 2023). Thus, disrupting the TAD structure could break the enhancer-promoter interaction responsible for *MNX1* expression. To investigate this, I first used the Hi-C dataset of ChiPSC22 (induced pluripotent stem cells) differentiated to HSPCs (Weichenhan et al., 2024) to assess the TAD structures driving *MNX1* expression (Figure 10B). The findings from all DAC-treated replicates revealed that 5 potential CTCF binding sites became accessible upon DAC. The appearance of those newly accessible CTCF peaks may suggest the formation of new TAD boundaries for *de novo* TAD structures. This could potentially lead to excluding the *AHI/MYB* enhancer(s) or *MNX1* promoter from the TAD structure. To test whether the interaction between *AHI/MYB* enhancer(s) and *MNX1* promoter is preserved upon DAC treatment, 4C-seq experiments using 1 biological replicate of DAC, DMSO-treated, and untreated GDM-1 samples were performed.

Previously, we showed an interaction between the *MYB/AHI1* region and *MNX1* promoter when we used the *MNX1* region as a viewpoint (Paper_WT in Figure 11) (Weichenhan et al., 2023). The findings from 4C-seq revealed that the interactions between the *MNX1* promoter and

MYB/AHI1 region were preserved in DAC, DMSO-treated, and untreated (WT) samples, which are represented as green peaks when the *MNX1* promoter is used as a viewpoint. This suggests that DAC does not interfere with the interaction of *MNX1* promoter and enhancers from the *AHI1/MYB* region (Figure 11). Next, the 4C-seq experiment using 3 further biological replicates of DAC and DMSO-treated GDM-1 samples was performed to consolidate the data of one biological replicate. The new 4C-seq data identified that when the *MNX1* promoter is used as a viewpoint, only DMSO replicate number 1 showed an interaction with the *AHI1/MYB* region. Unfortunately, this 4C-seq experiment uncovered only a few reads (Figure 11). The number of reads and whole genomic interactions from this second 4C-seq experiment did not show interactions with regions other than the viewpoint (Supplementary Table 19).

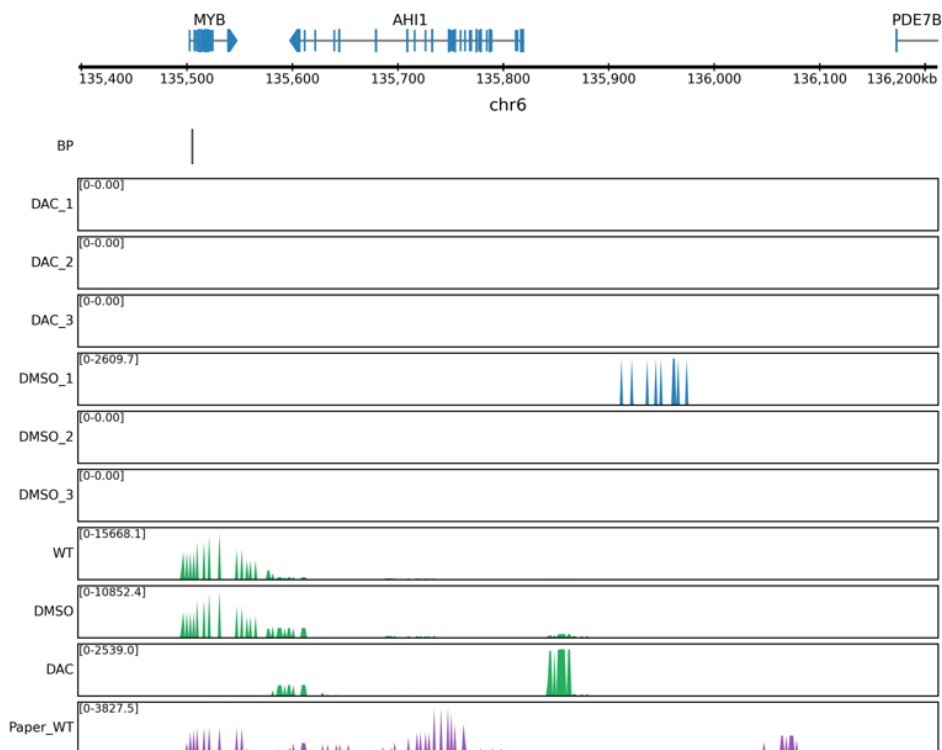


Figure 11: Representation of 4C-seq results when *MNX1* viewpoint is used.

Sequencing reads from the *AHI1/MYB* region when the *MNX1* viewpoint was used. Each blue line represents the sequencing reads from the second 4C-seq experiment using DAC or DMSO-treated replicates, whereas each green line represents the previously prepared samples. BP depicts the breakpoint of t(6;7).

Based on CTCF ACT-seq and 4C-seq data from the first biological replicate, I rejected the hypothesis that DAC treatment may disrupt the enhancer-promoter interaction driving *MNX1* expression via demethylating not-accessible CTCF sites.

4.3.2. Hypothesis 2: CAT7 and PRC1 recruitment to the *MNX1* promoter region could explain the observed *MNX1* downregulation.

The second hypothesis was that the downregulation of *MNX1* may be explained by the recruitment of CAT7 and PRC1 to the *MNX1* promoter region.

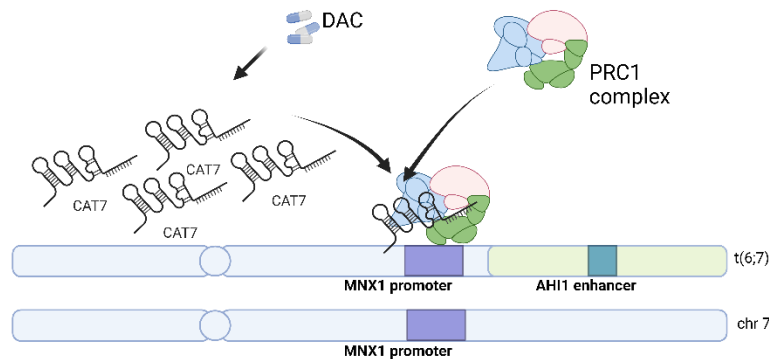


Figure 12: The illustration of the second hypothesis tested.

DAC treatment might upregulate CAT7, and upregulated CAT7 can be recruited to the *MNX1* promoter, enabling recruitment of the PRC1 complex, which is responsible for forming the compacted chromatin.

PRCs are responsible for compacting the genome and repressing transcription and are regulated by lncRNAs in several ways (Trotman et al., 2021). One mechanism, described in the case of CAT7 lncRNA, is the recruitment of PRC1 to the promoter region of *MNX1*. In this scenario, *MNX1* expression in neurons was increased upon knockdown of CAT7 lncRNA, which recruits the PRC1 complex to the promoter region of *MNX1* (Ray et al., 2016). Therefore, to test the hypothesis that DAC treatment of GDM-1 may activate CAT7, thus enabling the recruitment of PRC1 to the *MNX1* promoter and silencing the gene (Figure 12), I assessed the expression of CAT7 upon DAC treatment.

CAT7 is located on chromosome 7 between 156,309,438 and 156,310,990 (Ray et al., 2016). I analyzed transcription levels in this region using our previously generated RNA-seq data, which revealed that CAT7 is not expressed either in DAC-treated (48h or 120h) or DMSO-treated (48h or 120h) conditions (Figure not shown). For confirmation, I assessed the CAT7 expression via qPCR. However, I obtained no Ct values, so I could not detect any CAT7 expression via qPCR. I validated via Sanger sequencing that the qPCR primers are specifically amplifying the CAT7 region (Supplementary Figure 1).

RNA-seq, qPCR, and sequencing data showed that CAT7 is not expressed in DMSO or DAC-treated GDM-1 cells, so this hypothesis was also rejected.

4.4. Chapter 4: miRNA-dependent mechanisms behind *MNX1* downregulation upon DAC treatment

DAC treatment is known to result in the upregulation of miRNAs, including some tumor-suppressor miRNAs (Tanaka et al., 2011), which can lead to reduced expression of oncogenes (Cao et al., 2020). MiRNAs can also regulate *MNX1*, an oncogene in AML (Waraky et al., 2024); for example, miR-200a and miR-141-3p bind to *MNX1* RNA, resulting in its degradation (Chen et al., 2020; Mu et al., 2016). This background led us to hypothesize that epigenetically silenced miRNA(s), upregulated upon DAC treatment, may target *MNX1* (Figure 13).

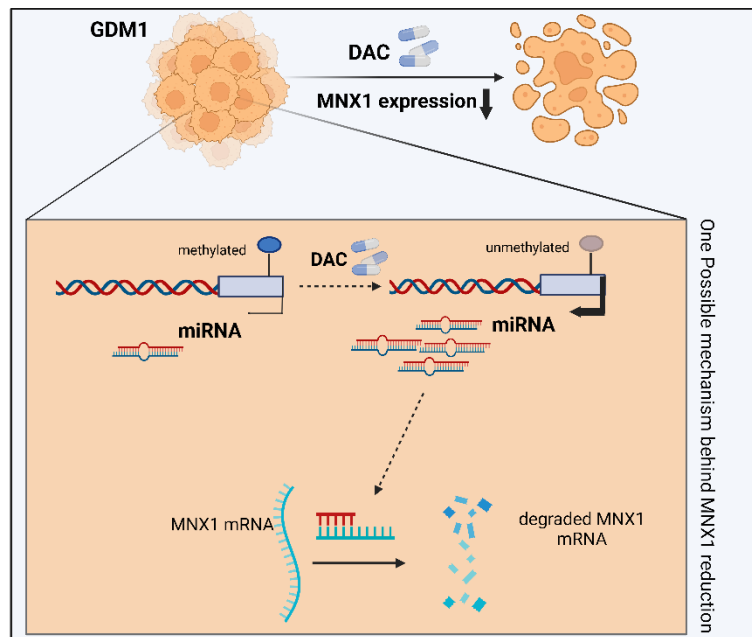


Figure 13: The illustration of the third hypothesis tested.

DAC treatment might hypomethylate the promoter region of miRNA(s), which binds to *MNX1* 3'UTR and results in degradation. This might reduce *MNX1* expression and the viability of *MNX1*-dependent cells.

4.4.1. miRNA-seq results

qPCR, microarrays, and NGS are the three most common techniques for miRNA profiling. Although microarrays cover the most commonly known miRNAs, NGS-based techniques such as small RNA-seq allow the identification of novel miRNAs, their isomiRs, and genome-wide miRNA profiling (Benesova et al., 2021).

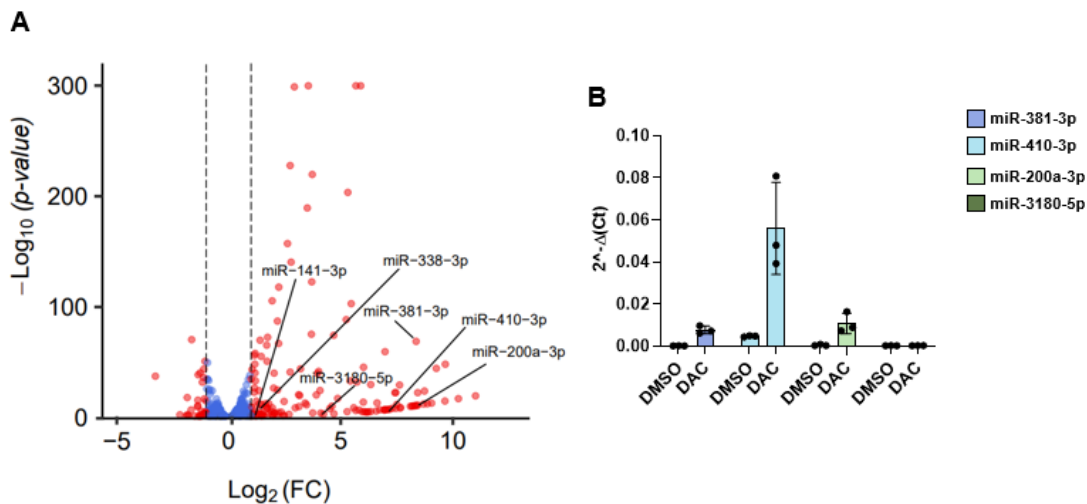
I performed a miRNA-seq and submitted the library to the NGS core facility (DKFZ, Heidelberg). MiRNA-seq revealed significant upregulation of 6 miRNAs predicted to target the *MNX1* 3'UTR

in at least two tested miRNA prediction tools, TargetScan, miRDB, and miRTarBase (Figure 14A). These miRNAs are miR-381-3p, miR-338-3p, miR-410-3p, miR-200a-3p, miR-141-39, and miR-3180-5p. Of these, I selected miRNAs that were not expressed in DMSO-treated but expressed in DAC-treated conditions for further analysis (Table 3).

qPCR data confirmed the upregulation of miR-381-3p, miR-410-3p, and miR-200a-3p. I could detect the expression of miR-3180-5p, but it is unchanged upon DAC treatment (Figure 14B, Table 3). Upon overexpressing miR-200a-3p individually (5 nM) or all three miRNAs in a mix (1.67 nM of each), Western blot analysis showed a statistically significant reduction in MNX1 protein levels (p-value = 0.0061) (Figure 14C). When I increased the concentration of miR-200a-3p mimic to 10nM, I observed that MNX1 protein levels were reduced by more than 70 percent, similar to that was observed upon DAC treatment (Figure 14D) (p-value = 0.0091).

Table 3: The list of miRNAs predicted to target *MNX1* 3'UTR and get upregulated upon DAC treatment.

miRNA	DMSO expression	<i>In vitro</i> validation	p-value
miR-381-3p	Not expressed	Validated	0.0095
miR-410-3p	Not expressed	Validated	0.0276
miR-200a-3p	Not expressed	Validated	0.0350
miR-3180-5p	Not expressed	Not validated	0.2614
miR-338-3p	Expressed		
miR-141-3p	Expressed		



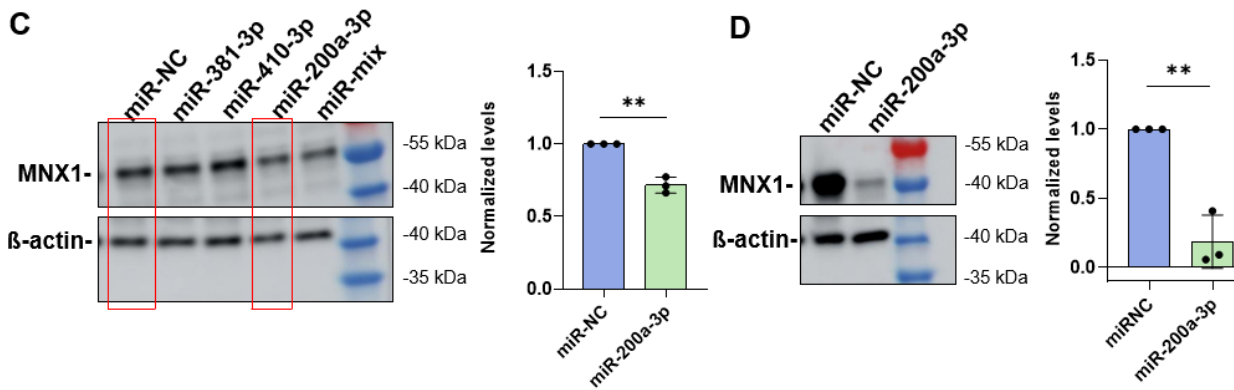


Figure 14: Changes in miRNA transcriptomics upon DAC treatment.

A. Volcano plot shows the differentially expressed miRNAs during DAC treatment. Red dots represent the expression of miRNAs whose FDR-adjusted p-value is less than 0.05 and whose absolute($\log_2(\text{Fold Change})$) is more than 1. **B.** Bar plot shows the mean expression of 4 miRNAs using the same samples submitted for miRNA-seq. **C.** A representative image of a Western blot analysis performed on either individual (5 nM) or a mixture of miRNAs (1.6 nM of each) overexpressed GDM-1 cells. The red squares emphasize MNX1 and β -actin protein levels in miRNA negative control (miR-NC) and miR-200a-3p overexpressed samples. The bar plot on the right shows the quantification of the treatments in 3 biological replicates. **D.** A representative image of a Western blot analysis performed on 10 nM miRNA-NC or miR-200a-3p overexpressed GDM-1 cells. The bar plot on the right shows the quantification of the treatments in 3 biological replicates. A one-tailed t-test was used to analyze the data, and a p-value less than or equal to 0.05 was considered significant according to the test results. (* p-value ≤ 0.05 , **p-value ≤ 0.01 , *** p-value ≤ 0.001).

Luciferase assay data revealed a statistically significant signal reduction in the HEK293T cells, transfected with the *MNX1* 3'UTR LUC cassette and miR-200a-3p mimic, as compared to those transfected with miR-NC mimic (a miRNA mimic targeting none of the miRNAs, miRNA negative controls) (p-value = 0.0075). In samples transfected with a *MNX1* 3'UTR LUC cassette containing mutations in the binding site of miR-200a-3p, there was no reduction in the luciferase signals (Figure 15B).

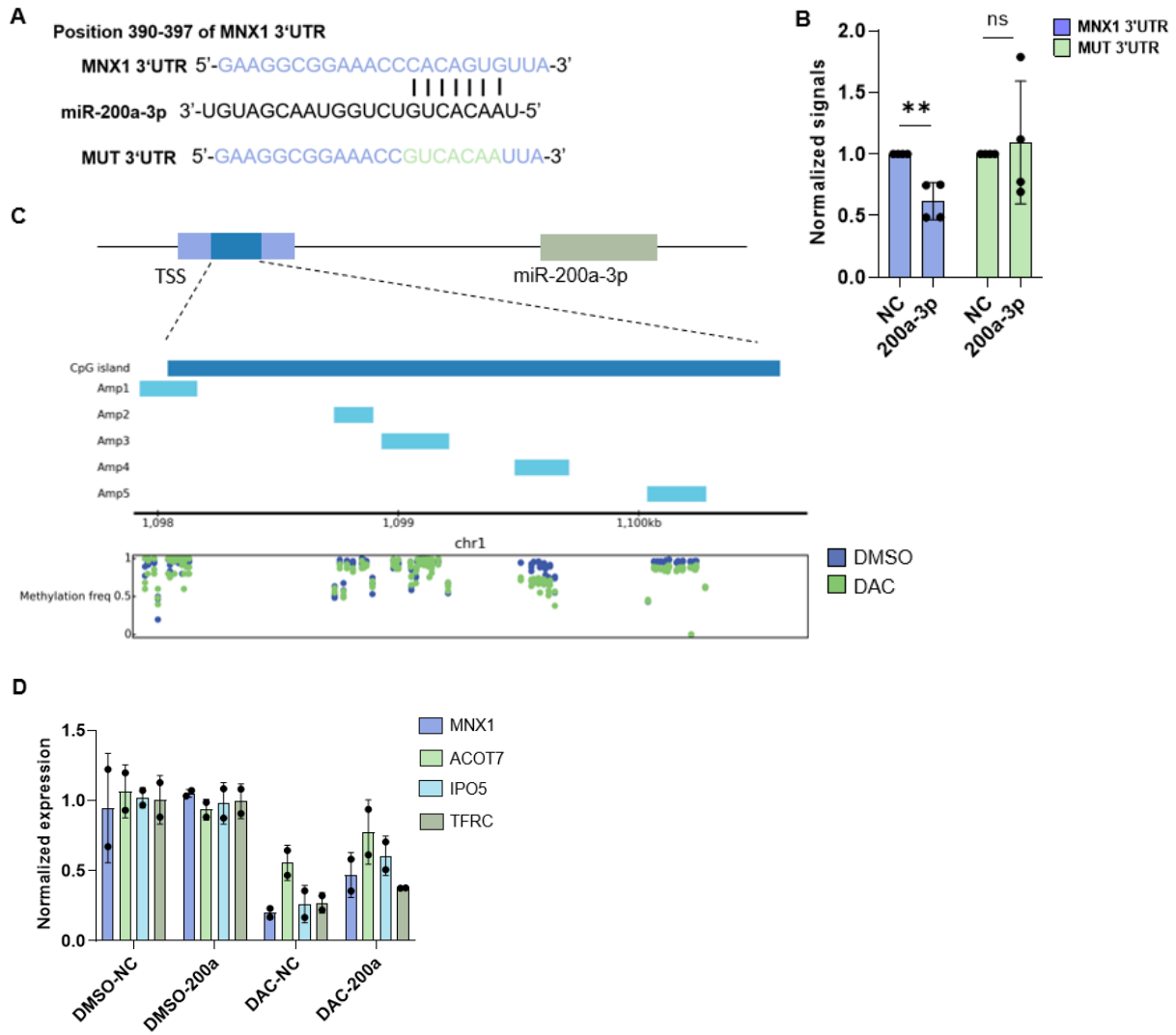


Figure 15: Elucidation of miR-200a-3p-dependent *MNX1* reduction.

A. Representation of the miR-200a-3p sequence and where it may bind on the *MNX1* 3'UTR (on the top). **B.** Bar plot shows the mean luciferase signals from four biological replicates. NC represents the samples where the miRNA negative control is overexpressed, and 200a-3p represents the samples where miR-200a-3p is overexpressed via miR-200a-3p mimic. **C.** Figure shows the Mi-Seq result on the CpG island (chr1: 1096414-1124603) of TSS of miR-200a-3p. Methylation frequency was measured before (blue dots) and after the DAC treatment (green dots), as shown below. **D.** Bar plot shows the mean expression of 4 genes that are known targets of miR-200a-3p and were found to be downregulated by DAC in our RNA-Seq analysis. The 2 biological replicates of DMSO and NC (miRNA negative control inhibitor), DMSO and miR-200a-3p antagomir, DAC and NC, and DAC and miR-200a-3p antagomir treated samples were used. A two-tailed t-test was used to analyze the data in Figure 16B, and a p-value less than or equal to 0.05 was considered significant according to the test results. (* p-value \leq 0.05, **p-value \leq 0.01, *** p-value \leq 0.001).

The transcription start site (TSS) of miR-200a-3p is around 2kbp upstream of miR-200b, miR-200a, and miR-429 and contains a CpG island (Wiklund et al., 2011). DNMT1 and EZH2 bind and downregulate the expression of the miR-200 family (Ning et al., 2015). Additionally, the binding of DNMT3A and MYC to the TSS downregulated the expression of miR-200b in Triple Negative Breast Cancer cells (Pang et al., 2018). Previous studies also found that HDAC4 regulates the TSS of the miR-200 family, and overexpression of HDAC4 leads to downregulation of miR-200b, induction of epithelial to mesenchymal transition (EMT), and resistance against anti-cancer drugs in lung cancer (Chen et al., 2014). Therefore, I analyzed the CpG island methylation on the miR-200a-3p TSS by local deep bisulfite sequencing via MiSeq. MiSeq results revealed a statistically significant hypomethylation in 4 out of 5 amplicons on the CpG island upon DAC treatment (Figure 15C, Supplementary Figure 2). I also found in the miRNA-seq results that the expression of miR-200b and miR-429, which share the same promoter with miR-200a, are significantly increased upon DAC treatment (Figure not shown).

MiRNA antagomirs can efficiently eliminate miRNA function. These 21-23 nucleotide-long modified antisense single-stranded oligonucleotides bind specifically to their target miRNAs (Mattes et al., 2007). The findings from the qPCR revealed a marginal increase upon miR-200a-3p antagomir treatment in both *MNX1* RNA levels and other predicted targets of miR-200a-3p, which were downregulated upon DAC treatment (Figure 15D). However, this experiment should be repeated with more replicates, and protein levels should be assessed in each replicate.

These results showed that DAC treatment leads to hypomethylation of the promoter region of miR-200a-3p, which binds to *MNX1* 3'UTR and downregulates *MNX1* levels. However, analysis of the expression changes of *MNX1* without 3'UTR upon DAC treatment would further prove the effect of miR-200a-3p on *MNX1* regulation. Furthermore, ectopic expression of *MNX1* without 3'UTR might rescue the DAC-induced GDM-1 cell death.

4.4.2. Overexpression of *MNX1* without 3'UTR

I overexpressed the *MNX1 ORF* fused with GFP and HA tags (MNX1-ORF) in a lentiviral expression vector under the EF1alpha promoter. I also generated an empty vector (EV) by removing the *MNX1 ORF* with *EcoRI* and *BstBI* restriction enzymes and ligating the ends of the vector (Figure not shown). I generated lentiviruses using EV and MNX1-ORF. I observed that during lentivirus generation of MNX1-ORF, HEK293T cells express GFP in their nuclei, meaning that the construct was able to express the fusion MNX1-GFP-HA TF, which is, as expected, located in the nuclei (Figure 16A). After the lentiviral transduction of GDM-1, I sorted GFP+ cells. Only 1% of the entire cell population of both EV and MNX1-ORF overexpressing GDM-1 cells were GFP+ (Figure 16B). Sorted MNX1-ORF or EV overexpressing GDM-1 cells were expanded and treated with DAC (Figure 17A).

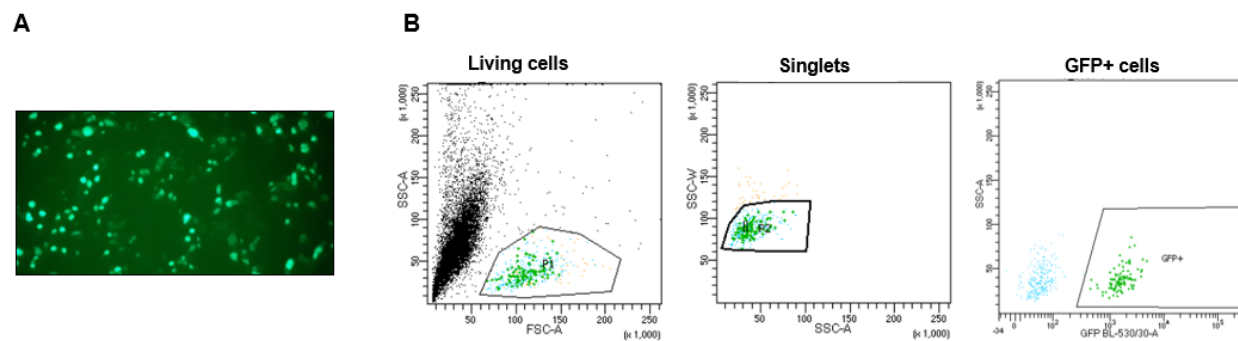


Figure 16: Generation of GDM-1 cells stably expressing MNX1-ORF fused with GFP and HA or EV with GFP and HA.

A. A picture of HEK293T cells during the production of lentiviruses. **B.** FACS images of GDM-1 cells infected with vMNX1-ORF. Single live cells were discriminated by FSC/SSC (first two graphs), and the GFP+ cells were sorted (the last graph).

I could discriminate the expression of exogenous MNX1 (MNX1-ORF) from endogenous MNX1 in GDM-1-MNX1 samples because the cDNA sequence of MNX1-ORF was codon optimized upon cloning and, hence, had a different sequence. qPCR analysis revealed no significant downregulation of exogenous MNX1 (MNX1-ORF) levels in GDM-1-MNX1 samples treated with DAC (Figure 17B) (p-value = 0.1563). Besides, Western blot data uncovered a statistically significant difference in endogenous MNX1 protein levels in the GDM-1-EV upon DAC treatment compared to the exogenous MNX1-ORF protein levels upon DAC treatment (Figure 17C) (p-value = 0.0083). Next, to determine if MNX1 overexpression could rescue the DAC-mediated increased cell death, I measured the viabilities of GDM-1-MNX1 and GDM-1-EV after the treatment with DAC. However, cell viability data revealed only a marginal recovery in the viability of GDM-1-MNX1 compared to GDM-1-EV (Figure 17D).

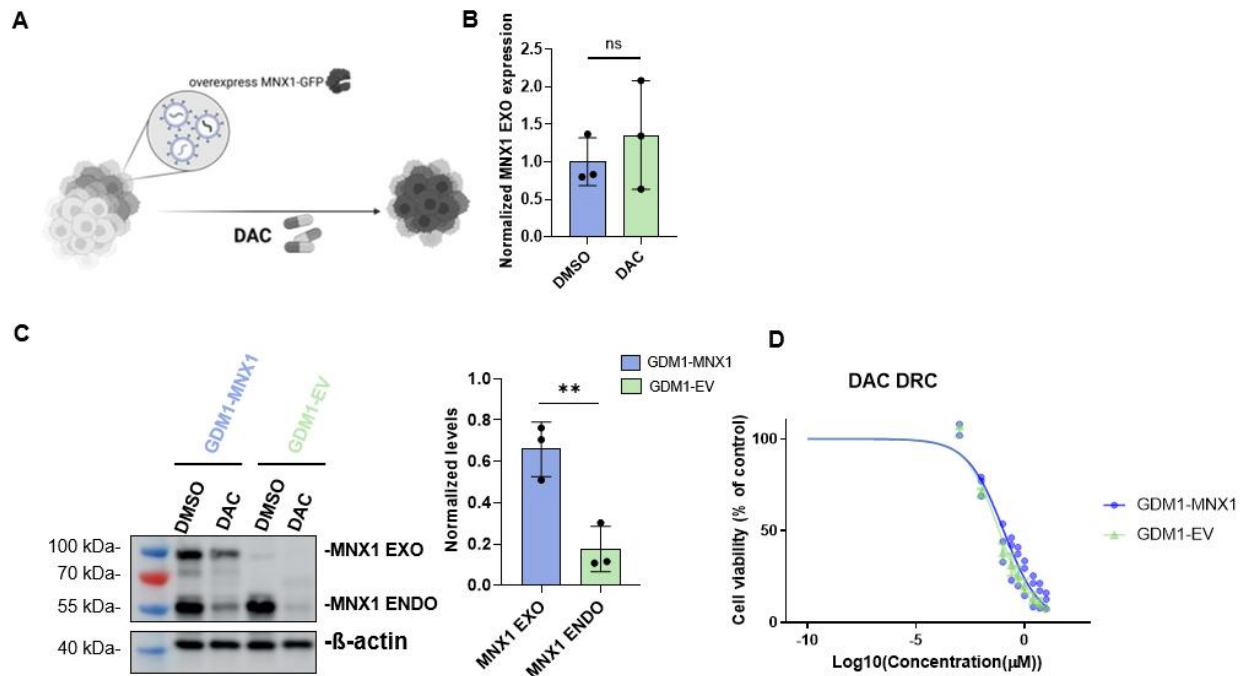


Figure 17: Changes in the expression of MNX1-ORF without 3'UTR upon DAC treatment.

A. Representation of the treatment of GDM-1-MNX1 and GDM-1-EV. **B.** Bar plot shows the mean expression of exogenous (on the left) and endogenous MNX1 (on the right) in GDM-1-MNX1 samples treated with DMSO or DAC. **C.** A representative image of a Western blot analysis performed on the treated cells in Figure A. The bar graph on the right shows the quantification of exogenous MNX1 in GDM-MNX1 and endogenous MNX1 levels in GDM-1-EV after DAC treatment. **D.** DAC dose-response curve of GDM-1-EV and GDM-1-MNX1. A one-tailed t-test was used to analyze the data in Figure 18B, and a p-value less than or equal to 0.05 was considered significant according to the test results. (* p-value \leq 0.05, **p-value \leq 0.01, *** p-value \leq 0.001). A one-tailed unpaired t-test was used to analyze the data in Figure 18C, and a p-value less than or equal to 0.05 was considered significant according to the test results. (* p-value \leq 0.05, **p-value \leq 0.01, *** p-value \leq 0.001).

After DAC treatment, Western blot analysis indicated a 20% reduction in the exogenous MNX1 protein levels in GDM-1-MNX1 cells (Figure 18A) (p-value = 0.0234). I considered the hypothesis that DAC may increase the induction of ubiquitinylation of this exogenous MNX1 protein.

Ubiquitin-tagged proteins undergo proteasomal degradation (Popovic et al., 2014; Sheng et al., 2024). Proteasomal inhibitors, such as MG132 (Sun et al., 2024), prevent ubiquitin-mediated protein degradation (Deng et al., 2020). Therefore, I treated GDM-1-MNX1 cells with MG-132 during DAC treatment to assess the changes in MNX1-ORF expression upon inhibition of the proteasomal process. Western blot data from Marion Bähr (DKFZ, Heidelberg) identified no upregulation of the MNX1-ORF levels upon MG-132 treatment (Figure 18B). However, I could

not prove that the MG132 treatment worked because the Western blot analysis showed no increased smear-like band pattern upon MG132 treatment in the MG132 treated samples (Figure 18C). Therefore, the MG-132 treatment and Western blot analysis should be repeated with more replicates and proper loading.

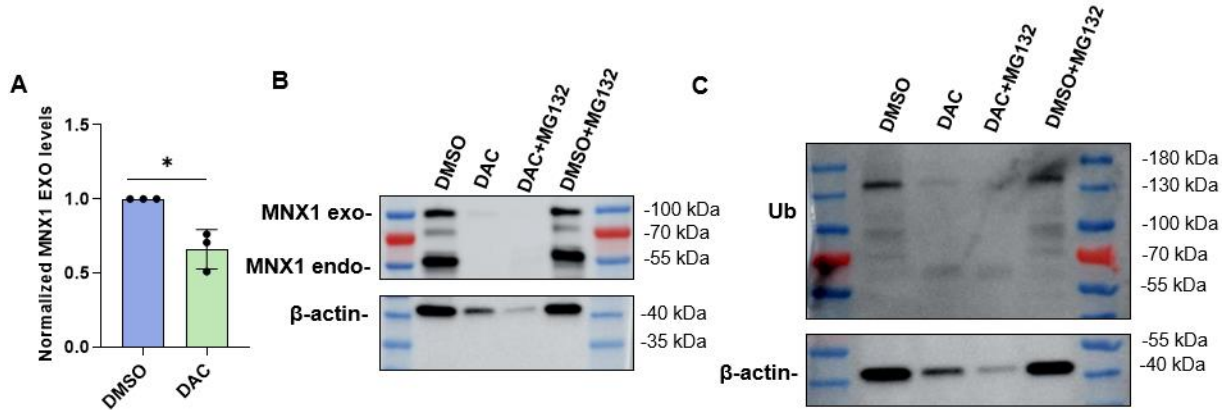


Figure 18: Changes in the levels of MNX1-ORF without 3'UTR upon proteasomal inhibition.

A. The bar plot shows the mean exogenous MNX1 expression levels of GDM-1-MNX1 during the treatment with DAC treatment. **B.** Representative image of a Western blot analysis using an antibody against MNX1 was performed on the MG132-treated cells. **C.** Representative image of a Western blot analysis using an antibody against ubiquitin was performed on the MG132-treated cells. A one-tailed t-test was used to analyze the data, and a p-value less than or equal to 0.05 was considered significant according to the test results. (* p-value ≤ 0.05 , **p-value ≤ 0.01 , *** p-value ≤ 0.001).

These results showed that DAC treatment reduces both exogenous and endogenous MNX1 levels. Further analysis should be carried out to investigate the reasons behind DAC-induced downregulation of exogenous MNX1 levels.

I concluded that DAC treatment causes hypomethylation of the miR-200a-3p promoter, which subsequently binds to the *MNX1* 3'UTR and decreases the MNX1 expression level in GDM-1. The next step is to validate these in other *MNX1*-expressing models.

4.4.3. Validation experiments with PDX samples

PDX models are generated by implanting tumor tissues from patients into humanized or immunocompromised mice. These models recapitulate the characteristics of human tumors better than cell lines; for example, they allow for more meaningful studies of intratumor heterogeneity and compound screening *in vivo* (Liu et al., 2023). Therefore, I decided to use AML PDX models expressing MNX1 to assess whether I could recapitulate the phenotypes I observed in GDM-1

cells. Two PDX models, PDX491 and PDX661, were generated by Binje Vick (Helmholtz Zentrum Munich, Germany) from an *MNX1* expressing del(7q) patient at first and second relapse.

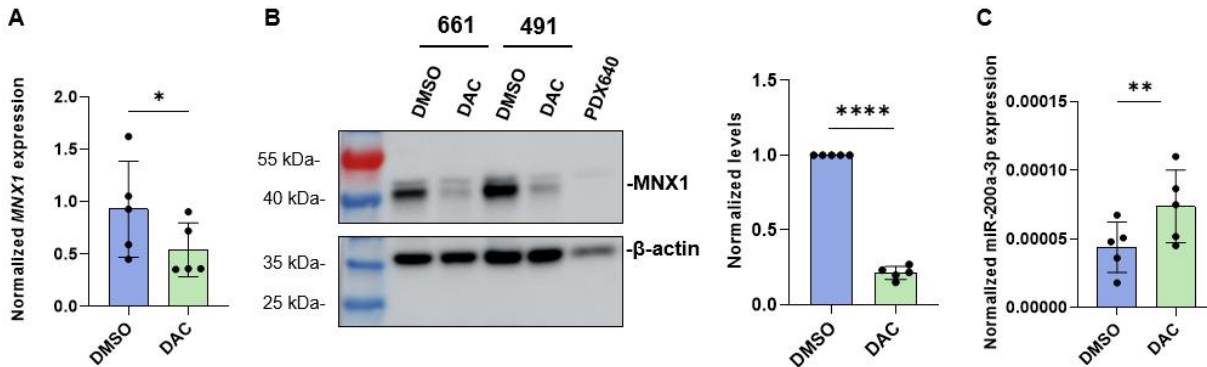


Figure 19: Changes in PDX samples upon DAC treatment.

A. Bar plot shows the mean of *MNX1* expression levels in PDX samples (491 and 661) upon the treatment with DAC. **B.** A representative image of a Western blot analysis using an antibody against MNX1, which was performed on the DAC-treated cells from PDX samples. PDX640, a PDX sample that does not express MNX1, is a negative control. The bar plot on the right shows the quantification of the treatments in 3 biological replicates. **C.** Bar plot shows the mean of miR-200a-3p expression levels of PDX samples (491 and 661) upon the treatment with DAC. A one-tailed t-test was used to analyze the data, and a p-value less than or equal to 0.05 was considered significant according to the test results. (* p-value ≤ 0.05 , **p-value ≤ 0.01 , *** p-value ≤ 0.001).

In vitro DAC treatment of PDX samples showed a statistically significant reduction of *MNX1* RNA levels (Figure 19A) (p-value = 0.0110) and around 70 percent reduction in protein levels (Figure 19B) (p-value < 0.0001). This reduction may be induced by miR-200a-3p-mediated degradation of MNX1, as I observed a statistically significant upregulation of miR-200a-3p upon DAC treatment (Figure 19C) (p-value = 0.0467). Binje Vick (Helmholtz Zentrum Munich, Germany) shared her results on the *in vivo* treatment of the PDX491 sample with 5-AZA. She observed that the tumor burden continued to decrease, even after stopping the treatment with 5-AZA, compared to the results of another PDX sample, PDX372, generated from a ck-AML patient that does not express *MNX1* (Figure not shown).

5. Discussion

5.1. Epigenetic compound screening in GDM-1

The effect of sinefungin, a SAM and methylation inhibitor, has previously been investigated in an AML mouse model retrovirally overexpressing *MNX1*. While this treatment prevented the expression of target genes, it did not result in *MNX1* downregulation (Waraky et al., 2024). A recent study highlighted the importance of finding a candidate compound to target *MNX1* therapeutically in t(7;12) AML cases (Ragusa et al., 2023). To date, no such strategy exists.

In a recent review, Lazaro and Delwel discussed the importance of targeting oncogenic enhancers as a potential therapeutic strategy in leukemia. They mentioned that one option could be to screen epigenetic compounds to reduce super-enhancer activity in AML (Mulet-Lazaro & Delwel, 2024). Additionally, researchers used epigenetic compound libraries and found that a broad spectrum of inhibitors of HDACs, KDMs, and DNMTs were among the top candidates when they measured the viabilities of chordoma or IDH1-mutant glioma cell lines (Cottone et al., 2020; Kayabolen et al., 2022). Therefore, in this thesis, I decided to screen epigenetic compounds that may lead to the downregulation of *MNX1*, a known oncogene in AML (Waraky et al., 2024), and a putative cancer biomarker (Ragusa, Tosi, et al., 2022). I used GDM-1 as a cell line model for this screening and downstream experiments. This cell line was chosen because it is the only AML cell line with *MNX1* expression (Nagel et al., 2005; Weichenhan et al., 2023). I also utilized various non-*MNX1*-expressing AML cell lines and PDX models expressing *MNX1* throughout this project to test whether my findings were unique to *MNX1*-expressing cells.

I first used shRNA-mediated knockdown constructs to knockdown *MNX1* in GDM-1 and observed a statistically significant reduction in GDM-1 viability upon *MNX1* knockdown (Figure 4D). Mariam Hakobyan (DKFZ, Heidelberg) also found in her master's project that shRNA-mediated knockdown affects the growth kinetics of GDM-1. Both findings match and show the importance of *MNX1* in both growth kinetics and viability. Further research is necessary to investigate the effect of *MNX1* downregulation on the viability of *MNX1*-expressing t(7;12) or del(7q) or ck iPSCs-derived HSPCs or AML patient samples or *in vivo* models.

I hypothesized that *MNX1* overexpression may drive AML, and epigenetic compound(s) might regulate *MNX1* expression and affect viability. My comprehensive epigenetic compound screening revealed a significant reduction in the viability of GDM-1 upon DAC treatment as compared to the other *MNX1*(-) cell lines (Figure 6B). Extensive analyses showed that DAC was the only substance among those tested which reduced *MNX1* expression. JQ1 treatment led to a marginal but not significant reduction of *MNX1* expression. JQ1 is known to reduce super-enhancer activity via loss of BRD4 (Loven et al., 2013). Inhibition of BRD4 was previously shown to disrupt enhancer-promoter interactions (Wang et al., 2021). Therefore, JQ1 might affect the enhancer-

promoter interaction driving *MNX1* expression in GDM-1 (Weichenhan et al., 2023), though only marginally.

5.2. Effect of DAC treatment in GDM-1 cells

Using Infinium Methylation EPIC array data before and after DAC treatment, I confirmed that the treatment leads to global hypomethylation, as expected due to DNMT inhibition. Upon DAC treatment, I observed hypomethylation in the *MNX1* 3'UTR, promoter, and gene body region (Figure 7). The decrease in methylation may be due to hypomethylation of the WT allele. One study shows that *MNX1* is expressed on the WT allele but not on the translocated allele (Federico et al., 2017). However, in-house, Etienne Sollier showed, using nanopore sequencing, that the promoter region of the translocated allele is hypomethylated in GDM-1 (Figure not shown). In contrast, the same area is hypermethylated on the WT allele, which suggests that the translocated allele is responsible for the expression. Therefore, I concluded that if the observed semi-hypomethylation upon DAC treatment is due to hypomethylation of the WT allele, it should not affect the expression of *MNX1* as the WT allele is not responsible for the expression.

My thesis revealed a statistically significant downregulation of *MNX1* RNA and protein levels upon global hypomethylation with DAC treatment in GDM-1. Sinefungin (SAM inhibitor) treatment reduced the expression of *MNX1* target genes. However, the authors did not observe a reduction in *MNX1* RNA expression (Waraky et al., 2024). Upon DAC treatment, I revealed a statistically significant downregulation of *MNX1* RNA and protein levels (Figure 8). Although Waraky et al. contradicted our findings, there could be several reasons why they did not observe a reduction in *MNX1* RNA expression. A notable difference in their experiments is that they used retroviral overexpression of *MNX1* *in vivo*. Their sequence lacks the 3'UTR region of *MNX1*, so miRNA-dependent inhibition of *MNX1* may not be possible. The Infinium Methylation EPIC array of Mahmood et al. revealed that sinefungin treatment led to more DNA hypermethylation than hypomethylation. Mahmood et al. combined sinefungin with DAC and observed more hypomethylation in the vicinity of promoter regions but more hypermethylation in the intergenic region (Mahmood et al., 2020). Therefore, sinefungin treatment might also not result in hypomethylation of the promoter region of miR-200a-3p.

5.3. miRNA-independent mechanisms behind *MNX1* downregulation upon DAC treatment

DAC treatment leads to passive global hypomethylation and restoration of genes whose promoters are silenced via hypermethylation (Si et al., 2010). However, I observed a statistically significant reduction in *MNX1* gene expression upon DAC treatment. To explain one of the possible mechanisms behind this reduction, CTCF ACT-seq was performed. I found *five* demethylation-mediated accessible CTCF peaks in DAC-treated samples but could not find enrichment of a CTCF

motif in these regions. There is, however, the possibility that CTCF may be recruited to these regions by other TFs or chromatin remodelers. For example, Wagner et al. showed recruitment of CTCF to the low-affinity SIRT1 promoter upon oxidative stress-mediated posttranslational modification of CTCF (Wagner et al., 2024). Interaction between the *MNX1* promoter and the enhancer(s) in or close to the juxtaposed *AH11/MYB* region drives the expression of *MNX1* in GDM-1 (Weichenhan et al., 2023). Observations from CTCF ACT-seq suggest that the TAD structure encapsulating the enhancer-promoter interaction, driving *MNX1* expression, may be disrupted. To check if the enhancer-promoter interaction is preserved after DAC treatment, 4C-seq experiments were performed. Interactions between the *AH11/MYB* region and *MNX1* appeared to be maintained after DAC treatment. Therefore, this hypothesis was rejected. However, performing a Hi-C sequencing is recommended as a future outlook to assess if the TAD structures before and after DAC treatment are preserved, focusing on the TAD encapsulating the enhancer-*MNX1* promoter interaction.

To test the hypothesis that the expression of *CAT7*, a lncRNA known to regulate *MNX1* expression (Ray et al., 2016), is increased upon DAC treatment and that *CAT7* recruits PRC1 complexes to the *MNX1* promoter, I assessed the expression of *CAT7* in our RNA-seq and performed a qPCR assay to determine the expression of *CAT7*. I found that *CAT7* was not expressed in this system, neither under treated nor under untreated conditions. It may be that the promoter of *CAT7* does not get hypomethylated upon DAC treatment or that the other epigenetic mechanisms are required for *CAT7* activation, which may not be present in hematopoietic cells. I could have checked the promoter methylation of *CAT7* using the Infinium Methylation EPIC array data I generated. However, the authors did not share the promoter information for this lncRNA that they discovered and annotated (Ray et al., 2016). I rejected the hypothesis since I did not detect any expression in treated or untreated conditions. If *CAT7* is not expressed, I expect the PRC1 complex may not be recruited or may still be recruited via other mechanisms. Therefore, as an outlook, one should check PRC1 and H3K27me3 levels on the *MNX1* promoter upon DAC treatment via ChIP-qPCR, which is a method to quantify the enrichment of immunoprecipitated DNA fragments that are bound by the protein of interest (Kim & Dekker, 2018).

5.4. miRNA-dependent mechanisms behind *MNX1* downregulation upon DAC treatment

The activation of epigenetically silenced miRNAs via epigenetic regulations has been studied in multiple cancer types and may have therapeutic potential (Baer et al., 2013; Fabbri et al., 2013). For instance, activation of miR-135a-5p via DAC treatment increased apoptosis of HL-60 via activation of LINC00599 and downregulation of *Bcl-2* (Du et al., 2023). As another example, upon DAC treatment, miRNA-345 got upregulated, resulting in the degradation of viral oncogenes like E6 and E7 in high-risk human papillomavirus-associated cancers (Stich et al., 2017). This background led me to hypothesize that epigenetically silenced miRNA(s) targeting *MNX1* could

be reactivated upon DAC treatment. Using the miRNA-seq, I revealed the upregulation of six miRNAs (miR-381-3p, miR-410-3p, miR-200a-3p, miR-3180-5p, miR-338-3p, and miR-141-3p) that are predicted to bind *MNX1* 3'UTR. Since *MNX1* is highly expressed in GDM-1 cells (D. Weichenhan et al., 2023) (Figure 8), we considered it unlikely that a miRNA targeting *MNX1* would be expressed at low baseline levels in DMSO-treated conditions. Therefore, of these six miRNAs, I decided to focus further experiments on those activated upon DAC treatment. One of those is miR-200a-3p, which Mu et al. showed to reduce *MNX1* expression upon overexpression (Mu et al., 2016).

Song et al. found that the TET family of methylases regulates the expression of miR-200a via demethylation inhibition on the promoter region, leading to EMT (Song et al., 2013). Another observation is the TET-dependent downregulation of miR-200s, miR-429, and miR-141 expressions during somatic cell reprogramming (Hu et al., 2014). These studies have described the critical role of DNA methylation in regulating miR-200 family members. In my thesis, I identified a significant and novel finding: DAC treatment activated miR-200a-3p, downregulating *MNX1*. This previously unknown mechanism has potential implications for AML therapy because of the specific regulation of *MNX1* by miR-200a-3p upon DAC treatment.

I observed a statistically significant downregulation of MNX1 protein levels upon miR-200a-3p overexpression at 5nM and 10nM concentrations. I confirmed the interaction with *MNX1* 3'UTR and miR-200a-3p via luciferase assay. Upon DAC treatment, I also validated the hypomethylation on the promoter region of miR-200a-3p. I assessed the expression of the genes targeted by miR-200a-3p and downregulated upon DAC treatment: *ACOT7*, *IPO5*, *TFRC*, *MNX1* after miR-200a-3p antagomir treatment. I observed a marginal increase in these genes upon miR-200a-3p antagomir transfection and DAC treatment (Figure 15D). This suggests that the inhibition of miR-200a-3p rescues the DAC-mediated MNX1-downregulation. However, further research should include optimizing the concentration of antagomir or stable inducible overexpression of the antagomir lentivirally. Another possibility is to knock out miR-200a-3p or siRNA-mediated knockdown of DICER, DROSHA, and AGO complexes.

Taken together, I provided experimental evidence that activation of miR-200a-3p upon demethylation of its promoter after DAC treatment is the mechanism behind DAC-mediated *MNX1* downregulation in GDM-1.

5.5. Overexpression of *MNX1* without 3'UTR

Cottone et al. showed that treating chordoma cell lines and patient samples with the KDM6A/6 B inhibitor KDOBA67 reduced the expression of the oncogene *TBXT* and induced cell death. They overexpressed TBXT-HA under a strong promoter and observed that the exogenous TBXT-HA is not sensitive to KDOBA67 treatment, and overexpression rescued the treatment-associated cell death (Cottone et al., 2020). In line with this, I designed a lentivirus construct with *MNX1* ORF fused with GFP and HA. I used the T2A self-cleavage sequence (Wang et al., 2015) to cleave

puromycin from the fusion protein, which enabled a possibility of puromycin-dependent selection as well. A critical feature of this construct is that exogenous *MNX1* lacks 3'UTR; therefore, there is no possibility of miRNA-mediated degradation. miRNAs can bind to 5'UTR or ORF as well (Oliveto et al., 2017). However, using miRNA-seq, we revealed no significant upregulation of miRNAs upon DAC treatment, which are predicted to bind MNX1 5'UTR or ORF (Figure not shown).

I could not rescue the DAC-induced cell death upon MNX-ORF overexpression (Figure 17D). The reason could be that the exogenous MNX1-GFP-HA is still fused with the puromycin-resistance gene. Self-cleavage efficiency could be too low, and most cells express the fusion protein with puromycin. Therefore, there is a possibility that the MNX1-ORF-GFP-HA-puromycin fusion protein cannot function as a TF anymore because of its size. This might explain why GDM-1-MNX1 behaves similarly to GDM-1-EV in the DAC treatment. TFs are usually around 50 kDa in size, and large TFs can not enter through the chromatin domains on the target sites. Hence, the size of TFs is a major determinant of their function and binding capacity (Maeshima et al., 2015).

Western blot analysis showed that the levels of exogenous MNX1 protein get downregulated marginally. The codon-optimized exogenous sequence does not have a miR-200a-3p binding site or 3'UTR and 5'UTR, eliminating the possibility of miR-200a-3p-mediated degradation. Given that I did not observe a downregulation in mRNA levels but rather in the exogenous protein levels, I hypothesized that DAC treatment might increase the ubiquitin-mediated degradation of exogenous MNX1. I treated the cells with a ubiquitin inhibitor, MG-132, during DAC treatment. I observed no change in MNX1 or ubiquitination levels. If MNX1 was degraded, an increase in its ubiquitinylation would be expected upon DAC treatment, which was not the case (Figure 18C).

To summarize, the main limitation of this thesis is the conflicting results observed after overexpression of *MNX1* without 3'UTR. I observed a marginal but significant downregulation that miRNA-dependent mechanisms can not explain. MG-132 treatment and Western blot analyses should be repeated to elucidate the mechanism behind the reduction of exogenous *MNX1* without 3'UTR upon DAC treatment. Additionally, overexpression of *MNX1* without 3'UTR did not rescue the viability of GDM-1 after DAC treatment, possibly because the exogenous MNX1 protein might not function like the endogenous one. Further experiments overexpressing *MNX1* without 3'UTR with small tags are recommended.

Validation of phenotypes observed in cell lines using other models is essential. Therefore, I checked if the same effects occurred in PDX models as in cell lines. I revealed that the phenotypes observed in GDM-1, which are reduction in *MNX1* expression (both mRNA and protein) and upregulation of miR-200a-3p upon DAC treatment, can be recapitulated in PDX models with *MNX1* expression, PDX491, and PDX661. Furthermore, when Binje Wick (Helmholtz Zentrum Munich, Germany) observed a continuous tumor burden in PDX491 (MNX1+) after she stopped 5-AZA treatment compared to the spectrum of PDX372 (MNX1-), this could be due to the reduction of *MNX1* expression during 5-AZA and impaired recovery from this after 5-AZA

treatment stopped. Further research is necessary to explore the development of leukemogenesis and changes in MNX1 levels using the same PDX samples *in vivo*.

This thesis revealed the mechanism underlying the downregulation of *MNX1* RNA and protein levels in GDM-1 and PDX models. Additionally, my study uncovered the vital role of MNX1 in the viability of GDM-1. Considering the downregulation of MNX1 upon DAC treatment, DAC might be used in clinics against *MNX1*-expressing AML. However, AML patients treated with DAC develop resistance (Simonicova et al., 2022). Combinatorial therapies with DAC might be a possible way to overcome this. Further research on the identification of an epigenetic compound that has a synergism with DAC is warranted. One possibility is to screen the same epigenetic compounds used in the thesis on the DAC-treated *MNX1*-expressing AML cells.

6. Conclusion and Outlook

The main remark of this thesis is that an epigenetically silenced miRNA, miRNA-200a-3p, gets upregulated upon DAC treatment and downregulates *MNX1*. However, there could be other mechanisms that could explain DAC-mediated *MNX1* downregulation. For example, the changes in the methylation of the *MNX1* gene might play a role in regulating *MNX1* expression. Upon DAC treatment, hypomethylation of the gene body of *MNX1* should be investigated via long-read sequencing. Also, its effect on the *MNX1* expression should be assessed. Lentivirally expression of CRISPR-dCAS9 coupled with a TET enzyme targeting the *MNX1* gene body would phenocopy the hypomethylation observed upon DAC treatment. Later, a comparison of the *MNX1* expression in the conditions with and without CRISPR-dCAS9 would reveal whether this hypothesis should be rejected.

Peptidomimetic inhibitor of MYB (MYBmim) treatment led to decreased recruitment of MYB to hijacked *BCL2* enhancer, which is responsible for *EVII* expression in inv(3) and t(3;3) AML cases. This led to downregulation of *EVII* expression and induction of differentiation (Smeenk et al., 2021). To downregulate *MNX1* expression, future studies could focus on developing peptidomimetic inhibitors against either *MNX1* itself or the TFs regulating *MNX1* expression. MYB regulates its expression (Nicolaidis et al., 1991). It may also be worthwhile to attempt MYBmim in GDM-1, given that the hijacked enhancers responsible for driving *MNX1* expression are located within the *AH11/MYB* region.

MiRNA mimics or antagomirs have been used as therapeutic agents against several cancers (Seyhan, 2024). However, the challenges of miRNA mimic therapeutics are the possibility of degradation by RNases during delivery, and the instability of those miRNA mimic therapeutics. To overcome these, studies on advancing miRNA chemistry via changing the miRNA backbone to resist RNases (via methylation, addition of phosphorothioate members, or use of nucleotide analog locked nucleic acid [LNA]) or lipid nanoparticle-based delivery approaches have enabled mimics to move into clinical trials (Rupaimoole & Slack, 2017). Therefore, considering the results in this thesis, advancing miR-200a-3p mimic chemistry and covering it with lipid nanoparticles are recommended. This mimic can be combined with DAC against *MNX1*-expressing AML in clinics.

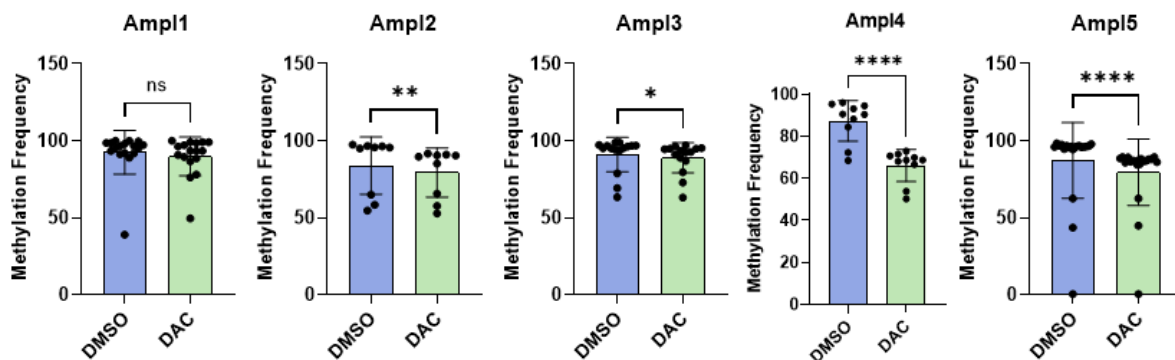
7. Supplementary Figures and Tables

7.1. Supplementary figures



Supplementary Figure 1: CAT7 qPCR results.

Snagene view of the sequencing result of CAT7 qPCR product with the qPCR primer I designed (upper panel) and the sequence that the CAT7 qPCR should amplify (lower panel). The blue-highlighted region shows the sequence amplified after the qPCR.



Supplementary Figure 2: Methylation frequencies of each CpG on the amplicons represented in Figure 15.

A two-tailed paired t-test was used, and a p-value less than or equal to 0.05 was considered significant according to the test results. (* p-value \leq 0.05, **p-value \leq 0.01, *** p-value \leq 0.001).

7.2. Supplementary tables

Supplementary Table 1: Authentication of cell lines

Cell lines	Cell line number	Authentication date
K562	CVCL_0004	12.07.2023
OCIAML3	CVCL_1844	14.12.2023
MOLM13	CVCL_2119	14.12.2023
HL60	CVCL_0002	14.12.2023
GDM-1	CVCL_1230	07.03.2023
HEK293T	CVCL_0063	16.11.2023

Supplementary Table 2: Cell culture media/reagents

Reagents/Media	Ordering details
RPMI Medium 1640 + L-glutamine	Thermo Fischer, Catalog number: 21875-034
Fetal Bovine Serum	Superior, Thermo Fischer, Catalog number: S0615
Penicillin/Streptomycin	10.000units, Sigma, Catalog number: P0781-100ml
Trypsin-EDTA (0.25%) with phenol red	1X, Thermo Fischer, Catalog number: 252000-56
DPBS without magnesium and calcium	1X, Thermo Fischer, Catalog number: 14190-094
DMEM (1X) +4.5 g/L D-glucose, L-glutamine (-) pyruvate	Thermo Fischer, Catalog number:41965-039

OPTIMEM (+HEPES, +2.4 g/L sodium bicarbonate, + L-glutamine)	Thermo Fischer, Catalog number: 2407807
PDX Media (kindly provided by Binje Vick)	
StemPro-34 and nutrient supplement medium	Thermo Fischer, Catalog number:10639011
100X Pen/Strep (10,000 U/ml)	Gibco, Catalog number:15140-100
1000X Gentamicin (50 mg/ml)	Lonza, Catalog number: 17518L
100X L-Glutamine (200mM)	Gibco, Catalog number:25030-024
rhFLT3L (Stock: 100µg/ml PBS + (at least) 0.1%BSA)	R&D Systems, Catalog number:308-FKN-100
rhSCF (Stock: 50µg/ml water)	Peprotech, Catalog number:300-07-100
rhTPO (Stock: 50µg/ml water)	Peprotech, Catalog number:300-18-100
rhIL3 (Stock: 50µg/ml water)	Peprotech, Catalog number:200-03-100

Supplementary Table 3: Epigenetic compounds in the library.

Compounds	Functions	Compounds are shown in the Figure 5A .	Numbers
(+)-JQ1	Bromodomains - BRD2, BRD3, BRD4, BRDT (BET)	XZL-1	1
(-)-JQ1 (inactive)	Bromodomains - Negative control	Mocetinostat	2
PFI-1	Bromodomains - BRD2, BRD3, BRD4, BRDT (BET)	J556-63R	3
I-BET	Bromodomains - BRD2/3/4	Romidepsin	4
Bromosporine	Bromodomains - pan-Bromodomain	PCI-24781	5
CBP/BRD4 (0383)	Bromodomains - CBP, BRD4(1)	KDOBA67	6
SGC-CBP30	Bromodomains - CREBBP, EP300	SAHA	7
I-CBP112	Bromodomains - CREBBP, EP300	GSK J4	8
RVX-208	Bromodomains - BRD2, BRD3, BRD4, BRDT (BET, BD2)	GSK484	9

SMARCA	Bromodomains - SMARCA, PB1	RGFP966	10
PB1/SMARCA	Bromodomains - SMARCA, PB1	SGC-CBP30	11
PFI-3	Bromodomains - SMARCA2/4, PB1(5)	MZ1	12
GSK2801	Bromodomains - BAZ2A, BAZ2B	ACBI1	13
PFI-4	Bromodomains - BRPF1B	Chaetocin	14
TRIM24/BRPF	Bromodomains - TRIM24/BRPF	CHR-6494	15
OF-1	Bromodomains - pan-BRPF	A-485	16
Belinostat	HDAC - hydroxamic acids	5-Azadeoxycytidine	17
CXD101	HDAC -	Rocilinostat	18
Valproic acid	HDAC - aliphatic acid compounds	NVS-CECR2-C	19
Entinostat	HDAC - ortho-amino anilides	5-Azacitidine	20
SAHA	HDAC - hydroxamic acids	IOX1	21
Trichostatin A	HDAC - hydroxamic acids - Class I & II	AZD5153	22
SRT1720	HDAC - SIRT1 (indirect?) activator	GSK959	23
EX 527	HDAC - SIRT1	I-BET	24
CI-994	HDAC - 1,2,3,(8)	I-BRD9	25
CPI-360	Histone methyltransferase - EZH2 and EZH1	Tranlycypromine	26
UNC0638	Histone methyltransferase - G9a, GLP	MAZ1392	27
UNC0642	Histone methyltransferase - G9a, GLP	Entinostat	28
A-366	Histone methyltransferase - G9a, GLP	J556-143	29
Chaetocin	Histone methyltransferase - SUV39H1	GSK2879552	30
PFI-2	Histone methyltransferase - SETD7	GSK9311	31
SGC0946	Histone methyltransferase - DOT1L	GSK591	32
GSK343	Histone methyltransferase - EZH2	MS003	33

UNC1999	Histone methyltransferase - EZH2	Valproic acid	34
LLY-507	Histone methyltransferase - SMYD2	ZXH-3-26	35
Tranylcypromine	Lysine demethylases - LSD1	Belinostat	36
GSK-LSD1 (irreversible)	Lysine demethylases - LSD1	GSK-LSD1 (rev.)	37
GSK690	Lysine demethylases - LSD1	GSK-LSD1 (irrev.)	38
GSK J4	Lysine demethylases - JMJD3, UTX, JARID1B	(+)-JQ1	39
GSK J5 (inactive)	Lysine demethylases - Negative control	5-Iodotubercidin	40
IOX1 (5-carboxy-8HQ)	Lysine demethylases - pan-2-OG	ML324	41
Methylstat (Ester)	Histone demethylase	Tubastatin A HCl	42
(E)-JIB-04	Histone demethylase - Pan JmjC	J556-42R	43
ML324	Histone demethylase - JMJD2E	ACY-957	44
IOX2	Prolyl-Hydroxylases - PHD2 (EGLN1)	KDM5-C70	45
OICR-9429	Methyl Lysine Binder? - WDR5	GSK J5 (- cntrl)	46
UNC1215	Methyl Lysine Binder - L3MBTL3	PB1/SMARCA	47
5-Azacitidine	DNA methyltransferase (DNMT) -	VZ185	48
5-Azadeoxycytidine	DNA methyltransferase (DNMT) - DNMT1/3	SGC-iMLLT	49
Olaparib	Poly ADP ribose polymerase (PARP)	NVS-MLLT-1	50
Rucaparib	Poly ADP ribose polymerase (PARP)		
K00135	Kinase inhibitor - ATP competitive - PIM		
5-Iodotubercidin	Kinase inhibitor - ATP mimetic - Haspin		
C646	Histone acetyltransferase (HAT) p300/CBP		
DUAL1946			
GSK484	Peptidyl arginine deiminase (PAD4)		
KDOBA67	Histone demethylase		

BAZ2-ICR	Bromodomains - BAZ2A, BAZ2B		
NI-57	Bromodomains - pan-BRPF		
LP99	Bromodomains - BRD9, BRD7		
SGC707	Arginine methyltransferase - PRMT3		
RGFP966	HDAC - HDAC3		
PCI-34051	HDAC - HDAC8		
Rocilinostat	HDAC - HDAC6		
Tubastatin A HCl	HDAC - HDAC6		
KDOAM-25a	Lysine demethylases - JARID		
KDM5-C70	Histone demethylase - JARID1		
MAZ1805			
MAZ1392			
BI-9564	Bromodomains - BRD9, BRD7		
NVS-CECR2-1	Bromodomains - CECR2		
GSK106	Peptidyl arginine deiminase (PAD4)		
J556-42R	Arginine methyltransferase - PRMT5		
J556-63R	Arginine methyltransferase - PRMT5		
J556-70R	Arginine methyltransferase - PRMT5		
A-196	Histone methyltransferase - SUV420H1/H2		
BAY-598	Histone methyltransferase - SMYD2		
J556-143	Arginine methyltransferase - PRMT5		
MS049	Arginine methyltransferase		
MS023	Arginine methyltransferase - Type I PRMTs		
MS003	Arginine methyltransferase - negative control		
SGI-1776	Kinase inhibitor - Haspin		
CHR-6494	Kinase inhibitor - Haspin		
CPI-169	Histone methyltransferase - EZH2, EZH1		

UNC2400	Histone methyltransferase - EZH2		
GSK864	Dehydrogenase		
GSK8814	Bromodomains - ATAD2		
GSK8815	Bromodomains - ATAD2		
GSK959	Bromodomains - BRPF1		
NVS-CECR2-C	Bromodomains - CECR2		
BAY-299	Bromodomains - BRD1, TAF1		
PCI-24781	HDAC -		
Romidepsin	HDAC -		
Mocetinostat	HDAC -		
Santacruzamate	HDAC 2		
KDOAM32	Lysine demethylases - JARID		
MS409N	Arginine methyltransferase - PRMT4, PRMT6 inactive control		
TP-064	Arginine methyltransferase - PRMT4		
TP-064N	Arginine methyltransferase - PRMT4		
A-395	Methyl Lysine Binder - EED		
A-395N	Methyl Lysine Binder - EED		
I-BRD9	Bromodomains - BRD9		
TP-472	Bromodomains - BRD9		
TP-472N	Bromodomains - BRD9		
KDOPZ-32a	Lysine demethylases - KDM5		
KDOOA012000	Lysine demethylases KDM2		
AMI-1	Arginine methyltransferase - PRMT		
TMP269	HDAC -4, 5, 7 &9		
AGK2	HDAC - SIRT2		
GSK6853	Bromodomains - BRPF1/2/3		
GSK9311	Bromodomains - BRPF1/2/3		
LLY-283	Arginine methyltransferase - PRMT5		
TMP195	HDAC -4,5,7,9		
GSK2879552	Lysine demethylases - LSD1		
VinSpinIn	Methyl Lysine Binder/tudor domain -Spin1		

A-485	Histone acetyltransferase (HAT) p300/CBP		
A-486	Histone acetyltransferase (HAT) p300/CBP		
GSK4027	Bromodomains - PCAF, GCN5		
GSK4028	Bromodomains - PCAF, GCN5		
L-Moses	Bromodomains - PCAF, GCN5		
D-Moses	Bromodomains - PCAF, GCN5		
PFI-5	Histone methyltransferase - SMYD2		
YX39-31b	Methyl Lysine Binder/tudor domain -Spin1		
VinSpinIC	Methyl Lysine Binder/tudor domain -Spin1		
RTS-V5	protesome and HDAC		
dBRD9	Bromodomains - BRD9		
BI-7273	Bromodomains - BRD9/7 (IC50 19/117nM)		
CPI-621	Lysine demethylases - KDM5		
UNC6934	NSD2-PWWP1		
UNC7145	NSD2-PWWP1 neg ctrl		
BI9321	NSD3 (PWWP1)		
BI9466	NSD3 (PWWP1) -ve ctrl		
ACY-957	HDAC1/2		
ACY-738	HDAC6		
Ski73	PRMT4 (CARM1)		
SGC6870	PRMT6		
SGC6870N	PRMT6 neg ctrl		
BI9564	BRD9		
BI6354	BRD9 -ve		
MZ1	BET Protac		
cisMZ1	BET Protac -ve		
NVS-BPTF-C	BPTF- control		
NVS-BPTF-1	BPTF		
MOZ-IN-3	Lysine acetyltransferase KAT6A/MOZ		
PFI-5NC	Histone methyltransferase - SMYD2 -ve ctrl		
TP422	(neg ctrl)		

TP238	CECR2, BPTF (FALZ)		
UNC3866	CBX7/CBX4		
UNC4219	CBX7/CBX4 neg ctrl		
BAY6035	SMYD3		
ZXH 3-26	BRD4 degrader		
WM-1119	lysine acetyltransferase KAT6A/MOZ		
ACBI1	Bromodomain SMARCA2/4 PROTAC		
cisACBI1 (neg ctrl)	Bromodomain SMARCA2/4 PROTAC		
AZD5153	BRD2/4		
BI1347	Kinase CDK8		
BI1374 (neg ctrl)	Kinase CDK8 neg control		
XZL-1	KDM1		
CPTH2	HAT inhib,GCN5, KAT3B		
dTRIM24	Trim24		
GSK591	PRMT5		
IACS9571	Trim24		
MRK-740-NC	PRDM9 neg control		
NVS-MLLT-1	MLLT1		
SGC3027	PRMT7		
SGC3027N	PRMT7		
Tazemetostat (EPZ-6438)	EZH2		
TTK21	HAT activator		
VZ185	Bromodomain BRD7, BRD9 PROTAC		
cis VZ185 (neg ctrl)	Bromodomain BRD7, BRD9 PROTAC		
YX116-56B	SPIN1		
YX49-92B	SPIN1		
YX85-35	SPIN1		
SGC-iMLLT	MLLT1		

Supplementary Table 4: The IC₈₀ concentrations of the epigenetic compounds tested.

Compounds	Concentrations used (μM)
A485	0.9
ACBI1	0.1
JQ1	1.4
GSKJ4	7
SGCCBP30	5
GSKLSD1	1.5
GSK591	1.5
MZ1	1
IBRD9	8.5
DAC	2.3

Supplementary Table 5: Buffers

Western blot buffers

Name	Ingredients	Purpose
Tris/Glycine/SDS (TGS) Buffer (1X)	100 ml of 10X TGS buffer (Biorad, Catalog number:1610772) + 900 ml of Distilled water	Running buffer
Blocking buffer (1X)	40 ml of 1XTBS-T + 2 grams of Milk Powder (ROTH, Catalog number: T145.2)	Blocking buffer
10xTBS buffer	80 grams of NaCl (Sigma, Catalog number: 30620), 24.4 grams of Tris-Cl (Sigma, Catalog number: T1503-1kg), 1L of Distilled water, and adjusted pH to 7.6	Washing buffer(10X)
1X TBS-T buffer	100 ml of 10XTBS buffer, 900 ml of Distilled water, and 1 ml of Tween-20 (Sigma, Catalog number: SZBF3300V)	Washing buffer
Transfer buffer (10X)	30,3 grams of Tris-Cl (Sigma, Catalog number: T1503-1kg), 144 grams of Glycine (Sigma, Catalog number: 33226-1 kg), 1L of RNase-free water	Transfer buffer(10X)
Transfer buffer (1X)	100 ml of 10X Transfer buffer, 200 ml Methanol (Sigma, Catalog number: 32213-2.5L-M), and 700 ml of Distilled water	Transfer buffer

Agarose gel electrophoresis buffer

10xTris- borate-EDTA (TBE) buffer	Roth, Catalog number: 13061.2
-----------------------------------	-------------------------------

ACT-seq buffers

Wash buffer	50 mM Tris, pH 8.0 (500 µl of 1 M Tris, pH 7.5) (Sigma, Catalog number: T1503-1kg),
-------------	---

	150 mM NaCl (375 µl of 4 M NaCl) (Sigma, Catalog number: 30620)
	0.05% Triton X-100 (50 µl of 10% Triton X-100) (Sigma, Catalog number: 114H0521)
	9.075 ml H ₂ O
2X DMC buffer	100 mM Tris, pH 8.0 (1 ml of 1 M Tris, pH 7.5)
	0.3 M NaCl (0.75 ml of 4 M NaCl)
	0.1% of Triton X-100 (100 µl of 10% Triton X-100) (Sigma, Catalog number: 114H0521)
	25% of glycerol (2.5 ml of 100% glycerol) (Sigma, Catalog number: 15523-1L-R)
	5.65 ml H ₂ O (Ultrapure RNase-free water, Invitrogen, Catalog number: 10977-035)

4C-seq buffers

Ingredient	Final Concentration
500 µl of 1M TRIS pH 7.5 (Sigma, Catalog number: T1503-1kg)	50 mM
300 µl of 5M NaCl (Sigma, Catalog number: 30620)	150 mM
100 µl of 0.5M EDTA (Thermo Fischer, Catalog number: 00490837)	5 mM
500 µl of 10% NP-40 (Thermo Scientific, Catalog number: J60766-AP)	0.5%
500 µl of 20% Triton X-100 (Sigma, Catalog number: 114H0521)	1%
100 µl of 100X Proteasome inhibitor (Roche, Catalog number: 04693159001)	1X
8000 µl of H ₂ O	

HOT lysis buffer

Tris/ HCL pH 6.8	2.5 ml of 0.5 M (end concentration is 0.0625 M)	Sigma, Catalog number: T1503-1kg)
SDS	4 ml of 10% (end concentration is 2%)	ROTH, Catalog number: 0183.1

Glycerol	2 ml of 100% (end concentration is 10%)	Sigma, Catalog number: 15523-1L-R
DTT	20 μ l of 1 M (end concentration is 1mM)	Gerbu, Catalog number: 1008
Protease inhibitor	1 tablet	Roche, Catalog number: 04693159001
Sodium Orthovanadate	100 μ l of 200 mM (end concentration is 1mM)	Sigma, Catalog number: 6508
Sodium fluoride	200 μ l of 500 mM (end concentration is 5mM)	Sigma, Catalog number: 7920
PhosStop	2 tablets	Roche, Catalog number: 040906837001
H ₂ O	Up to 20 ml	(Ultrapure Distilled water, Invitrogen, Catalog number: 10977-035)

Supplementary Table 6: Kits

DNA isolation	DNeasy blood and tissue kit, Qiagen, Catalog number: 69506
RNA isolation	RNeasy plus mini kit, Qiagen, Catalog number: 74134
MiRNA isolation	RNeasy plus mini kit and RWT buffer (Qiagen, Catalog number: 1067933)
Qubit dsDNA HS kit	Invitrogen, Catalog number: Q32854
Qubit dsDNA BR kit	Invitrogen, Catalog number: Q32853
Qubit RNA HS kit	Invitrogen, Catalog number: Q32855
Qubit RNA BR kit	Invitrogen, Catalog number: Q10211
miRNA cDNA kit	miRCURY LNA RT kit, Qiagen, Catalog number: 339340
miRNA qPCR kit	miRCURY LNA SYBR Green PCR Kits, Qiagen, Catalog number: 339346
Plasmid isolation kit	Nucleospin plasmid transfection grade, MN, Catalog number: 740490.250
HiPure plasmid maxi prep isolation kit	Purelink, Catalog number: K210007
Neon Electroporation (10 μ l kit)	Invitrogen, Catalog number: MPK1096B
EZ DNA methylation kit	Zymo Research, Catalog number: D5002
Tapestation Highsensitivity DNA D1000	Agilent Technologies, Catalog number: 5067-5603, Lot number: 0006745365
Tapestation RNA	Agilent Technologies, Catalog number: 5067-5576, Lot number: 0202692145
NEBNext Small RNA Library Prep Set for Illumina Kit	NEB, catalog number: E7300S
Monarch PCR and DNA cleanup kit	NEB, catalog number: T1030S
MinElute kit	Qiagen, Catalog number: 28006

Supplementary Table 7: PCR reagents

Reagent	Ordering details
dNTP mix	Thermo Fischer, Catalog number: 0192
GC enhancer	Biolabs, Catalog number: B9028A
Q5 high-fidelity polymerase	Biolabs, Catalog number: M0491S
Water	Ultrapure Distilled water, Invitrogen, Catalog number: 10977-035
Q5 Reaction buffer	Biolabs, Catalog number: B9027S
25 mM MgCl ₂	Qiagen, Catalog number: 1005482
10X PCR buffer	Qiagen, Catalog number: 1005479
Hotstart Taq Polymerase-5 units/ μ l	Qiagen, Catalog number: 1007837

Supplementary Table 8: Primers

qPCR, cloning, and local deep bisulfite sequencing Miseq primers

Target gene	Forward Sequence	Reverse Sequence	Purpose	Hg19 coordinates
<i>MNX1-variant1</i>	GCCTAAGATG CCCGACTTC	GGTACTTGT TGAGCTTGA ACTGG	qPCR	Chr7: 156802358- 156802376 (forward) Chr7: 156799229- 156799251 (reverse)
<i>GAPDH</i>	GCCCAATACG ACCAAATCC	AGCCACATC GCTCAGACA C	qPCR	Chr6: 6643913- 6643933(forward) Chr6: 6643979- 6643997(reverse)
<i>LTR12C</i>	TCACTCTTTGG GTCCACACT	TGGAGTTGT TCGTTCCTC CC	qPCR	Multiple LTR12c
<i>MAGEA3</i>	TCCTGTGATCT TCAGCAAAGC TT	GGGTCCACT TCCATCAGC TC	qPCR	ChrX:151935655- 151935675(forward) ChrX: 151935706- 151935726 (reverse)
<i>NYES01</i>	TGCAGACCAC CGCCAACT	TCCACATCA ACAGGGAA AGCT	qPCR	chrX:153814797- 153814817 (forward) ChrX: 153814844- 153814864 (reverse)
<i>MNX1</i> exogenous	CTGCGCGACC TGAGAGATAG	GTTGCTGTA GGGGAAGT GGT	qPCR	-
<i>CAT7_1</i>	CTGCATCAGG GAGGCTATGT	TCATGACAG CCTCCTTCA CA	qPCR	Chr7:156309784- 156309804 (forward) Chr7:156309854- 156309874 (reverse 1)

				Chr7: 156310013-156310033 (reverse2)
<i>CAT7_2</i>	CAAGCACACC TCTGACGGAT	GCCATTGTG AATAGCACC GC	qPCR	Chr7: 156310865-156310885 (forward) Chr7: 156310945-156310965 (reverse)
<i>MNX1-AS1</i>	CCAAAGCTCT GCAGGTCGAA	GCTGCAGCA TTCTGGGAA AAG	qPCR	Chr7: 156803948-156803967 (forward) Chr7: 156808652-156808672 (reverse)
<i>MNX1-variant2</i>	TCCCCAGGAG GTTCGACT	GGGGGACT CTCAACAGT AGGT	qPCR	Chr7: 156799307-156799325 (forward) Chr7: 156801722-156801743(reverse)
<i>MNX1-AS2</i>	CAGCGCTAGA TGCCTCAGAC	TGGGTCAAT CCACTGCTA CC	qPCR	Chr7:156799075-156799095 (forward) Chr7: 156799639-156799659 (reverse)
<i>TFRC (CD17)</i>	ATCGGTTGGTG CCACTGAATGG	ACAACAGTG GGCTGGCAG AAAC	qPCR	Chr3: 195789731-195789752 (forward) Chr3: 195787080-195787101 (reverse)
<i>IPO5</i>	GTGGAGTACAC CGAACAGGTTG	TACTCAGGA CCACGGACT CTTG	qPCR	Chr13: 98664533-98664554 (forward) Chr13: 98666344-98666365 (reverse)
<i>ACOT7</i>	CTACACCTCCA AGCACTCTGTG	CCTTGTCCAC ATTCTTCAGC GAC	qPCR	Chr1: 6399533- 6399554 (forward) Chr1: 6393560- 6393582 (reverse)

Empty vector cloning forward and reverse	AATTCGGCTC CGGG	CGAACCCG GAGCCG	Cloning	-
Miseq Primer-Amplicon 1	TCGTCGGCAG CGTCAGATGT GTATAAGAGA CAGGGGGAGG TAGAGGTGGA GAG	GTCTCGTGG GCTCGGAG ATGTGTATA AGAGACAG ACAAATATA TCCCCTAAA CTCCC	Miseq	chr1:1097927-1097947 (forward) chr1:1098139-1098161 (reverse)
Miseq Primer-Amplicon 2	TCGTCGGCAG CGTCAGATGT GTATAAGAGA CAGYGTAGGT GATAGATGGG TTG	GTCTCGTGG GCTCGGAG ATGTGTATA AGAGACAG RTAAATCCA AAATAACTC CACAC	Miseq	chr1:1098736-1098755 (forward) chr1:1098851-1098893 (reverse)
Miseq Primer-Amplicon 3	TCGTCGGCAG CGTCAGATGT GTATAAGAGA CAGTAGGTAT GGGGTGTTTT AG	GTCTCGTGG GCTCGGAG ATGTGTATA AGAGACAG CRACCTCTA ACCAAAAA ATAC	Miseq	chr1:1098933-1098953 (forward) chr1:1099188-1099208 (reverse)
Miseq Primer-Amplicon 4	TCGTCGGCAG CGTCAGATGT GTATAAGAGA CAGTGGGAAT TGATTGATTAT GGTG	GTCTCGTGG GCTCGGAG ATGTGTATA AGAGACAG CCAACCATA	Miseq	chr1:1099486-1099508 (forward) chr1:1099684-1099707 (reverse)

		CTTTTAAAC ATTTC		
Miseq Primer- Amplicon 5	TCGTCGGCAG CGTCAGATGT GTATAAGAGA CAGYGTAGAG GGAAGAATTT GAGTG	GTCTCGTGG GCTCGGAG ATGTGTATA AGAGACAG CCRAATCCC ACCTACACA AAC	Miseq	chr1:1100038-1100060 (forward) chr1:1100258-1100277 (reverse)

4C-seq primers

<i>MNX1</i> exon2- intron2	BgIII_4CMNX1F	TCGTCGGCAGCGTCAGATGTGTATAA AGACAGTCGGGTTAATCATTAGATCT	Chr7:156802073-15680209
	NlaIII_4CMNX1R	GTCTCGTGGGCTCGGAGATGTGTATA GAGACAGCTGCCTGTAATTTGCGCTA T	Chr7:156800248-15680026
<i>MYB</i> intron4- intron5	BgIII_4CMYBR1	GTCTCGTGGGCTCGGAGATGTGTATA GAGACAGTCATTCTTCAGCGCCACAA ATCT	Chr6:135511182-13551120
	NlaIII_4CMYBF	TCGTCGGCAGCGTCAGATCTCTATAA AGACAGTCAGCTACCATTTTCCTGAT ACC	Chr6:135511885-13551190

Index primers

10 μ M Tn5mCP1n (Forward primer)	AATGATACGGCGAC CACCGAGATCTACA CTCGTCGGCAGCGTC	Miseq primers Index primers
10 μ M Tn5mCP1n- (reverse index primer 6)	CAAGCAGAAGACGG CATACGAGATCATGT CTCAGTCTCGTGGGC TCGG	Miseq primers Index primers
10 μ M Tn5mCP1n- (reverse index primer 8)	CAAGCAGAAGACGG CATACGAGATGTATC AGTCGTCTCGTGGGC TCGG	Miseq primers Index primers

10 μ M Tn5mCP1n- (reverse index primer 10)	CAAGCAGAAGACGG CATACGAGATCTAGT ACGGTCTCGTGGGCT CGG	Miseq primers Index primers
10 μ M Tn5mCP1n- (reverse index primer 16)	CAAGCAGAAGACGG CATACGAGATCCTCT CTGGTCTCGTGGGCT CGG	Miseq primers Index primers
10 μ M Tn5mCP1n- (reverse index primer 19)	CAAGCAGAAGACGG CATACGAGATTGCCT CTTGTCTCGTGGGCT CGG	Miseq primers Index primers
10 μ M Tn5mCP1n- (reverse index primer 20)	CAAGCAGAAGACGG CATACGAGATTCCTC TACGTCTCGTGGGCT CGG	Miseq primers Index primers
10 μ M Tn5mCP1n- (reverse index primer 9)	CAAGCAGAAGACGG CATACGAGATTCGCC TTAGTCTCGTGGGCT CGG	CTCF ACT-seq index primer
10 μ M Tn5mCP1n- (reverse index primer 10)	CAAGCAGAAGACGG CATACGAGATCTAGT ACGGTCTCGTGGGCT CGG	CTCF ACT-seq index primer
10 μ M Tn5mCP1n- (reverse index primer 11)	CAAGCAGAAGACGG CATACGAGATTTCTG CCTGTCTCGTGGGCT CGG	CTCF ACT-seq index primer

10 μ M Tn5mCP1n- (reverse index primer 12)	CAAGCAGAAGACGG CATACGAGATGCTC AGGAGTCTCGTGGG CTCGG	CTCF ACT-seq index primer
10 μ M Tn5mCP1n- (reverse index primer 13)	CAAGCAGAAGACGG CATACGAGATAGGA GTCCGTCTCGTGGGC TCGG	CTCF ACT-seq index primer
10 μ M Tn5mCP1n- (reverse index primer 14)	CAAGCAGAAGACGG CATACGAGATCATG CCTAGTCTCGTGGGC TCGG	CTCF ACT-seq index primer
10 μ M Tn5mCP1n- (reverse index primer 15)	CAAGCAGAAGACGG CATACGAGATGTAG AGAGGTCTCGTGGG CTCGG	IgG ACT-seq index primer
10 μ M Tn5mCP1n- (reverse index primer 16)	CAAGCAGAAGACGG CATACGAGATCCTCT CTGGTCTCGTGGGCT CGG	IgG ACT-seq index primer
10 μ M Tn5mCP1n- (reverse index primer 17)	CAAGCAGAAGACGG CATACGAGATAGCG TAGCGTCTCGTGGGC TCGG	IgG ACT-seq index primer
10 μ M Tn5mCP1n- (reverse index primer 18)	CAAGCAGAAGACGG CATACGAGATCAGC CTCGGTCTCGTGGGC TCGG	IgG ACT-seq index primer
10 μ M Tn5mCP1n- (reverse index primer 19)	CAAGCAGAAGACGG CATACGAGATTGCCT CTTGTCTCGTGGGCT CGG	IgG ACT-seq index primer

10 μ M Tn5mCP1n- (reverse index primer 20)	CAAGCAGAAGACGG CATACGAGATTCCTC TACGTCTCGTGGGCT CGG	IgG ACT-seq index primer
--	---	--------------------------

Supplementary Table 9: qPCR conditions

Temperature (°C)	Time per cycle	Number of cycles
95	3 min	1 cycle
95	15 sec	40 cycles
55	20 sec	
72	15-sec read	
Melting curve temperature (°C)	Melting curve time	Melting curve cycle number
95	5 sec	1 cycle
60	1 sec	
97	continuous	

Supplementary Table 10: Constructs used in the thesis.

pRCDEMP-EF1-GFP-HA-MNX1	Biocat, Germany
pRCDEMP-EF1-GFP-HA-EV	Generated via cloning
psiCheck2.0	Biocat, Germany
psiCHECK2.0-MNX13UTR	Biocat, Germany
psiCHECK2.0-mutMNX13UTR	Biocat, Germany
psPAX2	Plasmidfactory, Germany
pMD2.G	Plasmidfactory, Germany
BACe3.6	Kindly provided by Dieter Weichenhan (DKFZ, Heidelberg)
EcoRI cut BlueScriptII	Kindly provided by Dieter Weichenhan (DKFZ, Heidelberg)
pLVX-GFP-HA	Bought originally from Biocat, kindly provided by Dr. Ali Bakr, and used in publication PMID:34718742

Supplementary Table 11: miRNA qPCR probes

qPCR probes	Ordering details
miR-200a-3p	GeneGlobeID: YP00204707
miR-3180-5p	GeneGlobeID: YP02113327
miR-381-3p	GeneGlobeID: YP00205887
miR-410-3p	GeneGlobeID: YP00204042
U6 snRNA (v2)	GeneGlobeID: YP02119464
SNORD44	GeneGlobeID: YP00203902
Let-7b-3p	GeneGlobeID: YP00205653

Supplementary Table 12: miRNA mimics and qPCR conditions

Mimic	Ordering information	
Cel-miR-65-3p	Thermo Fischer, cat.no. MC22305	
Cel-miR-36-3p	Thermo Fischer, cat.no. MC10861	
Hsa-miR-381-3p	Qiagen, cat.no. MSY0000736	
Hsa-miR-410-3p	Qiagen, cat.no. MSY0002171	
Hsa-miR-200a-3p	Qiagen, cat.no. MSY0000682	
AllStars Negative Control siRNA (5nmol)	Qiagen, cat.no. SI03650318	
miRNA qPCR settings		
Step	Time	Temperature
Heat inactivation	2 mins	95°C
Denaturation	10 secs	95°C
Annealing/Extension	60 secs	56°C
Number of cycles	45	
Melting curve analysis		Between 60°C and 95°C

Supplementary Table 13: Antibodies

Antibodies	Ordering details	Purpose
Anti-MNX1	Bethyl, Catalog number: A303-184A	Western blot
Anti-B-actin	Santa-Cruz, Catalog number: 47778	Western blot
Anti-CTCF	Cell signaling, Catalog number:28995	ACT-seq
Anti-IgG	Merck, Catalog number: PP64	ACT-seq
Anti-HA	Sigma Aldrich, Catalog number: H6908	Western blot
Anti-GFP	Cell Signalling, Catalog number: 2956	Western blot
Anti-mouse IgG, HRP-linked secondary antibody	Cell Signalling, Catalog number: 7076P2	Western blot
Anti-rabbit	Cell Signalling, Catalog number: 7074	Western blot

Supplementary Table 14: Reagents used.

Reagent	Ordering information
2X Kapa 2G Robust HotStart ReadyMix	Kapa Biosystems, Catalog number: KK5702
2X SYBR Green buffer (primaquant)	Steinbrenner, Catalog number: SL-9902
4-Hydroxytamoxifen	Sigma, Catalog number: 508225
4X loading buffer (Protein)	Biorad, Catalog number: 1610474
5X- First strand buffer (cDNA)	Thermo Fischer, Catalog number: 902321
10X AMpute buffer	Kindly provided by Marion Bähr and Dr. Dieter Weichenhan
10X Ampure beads	Beckman Coulter, Catalog number: A63881
10X Cut smart buffer	NEB, Catalog number: B7200S
10X T4 ligase buffer with 10 mM ATP	Biolabs, Catalog number: B02025
100 μ M Oligo stock (cloning)	(NEB, Catalog number: N0440S)
Agarose	Boizym LE Agarose, Catalog number: 840004
Ampicilin-Soduim Salt	Merck, A918-56
AMPure XP beads	Beckman coulter, catalog number: A63880
Bacillol	HARTMANN, Reference number:973380-1000mL
Bacterial Peptone (Trypton/Pepton)	ROTH, Catalog number:6681.2
Betamercaptoethanol	PanReac, Applichem, Catalog number: A1108,0100
Benzoase 250 units/ μ l	ChemCruz, Catalog number: sc-202391
<i>Bg</i> III	NEB, Catalog number: R0143S
Bichinchoninic Acid solution (BCA)	Sigma, Catalog number: B9643-1L
BSA (Bovine serum albumin) - protein standard	Sigma, Catalog number: P0914-10Amp, Cas no: 9048-46-8
<i>Bst</i> BI restriction enzyme	Biolabs, Catalog number: R0519S
Cell Titer Blue	Promega, Catalog number: 68081
Chloroform	Analar Normapur, Catalog number: UN1888, Batch: 09F100512

Cocktail Phosphatase inhibitor PhosphoSTOP	Roche, Catalog number: 04096837001
Copper(II) Sulfate Solution	Sigma, Catalog number: C2284-25mL
DharmaFect transfection reagent	Dharmacon, Catalog number: T-2001-03
Dimethylsulfoxide (DMSO)	ROTH, Catalog number: 47204
DNA 100bp ladder	Invitrogen, Catalog number: 15628-050
DNase buffer (10X) with MgCl ₂ (cDNA)	Thermo Fischer, Catalog number: B43
DNase (1000U) (cDNA)	Thermo Fischer, Catalog number: EN0521
dNTP (cDNA)	Thermo Fischer, Catalog number: 0192
DTT (protein isolation)	Gerbu, Catalog number: 1008
DTT (0.1M) (cDNA)	Invitrogen, Catalog number: Y00147
NovEV ECL HRP Chemiluminescent Substrate Reagent Kit	Invitrogen, Catalog number: WP20005
<i>Eco</i> RI HF restriction enzyme	NEB, Catalog number: R3101S
EDTA (cDNA)	Thermo Fischer, Catalog number: 00490837
Ethyl alcohol	Sigma, Catalog number: 32205-2.5L-M
EtBr (Ethidium bromide)	Sigma, Catalog number: E-1510
Formaldehyde	Thermo Fischer, Catalog number: REF28906
Glycerol	Sigma, Catalog number: 15523-1L-R
Glycine	Sigma, Catalog number: 33226-1KG
Glycogen	Sigma, Catalog number: 501785294
HCl (Hydrochloric acid) (37%)	Fischer Scientific, Catalog number: AC450560050
High-fidelity NEB 2X PCR buffer (ACT-seq)	Biolabs, Catalog number: M05415
High-prep PCR beads	MagBio, Catalog number: AC60001E
Isopropyl alcohol	Honeywell, Catalog number: 33539-2.5L

Lambda HindIII	ROTH, Catalog number: X910.1
LB-Agar	BD, Reference number: 214010
Methanol	Sigma, Catalog number: 32213-2.5L-M
MG132	MedChemExpress, Catalog number: HY-13259
NaCl (Sodium Chloride)	Sigma, Catalog number: 71380-1KG-M
NEB3.1 buffer	NEB, Catalog number: B7203
NH ₄ .acetate	Serva, Catalog number: 39750
<i>Nla</i> III	NEB, Catalog number: R0125S
Phenol/Chloroform/Hydroxychlorin	Roth, Catalog number: A156.1
Proteinase K	Sigma, Catalog number: P-2308
Puromycin	Merck, Catalog number: P8833
Polybrene	Santa Cruz, Catalog number: sc-134220
Purple gel loading dye (6X)	Biolabs, Catalog number: B7024S
Qiazol	Qiagen, Catalog number: 5480397
Random hexamer (200ng/μl) (cDNA)	Thermo Fischer, Catalog number: 48190011
Ribolock RNase inhibitor	Invitrogen, Catalog number: E00381
RNaseA	Qiagen, Catalog number: 19101
PCR Buffer (10X)	Qiagen, Catalog number: 1005479
T4 Polynucleotide kinase	NEB, Catalog number: M0201S
T4 ligase	Biolabs, Catalog number: M0202L
T4 10X ligase buffer with 10 mm ATP	Biolabs, Catalog number: B02025
Tween-20	Sigma, Catalog number: P7949-100ml
<i>TransIT</i> -LT1	Mirus, Product number: MIR 2300
Triton X	Sigma, Catalog number: 114H0521
Trypan Blue stain 0.4%	Invitrogen, Reference number: T10282
SDS (Sodium dodecyl sulfate)	ROTH, Catalog number: 0183.1

Stabl3 competent cells	C737303, Thermo Fischer, and the cells were transformed to electrocompetent in-house by Oliver Mücke
SuperScript III reverse transcriptase	Invitrogen, Catalog number: 56575
Water (Ultrapure DNase and RNase free)	Invitrogen, Catalog number: 10977-035
Yeast extract	BB, Reference number: 212750

Supplementary Table 15: Consumables

Consumable	Ordering information
Combtips advanced (0.2 ml, 1 ml, 5 ml, 10 ml)	Eppendorf, Catalog number: 0030089642
DNA low bind tubes (1.5 ml, 2.0 ml)	Sarstedt, Catalog number: 72.706.700
Microtube (1.5 ml, 2.0 ml)	Sarstedt, Catalog number: 72.695.400
Parafilm	BEMIS, Catalog number: PM-996
PCR tubes-8er strips	Biozym, Catalog number: 23045
Plates	CellStar, Catalog number: 655180
Protein gels 4-20% TGX	Merck, Catalog number: PCG2016
Small (S) gloves	Starlab, Catalog number: SG-C-S

Supplementary Table 16: Machines used.

The first column shows the machines' names, and the second shows the brand and the purpose of using that machine.

Tapestation 4150	Agilent, quality control
Transilluminator	Amersham Imager 680, Western blot imaging
UV gel electrophoresis machine	Biorad, gel imaging
Nucleocounter NC250	Chemometec, cell counting
Shaker TH30	Edmund Bühler, bacterial shaker
Centrifuge 5424R	Eppendorf, centrifugation

Mastercycler ProS	Eppendorf, PCR
Thermomixer 1.5, 2.0 ml	Eppendorf, thermomixer
Multiporator	Eppendorf, electroporation
Duomax Shaker 1030	Heidolph, shaking
Sharp microwave	Inverter, microwave
Countess automatic cell counter	Invitrogen, cell counting
Qubit 2.0 fluorometer	Invitrogen, measuring DNA/RNA concentrations
SpectraMax iD3 plate reader	Molecular Devices, plate reader
Nanodrop Spectrometer	Reqlab, measuring DNA/RNA concentrations
Lightcycler 480 II	Roche, qPCR
Spanner	Sprout, spinning down
pH50 Benchmeter	Violab, pH meter
Vortexgenie 2	Vortexgenie2, Vortexing

Supplementary Table 17: Softwares used.

Adobe Illustrator	2024
SnapGene	7.0.1
Imagestudio	5.2.0
R studio	4.4.0
Graphpad	10.0
Spectramay iD3 Soft max	7.0

Supplementary Table 18: 4C-seq experiment PCR conditions.

Temperature	Conditions/Time
98°C	hold
98°C	30 seconds
98°C	15 seconds
54-49°C	20 seconds
72°C	120 seconds
98°C	15 seconds
49°C	20 seconds
72°C	120 seconds
72°C	3 minutes
10°C	hold

Supplementary Table 19: The names and the number of the reads obtained after the second 4C-seq.

vpname	nReads
40526MN_GDM-1_DMSO_rep1	1202926
40526MN_GDM-1_DAC_rep1	1079128
40526MN_GDM-1_DMSO_rep2	1498007
40526MN_GDM-1_DAC_rep2	1785456
40526MN_GDM-1_DMSO_rep3	1595207
40526MN_GDM-1_DAC_rep3	1246431
40526MY_GDM-1_DMSO_rep1	130128
40526MY_GDM-1_DAC_rep1	154713
40526MY_GDM-1_DMSO_rep2	203978
40526MY_GDM-1_DAC_rep2	652853
40526MY_GDM-1_DMSO_rep3	149404
40526MY_GDM-1_DAC_rep3	53849

8. References

- Abaza, Y., McMahon, C., & Garcia, J. S. (2024). Advancements and Challenges in the Treatment of AML. *Am Soc Clin Oncol Educ Book*, 44(3), e438662. https://doi.org/10.1200/EDBK_438662
- Achille, N. J., Othus, M., Phelan, K., Zhang, S., Cooper, K., Godwin, J. E., Appelbaum, F. R., Radich, J. P., Erba, H. P., Nand, S., & Zeleznik-Le, N. J. (2016). Association between early promoter-specific DNA methylation changes and outcome in older acute myeloid leukemia patients. *Leuk Res*, 42, 68-74. <https://doi.org/10.1016/j.leukres.2016.01.004>
- Agirre, X., Martinez-Climent, J. A., Otero, M. D., & Prosper, F. (2012). Epigenetic regulation of miRNA genes in acute leukemia. *Leukemia*, 26(3), 395-403. <https://doi.org/10.1038/leu.2011.344>
- Akerberg, B. N., & Pu, W. T. (2020). Genetic and Epigenetic Control of Heart Development. *Cold Spring Harb Perspect Biol*, 12(7). <https://doi.org/10.1101/cshperspect.a036756>
- Akhila Raj, T. V., Gopinath, P., Geetha Raj, J. A., Narayanan, G., Nair, S. G., Joy Philip, D. S., Raveendran, S., Geetha, P., & Sreedharan, H. (2022). Acute myeloid leukemia patients with variant or unusual translocations involving chromosomes 8 and 21 - A comprehensive cytogenetic profiling of three cases with review of literature. *J Cancer Res Ther*, 18(3), 697-703. https://doi.org/10.4103/jcrt.jcrt_190_21
- Aly, H. H., De Franco, E., Flanagan, S. E., & Elhenawy, Y. I. (2023). MNX1 mutations causing neonatal diabetes: Review of the literature and report of a case with extra-pancreatic congenital defects presenting in severe diabetic ketoacidosis. *J Diabetes Investig*, 14(4), 516-521. <https://doi.org/10.1111/jdi.13968>
- Arber, D. A., Orazi, A., Hasserjian, R. P., Borowitz, M. J., Calvo, K. R., Kvasnicka, H. M., Wang, S. A., Bagg, A., Barbui, T., Branford, S., Bueso-Ramos, C. E., Cortes, J. E., Dal Cin, P., DiNardo, C. D., Dombret, H., Duncavage, E. J., Ebert, B. L., Estey, E. H., Facchetti, F., Foucar, K., Gangat, N., Gianelli, U., Godley, L. A., Gokbuget, N., Gotlib, J., Hellstrom-Lindberg, E., Hobbs, G. S., Hoffman, R., Jabbour, E. J., Kiladjian, J. J., Larson, R. A., Le Beau, M. M., Loh, M. L., Lowenberg, B., Macintyre, E., Malcovati, L., Mullighan, C. G., Niemeyer, C., Odenike, O. M., Ogawa, S., Orfao, A., Papaemmanuil, E., Passamonti, F., Porkka, K., Pui, C. H., Radich, J. P., Reiter, A., Rozman, M., Rudelius, M., Savona, M. R., Schiffer, C. A., Schmitt-Graeff, A., Shimamura, A., Sierra, J., Stock, W. A., Stone, R. M., Tallman, M. S., Thiele, J., Tien, H. F., Tzankov, A., Vannucchi, A. M., Vyas, P., Wei, A. H., Weinberg, O. K., Wierzbowska, A., Cazzola, M., Dohner, H., & Tefferi, A. (2022). International Consensus Classification of Myeloid Neoplasms and Acute Leukemias: integrating morphologic, clinical, and genomic data. *Blood*, 140(11), 1200-1228. <https://doi.org/10.1182/blood.2022015850>
- Ardeljan, D., Taylor, M. S., Ting, D. T., & Burns, K. H. (2017). The Human Long Interspersed Element-1 Retrotransposon: An Emerging Biomarker of Neoplasia. *Clin Chem*, 63(4), 816-822. <https://doi.org/10.1373/clinchem.2016.257444>

- Baba, Y., Yagi, T., Sawayama, H., Hiyoshi, Y., Ishimoto, T., Iwatsuki, M., Miyamoto, Y., Yoshida, N., & Baba, H. (2018). Long Interspersed Element-1 Methylation Level as a Prognostic Biomarker in Gastrointestinal Cancers. *Digestion*, 97(1), 26-30. <https://doi.org/10.1159/000484104>
- Baer, C., Claus, R., & Plass, C. (2013). Genome-wide epigenetic regulation of miRNAs in cancer. *Cancer Res*, 73(2), 473-477. <https://doi.org/10.1158/0008-5472.CAN-12-3731>
- Balasubramanian, D., Borges Pinto, P., Grasso, A., Vincent, S., Tarayre, H., Lajoignie, D., & Ghavi-Helm, Y. (2024). Enhancer-promoter interactions can form independently of genomic distance and be functional across TAD boundaries. *Nucleic Acids Res*, 52(4), 1702-1719. <https://doi.org/10.1093/nar/gkad1183>
- Banerji, J., Olson, L., & Schaffner, W. (1983). A lymphocyte-specific cellular enhancer is located downstream of the joining region in immunoglobulin heavy chain genes. *Cell*, 33(3), 729-740. [https://doi.org/10.1016/0092-8674\(83\)90015-6](https://doi.org/10.1016/0092-8674(83)90015-6)
- Banuelos-Sanchez, G., Sanchez, L., Benitez-Guijarro, M., Sanchez-Carnerero, V., Salvador-Palomeque, C., Tristan-Ramos, P., Benkaddour-Boumzaouad, M., Morell, S., Garcia-Puche, J. L., Heras, S. R., Franco-Montalban, F., Tamayo, J. A., & Garcia-Perez, J. L. (2019). Synthesis and Characterization of Specific Reverse Transcriptase Inhibitors for Mammalian LINE-1 Retrotransposons. *Cell Chem Biol*, 26(8), 1095-1109 e1014. <https://doi.org/10.1016/j.chembiol.2019.04.010>
- Bauer, K., Hauswirth, A., Gleixner, K. V., Greiner, G., Thaler, J., Bettelheim, P., Filik, Y., Koller, E., Hoermann, G., Staber, P. B., Sperr, W. R., Keil, F., & Valent, P. (2024). BRD4 degraders may effectively counteract therapeutic resistance of leukemic stem cells in AML and ALL. *Am J Hematol*. <https://doi.org/10.1002/ajh.27385>
- Bejar, R., Lord, A., Stevenson, K., Bar-Natan, M., Perez-Ladaga, A., Zaneveld, J., Wang, H., Caughey, B., Stojanov, P., Getz, G., Garcia-Manero, G., Kantarjian, H., Chen, R., Stone, R. M., Neuberg, D., Steensma, D. P., & Ebert, B. L. (2014). TET2 mutations predict response to hypomethylating agents in myelodysplastic syndrome patients. *Blood*, 124(17), 2705-2712. <https://doi.org/10.1182/blood-2014-06-582809>
- Belgardt, B. F., Ahmed, K., Spranger, M., Latreille, M., Denzler, R., Kondratiuk, N., von Meyenn, F., Villena, F. N., Herrmanns, K., Bosco, D., Kerr-Conte, J., Pattou, F., Rulicke, T., & Stoffel, M. (2015). The microRNA-200 family regulates pancreatic beta cell survival in type 2 diabetes. *Nat Med*, 21(6), 619-627. <https://doi.org/10.1038/nm.3862>
- Benesova, S., Kubista, M., & Valihrach, L. (2021). Small RNA-Sequencing: Approaches and Considerations for miRNA Analysis. *Diagnostics (Basel)*, 11(6). <https://doi.org/10.3390/diagnostics11060964>
- Berson, A., Nativio, R., Berger, S. L., & Bonini, N. M. (2018). Epigenetic Regulation in Neurodegenerative Diseases. *Trends Neurosci*, 41(9), 587-598. <https://doi.org/10.1016/j.tins.2018.05.005>

- Bird, A., Taggart, M., Frommer, M., Miller, O. J., & Macleod, D. (1985). A fraction of the mouse genome that is derived from islands of nonmethylated, CpG-rich DNA. *Cell*, *40*(1), 91-99. [https://doi.org/10.1016/0092-8674\(85\)90312-5](https://doi.org/10.1016/0092-8674(85)90312-5)
- Bofill-De Ros, X., Hong, Z., Birkenfeld, B., Alamo-Ortiz, S., Yang, A., Dai, L., & Gu, S. (2022). Flexible pri-miRNA structures enable tunable production of 5' isomiRs. *RNA Biol*, *19*(1), 279-289. <https://doi.org/10.1080/15476286.2022.2025680>
- Briski, R., Garcia-Manero, G., Kantarjian, H., & Ravandi, F. (2023). The history of oral decitabine/cedazuridine and its potential role in acute myeloid leukemia. *Ther Adv Hematol*, *14*, 20406207231205429. <https://doi.org/10.1177/20406207231205429>
- Brown-Burke, F., Hwang, I., Sloan, S., Hinterschied, C., Helmig-Mason, J., Long, M., Chan, W. K., Prouty, A., Chung, J. H., Zhang, Y., Singh, S., Youssef, Y., Bhagwat, N., Chen, Z., Chen-Kiang, S., Di Liberto, M., Elemento, O., Sehgal, L., Alinari, L., Vaddi, K., Scherle, P., Lapalombella, R., Paik, J., & Baiocchi, R. A. (2023). PRMT5 inhibition drives therapeutic vulnerability to combination treatment with BCL-2 inhibition in mantle cell lymphoma. *Blood Adv*, *7*(20), 6211-6224. <https://doi.org/10.1182/bloodadvances.2023009906>
- Brown, E. J., Balaguer-Lluna, L., Cribbs, A. P., Philpott, M., Campo, L., Browne, M., Wong, J. F., Oppermann, U., Carcaboso, A. M., Bullock, A. N., & Farnie, G. (2024). PRMT5 inhibition shows in vitro efficacy against H3K27M-altered diffuse midline glioma, but does not extend survival in vivo. *Sci Rep*, *14*(1), 328. <https://doi.org/10.1038/s41598-023-48652-x>
- Bullinger, L., Dohner, K., & Dohner, H. (2017). Genomics of Acute Myeloid Leukemia Diagnosis and Pathways. *J Clin Oncol*, *35*(9), 934-946. <https://doi.org/10.1200/JCO.2016.71.2208>
- Cai, H., Kondo, M., Sandhow, L., Xiao, P., Johansson, A. S., Sasaki, T., Zawacka-Pankau, J., Tryggvason, K., Ungerstedt, J., Walfridsson, J., Ekblom, M., & Qian, H. (2022). Critical role of Lama4 for hematopoiesis regeneration and acute myeloid leukemia progression. *Blood*, *139*(20), 3040-3057. <https://doi.org/10.1182/blood.2021011510>
- Cancer Genome Atlas Research, N., Ley, T. J., Miller, C., Ding, L., Raphael, B. J., Mungall, A. J., Robertson, A., Hoadley, K., Triche, T. J., Jr., Laird, P. W., Baty, J. D., Fulton, L. L., Fulton, R., Heath, S. E., Kalicki-Veizer, J., Kandoth, C., Klco, J. M., Koboldt, D. C., Kanchi, K. L., Kulkarni, S., Lamprecht, T. L., Larson, D. E., Lin, L., Lu, C., McLellan, M. D., McMichael, J. F., Payton, J., Schmidt, H., Spencer, D. H., Tomasson, M. H., Wallis, J. W., Wartman, L. D., Watson, M. A., Welch, J., Wendl, M. C., Ally, A., Balasundaram, M., Birol, I., Butterfield, Y., Chiu, R., Chu, A., Chuah, E., Chun, H. J., Corbett, R., Dhalla, N., Guin, R., He, A., Hirst, C., Hirst, M., Holt, R. A., Jones, S., Karsan, A., Lee, D., Li, H. I., Marra, M. A., Mayo, M., Moore, R. A., Mungall, K., Parker, J., Pleasance, E., Plettner, P., Schein, J., Stoll, D., Swanson, L., Tam, A., Thiessen, N., Varhol, R., Wye, N., Zhao, Y., Gabriel, S., Getz, G., Sougnez, C., Zou, L., Leiserson, M. D., Vandin, F., Wu, H. T., Applebaum, F., Baylin, S. B., Akbani, R., Broom, B. M., Chen, K., Motter, T. C., Nguyen, K., Weinstein, J. N., Zhang, N., Ferguson, M. L., Adams, C., Black, A., Bowen, J., Gastier-

- Foster, J., Grossman, T., Lichtenberg, T., Wise, L., Davidsen, T., Demchok, J. A., Shaw, K. R., Sheth, M., Sofia, H. J., Yang, L., Downing, J. R., & Eley, G. (2013). Genomic and epigenomic landscapes of adult de novo acute myeloid leukemia. *N Engl J Med*, *368*(22), 2059-2074. <https://doi.org/10.1056/NEJMoa1301689>
- Cao, Y., Liu, Y., Shang, L., Wei, W., Shen, Y., Gu, Q., Xie, X., Dong, W., Lin, Y., Yue, Y., Wang, F., & Gu, W. (2020). Decitabine and all-trans retinoic acid synergistically exhibit cytotoxicity against elderly AML patients via miR-34a/MYCN axis. *Biomed Pharmacother*, *125*, 109878. <https://doi.org/10.1016/j.biopha.2020.109878>
- Carter, B., Ku, W. L., Kang, J. Y., Hu, G., Perrie, J., Tang, Q., & Zhao, K. (2020). Author Correction: Mapping histone modifications in low cell number and single cells using antibody-guided chromatin tagmentation (ACT-seq). *Nat Commun*, *11*(1), 4424. <https://doi.org/10.1038/s41467-020-18309-8>
- Carthew, R. W., & Sontheimer, E. J. (2009). Origins and Mechanisms of miRNAs and siRNAs. *Cell*, *136*(4), 642-655. <https://doi.org/10.1016/j.cell.2009.01.035>
- Chen, D. Q., Pan, B. Z., Huang, J. Y., Zhang, K., Cui, S. Y., De, W., Wang, R., & Chen, L. B. (2014). HDAC 1/4-mediated silencing of microRNA-200b promotes chemoresistance in human lung adenocarcinoma cells. *Oncotarget*, *5*(10), 3333-3349. <https://doi.org/10.18632/oncotarget.1948>
- Chen, H., Zeng, L., Zheng, W., Li, X., & Lin, B. (2020). Increased Expression of microRNA-141-3p Improves Necrotizing Enterocolitis of Neonates Through Targeting MNX1. *Front Pediatr*, *8*, 385. <https://doi.org/10.3389/fped.2020.00385>
- Chen, X., Yuan, L., Zhang, Y., Wang, F., Ma, X., Fang, J., Cao, P., Liu, Y., Liu, Z., Liu, M., Chen, J., Zhou, X., Liu, M., Jin, D., Wang, T., Lu, P., & Liu, H. (2024). Advances towards genome-based acute myeloid leukemia classification: A comparative analysis of WHO-HAEM4R, WHO-HAEM5, and International Consensus Classification. *Am J Hematol*, *99*(5), 824-835. <https://doi.org/10.1002/ajh.27249>
- Chen, Y., & Wang, X. (2020). miRDB: an online database for prediction of functional microRNA targets. *Nucleic Acids Res*, *48*(D1), D127-D131. <https://doi.org/10.1093/nar/gkz757>
- Chi, W., Xiu, B., Xiong, M., Wang, X., Li, P., Zhang, Q., Hou, J., Sang, Y., Zhou, X., Chen, M., Zheng, S., Zhang, L., Xue, J., Chi, Y., & Wu, J. (2023). MNX1 Promotes Anti-HER2 Therapy Sensitivity via Transcriptional Regulation of CD-M6PR in HER2-Positive Breast Cancer. *Int J Mol Sci*, *25*(1). <https://doi.org/10.3390/ijms25010221>
- Choi, P. W., Bahrapour, A., Ng, S. K., Liu, S. K., Qiu, W., Xie, F., Kuo, W. P., Kwong, J., Hales, K. H., Hales, D. B., Wong, K. K., Norwitz, E. R., Chow, C. K., Berkowitz, R. S., & Ng, S. W. (2020). Characterization of miR-200 family members as blood biomarkers for human and laying hen ovarian cancer. *Sci Rep*, *10*(1), 20071. <https://doi.org/10.1038/s41598-020-77068-0>
- Cimmino, L., Dolgalev, I., Wang, Y., Yoshimi, A., Martin, G. H., Wang, J., Ng, V., Xia, B., Witkowski, M. T., Mitchell-Flack, M., Grillo, I., Bakogianni, S., Ndiaye-Lobry, D., Martin, M. T., Guillamot, M., Banh, R. S., Xu, M., Figueroa, M. E., Dickins, R. A., Abdel-

- Wahab, O., Park, C. Y., Tsigirigos, A., Neel, B. G., & Aifantis, I. (2017). Restoration of TET2 Function Blocks Aberrant Self-Renewal and Leukemia Progression. *Cell*, *170*(6), 1079-1095 e1020. <https://doi.org/10.1016/j.cell.2017.07.032>
- Clement, T., Salone, V., & Rederstorff, M. (2015). Dual luciferase gene reporter assays to study miRNA function. *Methods Mol Biol*, *1296*, 187-198. https://doi.org/10.1007/978-1-4939-2547-6_17
- Conery, A. R., Centore, R. C., Neiss, A., Keller, P. J., Joshi, S., Spillane, K. L., Sandy, P., Hatton, C., Pardo, E., Zawadzke, L., Bommi-Reddy, A., Gascoigne, K. E., Bryant, B. M., Mertz, J. A., & Sims, R. J. (2016). Bromodomain inhibition of the transcriptional coactivators CBP/EP300 as a therapeutic strategy to target the IRF4 network in multiple myeloma. *Elife*, *5*. <https://doi.org/10.7554/eLife.10483>
- Cook, M. R., Karp, J. E., & Lai, C. (2022). The spectrum of genetic mutations in myelodysplastic syndrome: Should we update prognostication? *EJHaem*, *3*(1), 301-313. <https://doi.org/10.1002/jha2.317>
- Cottone, L., Cribbs, A. P., Khandelwal, G., Wells, G., Ligammari, L., Philpott, M., Tumber, A., Lombard, P., Hookway, E. S., Szommer, T., Johansson, C., Brennan, P. E., Pillay, N., Jenner, R. G., Oppermann, U., & Flanagan, A. M. (2020). Inhibition of Histone H3K27 Demethylases Inactivates Brachyury (TBXT) and Promotes Chordoma Cell Death. *Cancer Res*, *80*(20), 4540-4551. <https://doi.org/10.1158/0008-5472.CAN-20-1387>
- Craig, J. M., & Bickmore, W. A. (1994). The distribution of CpG islands in mammalian chromosomes. *Nat Genet*, *7*(3), 376-382. <https://doi.org/10.1038/ng0794-376>
- Creutzig, U., van den Heuvel-Eibrink, M. M., Gibson, B., Dworzak, M. N., Adachi, S., de Bont, E., Harbott, J., Hasle, H., Johnston, D., Kinoshita, A., Lehrnbecher, T., Leverger, G., Mejstrikova, E., Meshinchi, S., Pession, A., Raimondi, S. C., Sung, L., Stary, J., Zwaan, C. M., Kaspers, G. J., Reinhardt, D., & Group, A. M. L. C. o. t. I. B. S. (2012). Diagnosis and management of acute myeloid leukemia in children and adolescents: recommendations from an international expert panel. *Blood*, *120*(16), 3187-3205. <https://doi.org/10.1182/blood-2012-03-362608>
- Cusan, M., Cai, S. F., Mohammad, H. P., Krivtsov, A., Chramiec, A., Loizou, E., Witkin, M. D., Smitheman, K. N., Tenen, D. G., Ye, M., Will, B., Steidl, U., Kruger, R. G., Levine, R. L., Rienhoff, H. Y., Jr., Koche, R. P., & Armstrong, S. A. (2018). LSD1 inhibition exerts its antileukemic effect by recommissioning PU.1- and C/EBPalpha-dependent enhancers in AML. *Blood*, *131*(15), 1730-1742. <https://doi.org/10.1182/blood-2017-09-807024>
- da Costa-Nunes, J. A., & Noordermeer, D. (2023). TADs: Dynamic structures to create stable regulatory functions. *Curr Opin Struct Biol*, *81*, 102622. <https://doi.org/10.1016/j.sbi.2023.102622>
- Dalpatraj, N., Naik, A., & Thakur, N. (2023). GSK-J4: An H3K27 histone demethylase inhibitor, as a potential anti-cancer agent. *Int J Cancer*, *153*(6), 1130-1138. <https://doi.org/10.1002/ijc.34559>

- Damaschke, N. A., Gawdzik, J., Avilla, M., Yang, B., Svaren, J., Roopra, A., Luo, J. H., Yu, Y. P., Keles, S., & Jarrard, D. F. (2020). CTCF loss mediates unique DNA hypermethylation landscapes in human cancers. *Clin Epigenetics*, *12*(1), 80. <https://doi.org/10.1186/s13148-020-00869-7>
- Dang, L., White, D. W., Gross, S., Bennett, B. D., Bittinger, M. A., Driggers, E. M., Fantin, V. R., Jang, H. G., Jin, S., Keenan, M. C., Marks, K. M., Prins, R. M., Ward, P. S., Yen, K. E., Liao, L. M., Rabinowitz, J. D., Cantley, L. C., Thompson, C. B., Vander Heiden, M. G., & Su, S. M. (2009). Cancer-associated IDH1 mutations produce 2-hydroxyglutarate. *Nature*, *462*(7274), 739-744. <https://doi.org/10.1038/nature08617>
- Delhommeau, F., Dupont, S., Della Valle, V., James, C., Trannoy, S., Masse, A., Kosmider, O., Le Couedic, J. P., Robert, F., Alberdi, A., Lecluse, Y., Plo, I., Dreyfus, F. J., Marzac, C., Casadevall, N., Lacombe, C., Romana, S. P., Dessen, P., Soulier, J., Viguie, F., Fontenay, M., Vainchenker, W., & Bernard, O. A. (2009). Mutation in TET2 in myeloid cancers. *N Engl J Med*, *360*(22), 2289-2301. <https://doi.org/10.1056/NEJMoa0810069>
- Desai, P., Mencia-Trinchant, N., Savenkov, O., Simon, M. S., Cheang, G., Lee, S., Samuel, M., Ritchie, E. K., Guzman, M. L., Ballman, K. V., Roboz, G. J., & Hassane, D. C. (2018). Somatic mutations precede acute myeloid leukemia years before diagnosis. *Nat Med*, *24*(7), 1015-1023. <https://doi.org/10.1038/s41591-018-0081-z>
- Desai, R. H., Zandvakili, N., & Bohlander, S. K. (2022). Dissecting the Genetic and Non-Genetic Heterogeneity of Acute Myeloid Leukemia Using Next-Generation Sequencing and In Vivo Models. *Cancers (Basel)*, *14*(9). <https://doi.org/10.3390/cancers14092182>
- DiNardo, C. D., & Cortes, J. E. (2016). Mutations in AML: prognostic and therapeutic implications. *Hematology Am Soc Hematol Educ Program*, *2016*(1), 348-355. <https://doi.org/10.1182/asheducation-2016.1.348>
- DiNardo, C. D., Jonas, B. A., Pullarkat, V., Thirman, M. J., Garcia, J. S., Wei, A. H., Konopleva, M., Dohner, H., Letai, A., Fenaux, P., Koller, E., Havelange, V., Leber, B., Esteve, J., Wang, J., Pejsa, V., Hajek, R., Porkka, K., Illes, A., Lavie, D., Lemoli, R. M., Yamamoto, K., Yoon, S. S., Jang, J. H., Yeh, S. P., Turgut, M., Hong, W. J., Zhou, Y., Potluri, J., & Pratz, K. W. (2020). Azacitidine and Venetoclax in Previously Untreated Acute Myeloid Leukemia. *N Engl J Med*, *383*(7), 617-629. <https://doi.org/10.1056/NEJMoa2012971>
- Ding, M., Sun, X., Zhong, J., Zhang, C., Tian, Y., Ge, J., Zhang, C. Y., Zen, K., Wang, J. J., Zhang, C., & Wang, C. (2018). Decreased miR-200a-3p is a key regulator of renal carcinoma growth and migration by directly targeting CBL. *J Cell Biochem*, *119*(12), 9974-9985. <https://doi.org/10.1002/jcb.27326>
- Dixon, J. R., Xu, J., Dileep, V., Zhan, Y., Song, F., Le, V. T., Yardimci, G. G., Chakraborty, A., Bann, D. V., Wang, Y., Clark, R., Zhang, L., Yang, H., Liu, T., Iyyanki, S., An, L., Pool, C., Sasaki, T., Rivera-Mulia, J. C., Ozadam, H., Lajoie, B. R., Kaul, R., Buckley, M., Lee, K., Diegel, M., Pezic, D., Ernst, C., Hadjur, S., Odom, D. T., Stamatoyannopoulos, J. A., Broach, J. R., Hardison, R. C., Ay, F., Noble, W. S., Dekker, J., Gilbert, D. M., & Yue, F.

- (2018). Integrative detection and analysis of structural variation in cancer genomes. *Nat Genet*, 50(10), 1388-1398. <https://doi.org/10.1038/s41588-018-0195-8>
- Dohner, H., Wei, A. H., Appelbaum, F. R., Craddock, C., DiNardo, C. D., Dombret, H., Ebert, B. L., Fenaux, P., Godley, L. A., Hasserjian, R. P., Larson, R. A., Levine, R. L., Miyazaki, Y., Niederwieser, D., Ossenkoppele, G., Rollig, C., Sierra, J., Stein, E. M., Tallman, M. S., Tien, H. F., Wang, J., Wierzbowska, A., & Lowenberg, B. (2022). Diagnosis and management of AML in adults: 2022 recommendations from an international expert panel on behalf of the ELN. *Blood*, 140(12), 1345-1377. <https://doi.org/10.1182/blood.2022016867>
- Du, F., Jin, T., & Wang, L. (2023). Mechanism of Action of Decitabine in the Treatment of Acute Myeloid Leukemia by Regulating LINC00599. *Anal Cell Pathol (Amst)*, 2023, 2951519. <https://doi.org/10.1155/2023/2951519>
- Edwards, J. R., Yarychivska, O., Boulard, M., & Bestor, T. H. (2017). DNA methylation and DNA methyltransferases. *Epigenetics Chromatin*, 10, 23. <https://doi.org/10.1186/s13072-017-0130-8>
- El Amrani, Z., Natiq, A., Sbiti, A., Ratbi, I., Liehr, T., Sefiani, A., & Sahli, M. (2024). Currarino Syndrome in Two Moroccan Siblings with Inherited 7q36 Deletion due to Maternal t(7;21)(q36;p11)mat: A Case Report. *Mol Syndromol*, 15(2), 125-129. <https://doi.org/10.1159/000534432>
- Espersen, A. D. L., Noren-Nystrom, U., Abrahamsson, J., Ha, S. Y., Pronk, C. J., Jahnukainen, K., Jonsson, O. G., Lausen, B., Palle, J., Zeller, B., Palmqvist, L., & Hasle, H. (2018). Acute myeloid leukemia (AML) with t(7;12)(q36;p13) is associated with infancy and trisomy 19: Data from Nordic Society for Pediatric Hematology and Oncology (NOPHO-AML) and review of the literature. *Genes Chromosomes Cancer*, 57(7), 359-365. <https://doi.org/10.1002/gcc.22538>
- Ewing, A. D., Smits, N., Sanchez-Luque, F. J., Faivre, J., Brennan, P. M., Richardson, S. R., Cheetham, S. W., & Faulkner, G. J. (2020). Nanopore Sequencing Enables Comprehensive Transposable Element Epigenomic Profiling. *Mol Cell*, 80(5), 915-928 e915. <https://doi.org/10.1016/j.molcel.2020.10.024>
- Fabbri, M., Calore, F., Paone, A., Galli, R., & Calin, G. A. (2013). Epigenetic regulation of miRNAs in cancer. *Adv Exp Med Biol*, 754, 137-148. https://doi.org/10.1007/978-1-4419-9967-2_6
- Farnaby, W., Koegl, M., Roy, M. J., Whitworth, C., Diers, E., Trainor, N., Zollman, D., Steurer, S., Karolyi-Oezguer, J., Riedmueller, C., Gmaschitz, T., Wachter, J., Dank, C., Galant, M., Sharps, B., Rumpel, K., Traxler, E., Gerstberger, T., Schnitzer, R., Petermann, O., Greb, P., Weinstabl, H., Bader, G., Zoepfel, A., Weiss-Puxbaum, A., Ehrenhofer-Wolfer, K., Wohrle, S., Boehmelt, G., Rinnenthal, J., Arnhof, H., Wiechens, N., Wu, M. Y., Owen-Hughes, T., Ettmayer, P., Pearson, M., McConnell, D. B., & Ciulli, A. (2019). BAF complex vulnerabilities in cancer demonstrated via structure-based PROTAC design. *Nat Chem Biol*, 15(7), 672-680. <https://doi.org/10.1038/s41589-019-0294-6>

- Federico, C., Leotta, C. G., Bruno, F., Longo, A. M., Owoka, T., Tosi, S., & Saccone, S. (2017). Nuclear Repositioning of the Non-Translocated HLXB9 Allele in the Leukaemia Cell Line GDM-1 Harboring a t(6;7)(q23;q36). *Cytogenet Genome Res*, 153(1), 10-17. <https://doi.org/10.1159/000480745>
- Federico, C., Owoka, T., Ragusa, D., Sturiale, V., Caponnetto, D., Leotta, C. G., Bruno, F., Foster, H. A., Rigamonti, S., Giudici, G., Cazzaniga, G., Bridger, J. M., Sisu, C., Saccone, S., & Tosi, S. (2019). Deletions of Chromosome 7q Affect Nuclear Organization and HLXB9 Gene Expression in Hematological Disorders. *Cancers (Basel)*, 11(4). <https://doi.org/10.3390/cancers11040585>
- Ferrell, J. E., Jr. (2012). Bistability, bifurcations, and Waddington's epigenetic landscape. *Curr Biol*, 22(11), R458-466. <https://doi.org/10.1016/j.cub.2012.03.045>
- Fontana, A., Barbano, R., Dama, E., Pasculli, B., Rendina, M., Morritti, M. G., Melocchi, V., Castelvete, M., Valori, V. M., Ravaioli, S., Bravaccini, S., Ciuffreda, L., Graziano, P., Maiello, E., Copetti, M., Fazio, V. M., Esteller, M., Bianchi, F., & Parrella, P. (2021). Combined analysis of miR-200 family and its significance for breast cancer. *Sci Rep*, 11(1), 2980. <https://doi.org/10.1038/s41598-021-82286-1>
- Forsberg, M., & Konopleva, M. (2024). AML treatment: conventional chemotherapy and emerging novel agents. *Trends Pharmacol Sci*, 45(5), 430-448. <https://doi.org/10.1016/j.tips.2024.03.005>
- Fukumoto, K., Ito, K., Saer, B., Taylor, G., Ye, S., Yamano, M., Toriba, Y., Hayes, A., Okamura, H., & Fustin, J. M. (2022). Excess S-adenosylmethionine inhibits methylation via catabolism to adenine. *Commun Biol*, 5(1), 313. <https://doi.org/10.1038/s42003-022-03280-5>
- Furukawa, Y., Sutheesophon, K., Wada, T., Nishimura, M., Saito, Y., Ishii, H., & Furukawa, Y. (2005). Methylation silencing of the Apaf-1 gene in acute leukemia. *Mol Cancer Res*, 3(6), 325-334. <https://doi.org/10.1158/1541-7786.MCR-04-0105>
- Gao, H., He, X., Li, Q., Wang, Y., Tian, Y., Chen, X., Wang, J., Guo, Y., Wang, W., & Li, X. (2020). Genome-wide DNA methylome analysis reveals methylation subtypes with different clinical outcomes for acute myeloid leukemia patients. *Cancer Med*, 9(17), 6296-6305. <https://doi.org/10.1002/cam4.3291>
- Gardiner-Garden, M., & Frommer, M. (1987). CpG islands in vertebrate genomes. *J Mol Biol*, 196(2), 261-282. [https://doi.org/10.1016/0022-2836\(87\)90689-9](https://doi.org/10.1016/0022-2836(87)90689-9)
- Gillies, S. D., Morrison, S. L., Oi, V. T., & Tonegawa, S. (1983). A tissue-specific transcription enhancer element is located in the major intron of a rearranged immunoglobulin heavy chain gene. *Cell*, 33(3), 717-728. [https://doi.org/10.1016/0092-8674\(83\)90014-4](https://doi.org/10.1016/0092-8674(83)90014-4)
- Goyal, A., Bauer, J., Hey, J., Papageorgiou, D. N., Stepanova, E., Daskalakis, M., Scheid, J., Dubbelaar, M., Klimovich, B., Schwarz, D., Marklin, M., Roerden, M., Lin, Y. Y., Ma, T., Mucke, O., Rammensee, H. G., Lubbert, M., Loayza-Puch, F., Krijgsveld, J., Walz, J. S., & Plass, C. (2023). DNMT and HDAC inhibition induces immunogenic neoantigens from

- human endogenous retroviral element-derived transcripts. *Nat Commun*, 14(1), 6731. <https://doi.org/10.1038/s41467-023-42417-w>
- Gulino, G. M., Bruno, F., Sturiale, V., Brancato, D., Ragusa, D., Tosi, S., Saccone, S., & Federico, C. (2021). From FISH to Hi-C: The Chromatin Architecture of the Chromosomal Region 7q36.3, Frequently Rearranged in Leukemic Cells, Is Evolutionary Conserved. *Int J Mol Sci*, 22(5). <https://doi.org/10.3390/ijms22052338>
- Gunn, K., Myllykoski, M., Cao, J. Z., Ahmed, M., Huang, B., Rouaisnel, B., Diplas, B. H., Levitt, M. M., Looper, R., Doench, J. G., Ligon, K. L., Kornblum, H. I., McBrayer, S. K., Yan, H., Duy, C., Godley, L. A., Koivunen, P., & Losman, J. A. (2023). (R)-2-Hydroxyglutarate Inhibits KDM5 Histone Lysine Demethylases to Drive Transformation in IDH-Mutant Cancers. *Cancer Discov*, 13(6), 1478-1497. <https://doi.org/10.1158/2159-8290.CD-22-0825>
- Ha, M., & Kim, V. N. (2014). Regulation of microRNA biogenesis. *Nat Rev Mol Cell Biol*, 15(8), 509-524. <https://doi.org/10.1038/nrm3838>
- Hackanson, B., & Daskalakis, M. (2014). Decitabine. *Recent Results Cancer Res*, 201, 269-297. https://doi.org/10.1007/978-3-642-54490-3_18
- Hammitzsch, A., Tallant, C., Fedorov, O., O'Mahony, A., Brennan, P. E., Hay, D. A., Martinez, F. O., Al-Mossawi, M. H., de Wit, J., Vecellio, M., Wells, C., Wordsworth, P., Muller, S., Knapp, S., & Bowness, P. (2015). CBP30, a selective CBP/p300 bromodomain inhibitor, suppresses human Th17 responses. *Proc Natl Acad Sci U S A*, 112(34), 10768-10773. <https://doi.org/10.1073/pnas.1501956112>
- Han, H., Lee, H. J., Kim, K. S., Chung, J., & Na, H. S. (2024). Comparison of the performance of MiSeq and NovaSeq in oral microbiome study. *J Oral Microbiol*, 16(1), 2344293. <https://doi.org/10.1080/20002297.2024.2344293>
- Hanahan, D. (2022). Hallmarks of Cancer: New Dimensions. *Cancer Discov*, 12(1), 31-46. <https://doi.org/10.1158/2159-8290.CD-21-1059>
- Harrison, K. A., Thaler, J., Pfaff, S. L., Gu, H., & Kehrl, J. H. (1999). Pancreas dorsal lobe agenesis and abnormal islets of Langerhans in Hlx9-deficient mice. *Nat Genet*, 23(1), 71-75. <https://doi.org/10.1038/12674>
- Hayday, A. C., Gillies, S. D., Saito, H., Wood, C., Wiman, K., Hayward, W. S., & Tonegawa, S. (1984). Activation of a translocated human c-myc gene by an enhancer in the immunoglobulin heavy-chain locus. *Nature*, 307(5949), 334-340. <https://doi.org/10.1038/307334a0>
- Herceg, Z., & Vaissiere, T. (2011). Epigenetic mechanisms and cancer: an interface between the environment and the genome. *Epigenetics*, 6(7), 804-819. <https://doi.org/10.4161/epi.6.7.16262>
- Hinohara, K., Wu, H. J., Sebastien, V., McDonald, T. O., Igarashi, K. J., Yamamoto, K. N., Madsen, T., Fassl, A., Egri, S. B., Papanastasiou, M., Ding, L., Peluffo, G., Cohen, O., Kales, S. C., Lal-Nag, M., Rai, G., Maloney, D. J., Jadhav, A., Simeonov, A., Wagle, N., Brown, M., Meissner, A., Sicinski, P., Jaffe, J. D., Jeselsohn, R., Gimelbrant, A. A.,

- Michor, F., & Polyak, K. (2019). KDM5 Histone Demethylase Activity Links Cellular Transcriptomic Heterogeneity to Therapeutic Resistance. *Cancer Cell*, 35(2), 330-332. <https://doi.org/10.1016/j.ccell.2019.01.012>
- Hnisz, D., Day, D. S., & Young, R. A. (2016). Insulated Neighborhoods: Structural and Functional Units of Mammalian Gene Control. *Cell*, 167(5), 1188-1200. <https://doi.org/10.1016/j.cell.2016.10.024>
- Hofer, T., & Rodewald, H. R. (2018). Differentiation-based model of hematopoietic stem cell functions and lineage pathways. *Blood*, 132(11), 1106-1113. <https://doi.org/10.1182/blood-2018-03-791517>
- Hu, X., Zhang, L., Mao, S. Q., Li, Z., Chen, J., Zhang, R. R., Wu, H. P., Gao, J., Guo, F., Liu, W., Xu, G. F., Dai, H. Q., Shi, Y. G., Li, X., Hu, B., Tang, F., Pei, D., & Xu, G. L. (2014). Tet and TDG mediate DNA demethylation essential for mesenchymal-to-epithelial transition in somatic cell reprogramming. *Cell Stem Cell*, 14(4), 512-522. <https://doi.org/10.1016/j.stem.2014.01.001>
- Huang, F., Sun, J., Chen, W., He, X., Zhu, Y., Dong, H., Wang, H., Li, Z., Zhang, L., Khaled, S., Marcucci, G., Huang, J., & Li, L. (2020). HDAC4 inhibition disrupts TET2 function in high-risk MDS and AML. *Aging (Albany NY)*, 12(17), 16759-16774. <https://doi.org/10.18632/aging.103605>
- Huang, H. Y., Lin, Y. C., Cui, S., Huang, Y., Tang, Y., Xu, J., Bao, J., Li, Y., Wen, J., Zuo, H., Wang, W., Li, J., Ni, J., Ruan, Y., Li, L., Chen, Y., Xie, Y., Zhu, Z., Cai, X., Chen, X., Yao, L., Chen, Y., Luo, Y., LuXu, S., Luo, M., Chiu, C. M., Ma, K., Zhu, L., Cheng, G. J., Bai, C., Chiang, Y. C., Wang, L., Wei, F., Lee, T. Y., & Huang, H. D. (2022). miRTarBase update 2022: an informative resource for experimentally validated miRNA-target interactions. *Nucleic Acids Res*, 50(D1), D222-D230. <https://doi.org/10.1093/nar/gkab1079>
- Inaba, T., Honda, H., & Matsui, H. (2018). The enigma of monosomy 7. *Blood*, 131(26), 2891-2898. <https://doi.org/10.1182/blood-2017-12-822262>
- Ingenhag, D., Reister, S., Auer, F., Bhatia, S., Wildenhain, S., Picard, D., Remke, M., Hoell, J. I., Kloetgen, A., Sohn, D., Janicke, R. U., Koegler, G., Borkhardt, A., & Hauer, J. (2019). The homeobox transcription factor HB9 induces senescence and blocks differentiation in hematopoietic stem and progenitor cells. *Haematologica*, 104(1), 35-46. <https://doi.org/10.3324/haematol.2018.189407>
- Issa, H., Bhayadia, R., Winkler, R., Swart, L. E., Heckl, D., & Klusmann, J. H. (2023). Preclinical testing of miRNA-193b-3p mimic in acute myeloid leukemias. *Leukemia*, 37(7), 1583-1587. <https://doi.org/10.1038/s41375-023-01937-6>
- Itzykson, R., Kosmider, O., Cluzeau, T., Mansat-De Mas, V., Dreyfus, F., Beyne-Rauzy, O., Quesnel, B., Vey, N., Gelsi-Boyer, V., Raynaud, S., Preudhomme, C., Ades, L., Fenaux, P., Fontenay, M., & Groupe Francophone des, M. (2011). Impact of TET2 mutations on response rate to azacitidine in myelodysplastic syndromes and low blast count acute myeloid leukemias. *Leukemia*, 25(7), 1147-1152. <https://doi.org/10.1038/leu.2011.71>

- Iwakawa, H. O., & Tomari, Y. (2015). The Functions of MicroRNAs: mRNA Decay and Translational Repression. *Trends Cell Biol*, 25(11), 651-665. <https://doi.org/10.1016/j.tcb.2015.07.011>
- Jang, H. S., Shin, W. J., Lee, J. E., & Do, J. T. (2017). CpG and Non-CpG Methylation in Epigenetic Gene Regulation and Brain Function. *Genes (Basel)*, 8(6). <https://doi.org/10.3390/genes8060148>
- Jonas, B. A., & Pollyea, D. A. (2019). How we use venetoclax with hypomethylating agents for the treatment of newly diagnosed patients with acute myeloid leukemia. *Leukemia*, 33(12), 2795-2804. <https://doi.org/10.1038/s41375-019-0612-8>
- Kaluscha, S., Domcke, S., Wirbelauer, C., Stadler, M. B., Durdu, S., Burger, L., & Schubeler, D. (2022). Evidence that direct inhibition of transcription factor binding is the prevailing mode of gene and repeat repression by DNA methylation. *Nat Genet*, 54(12), 1895-1906. <https://doi.org/10.1038/s41588-022-01241-6>
- Kaushik, S., Liu, F., Veazey, K. J., Gao, G., Das, P., Neves, L. F., Lin, K., Zhong, Y., Lu, Y., Giuliani, V., Bedford, M. T., Nimer, S. D., & Santos, M. A. (2018). Genetic deletion or small-molecule inhibition of the arginine methyltransferase PRMT5 exhibit anti-tumoral activity in mouse models of MLL-rearranged AML. *Leukemia*, 32(2), 499-509. <https://doi.org/10.1038/leu.2017.206>
- Kayabolen, A., Yilmaz, E., Sahin, G. N., Seker-Polat, F., Cingoz, A., Isik, B., Acar, S., Wakimoto, H., Cahill, D. P., Solaroglu, I., Cribbs, A. P., Oppermann, U., & Bagci-Onder, T. (2022). Orthogonal targeting of KDM6A/B and HDACs mediates potent therapeutic effects in IDH1-mutant glioma. *bioRxiv*, 2020.2011.2026.400234. <https://doi.org/10.1101/2020.11.26.400234>
- Kayser, S., & Levis, M. J. (2022). Updates on targeted therapies for acute myeloid leukaemia. *Br J Haematol*, 196(2), 316-328. <https://doi.org/10.1111/bjh.17746>
- Kayser, S., & Levis, M. J. (2023). The clinical impact of the molecular landscape of acute myeloid leukemia. *Haematologica*, 108(2), 308-320. <https://doi.org/10.3324/haematol.2022.280801>
- Kellaway, S., Chin, P. S., Barneh, F., Bonifer, C., & Heidenreich, O. (2020). t(8;21) Acute Myeloid Leukemia as a Paradigm for the Understanding of Leukemogenesis at the Level of Gene Regulation and Chromatin Programming. *Cells*, 9(12). <https://doi.org/10.3390/cells9122681>
- Khoury, J. D., Solary, E., Abla, O., Akkari, Y., Alaggio, R., Apperley, J. F., Bejar, R., Berti, E., Busque, L., Chan, J. K. C., Chen, W., Chen, X., Chng, W. J., Choi, J. K., Colmenero, I., Coupland, S. E., Cross, N. C. P., De Jong, D., Elghetany, M. T., Takahashi, E., Emile, J. F., Ferry, J., Fogelstrand, L., Fontenay, M., Germing, U., Gujral, S., Haferlach, T., Harrison, C., Hodge, J. C., Hu, S., Jansen, J. H., Kanagal-Shamanna, R., Kantarjian, H. M., Kratz, C. P., Li, X. Q., Lim, M. S., Loeb, K., Loghavi, S., Marcogliese, A., Meshinchi, S., Michaels, P., Naresh, K. N., Natkunam, Y., Nejati, R., Ott, G., Padron, E., Patel, K. P., Patkar, N., Picarsic, J., Platzbecker, U., Roberts, I., Schuh, A., Sewell, W., Siebert, R.,

- Tembhare, P., Tyner, J., Verstovsek, S., Wang, W., Wood, B., Xiao, W., Yeung, C., & Hochhaus, A. (2022). The 5th edition of the World Health Organization Classification of Haematolymphoid Tumours: Myeloid and Histiocytic/Dendritic Neoplasms. *Leukemia*, 36(7), 1703-1719. <https://doi.org/10.1038/s41375-022-01613-1>
- Khrabrova, D. A., Yakubovskaya, M. G., & Gromova, E. S. (2021). AML-Associated Mutations in DNA Methyltransferase DNMT3A. *Biochemistry (Mosc)*, 86(3), 307-318. <https://doi.org/10.1134/S000629792103007X>
- Khwaja, A., Bjorkholm, M., Gale, R. E., Levine, R. L., Jordan, C. T., Ehninger, G., Bloomfield, C. D., Estey, E., Burnett, A., Cornelissen, J. J., Scheinberg, D. A., Bouscary, D., & Linch, D. C. (2016). Acute myeloid leukaemia. *Nat Rev Dis Primers*, 2, 16010. <https://doi.org/10.1038/nrdp.2016.10>
- Kikuchi, A., Onoda, H., Yamaguchi, K., Kori, S., Matsuzawa, S., Chiba, Y., Tanimoto, S., Yoshimi, S., Sato, H., Yamagata, A., Shirouzu, M., Adachi, N., Sharif, J., Koseki, H., Nishiyama, A., Nakanishi, M., Defossez, P. A., & Arita, K. (2022). Structural basis for activation of DNMT1. *Nat Commun*, 13(1), 7130. <https://doi.org/10.1038/s41467-022-34779-4>
- Kim, T. H., & Dekker, J. (2018). ChIP-Quantitative Polymerase Chain Reaction (ChIP-qPCR). *Cold Spring Harb Protoc*, 2018(5). <https://doi.org/10.1101/pdb.prot082628>
- Klever, M. K., Strang, E., Hetzel, S., Jungnitsch, J., Dolnik, A., Schopflin, R., Schrezenmeier, J. F., Schick, F., Blau, O., Westermann, J., Rucker, F. G., Xia, Z., Dohner, K., Schrezenmeier, H., Spielmann, M., Meissner, A., Melo, U. S., Mundlos, S., & Bullinger, L. (2023). AML with complex karyotype: extreme genomic complexity revealed by combined long-read sequencing and Hi-C technology. *Blood Adv*, 7(21), 6520-6531. <https://doi.org/10.1182/bloodadvances.2023010887>
- Klicka, K., Grzywa, T. M., Mielniczuk, A., Klinke, A., & Wlodarski, P. K. (2022). The role of miR-200 family in the regulation of hallmarks of cancer. *Front Oncol*, 12, 965231. <https://doi.org/10.3389/fonc.2022.965231>
- Klobuch, S., Steinberg, T., Bruni, E., Mirbeth, C., Heilmeyer, B., Ghibelli, L., Herr, W., Reichle, A., & Thomas, S. (2018). Biomodulatory Treatment With Azacitidine, All-trans Retinoic Acid and Pioglitazone Induces Differentiation of Primary AML Blasts Into Neutrophil Like Cells Capable of ROS Production and Phagocytosis. *Front Pharmacol*, 9, 1380. <https://doi.org/10.3389/fphar.2018.01380>
- Koldobskiy, M. A., Abante, J., Jenkinson, G., Pujadas, E., Tetens, A., Zhao, F., Tryggvadottir, R., Idrizi, A., Reinisch, A., Majeti, R., Goutsias, J., & Feinberg, A. P. (2020). A Dysregulated DNA Methylation Landscape Linked to Gene Expression in MLL-Rearranged AML. *Epigenetics*, 15(8), 841-858. <https://doi.org/10.1080/15592294.2020.1734149>
- Krijger, P. H. L., Geeven, G., Bianchi, V., Hilvering, C. R. E., & de Laat, W. (2020). 4C-seq from beginning to end: A detailed protocol for sample preparation and data analysis. *Methods*, 170, 17-32. <https://doi.org/10.1016/j.ymeth.2019.07.014>

- Krueger, F., & Andrews, S. R. (2011). Bismark: a flexible aligner and methylation caller for Bisulfite-Seq applications. *Bioinformatics*, 27(11), 1571-1572. <https://doi.org/10.1093/bioinformatics/btr167>
- la Torre, A., Lo Vecchio, F., & Greco, A. (2023). Epigenetic Mechanisms of Aging and Aging-Associated Diseases. *Cells*, 12(8). <https://doi.org/10.3390/cells12081163>
- Lagunas-Rangel, F. A., Chavez-Valencia, V., Gomez-Guijosa, M. A., & Cortes-Penagos, C. (2017). Acute Myeloid Leukemia-Genetic Alterations and Their Clinical Prognosis. *Int J Hematol Oncol Stem Cell Res*, 11(4), 328-339. <https://www.ncbi.nlm.nih.gov/pubmed/29340131>
- Langmead, B., & Salzberg, S. L. (2012). Fast gapped-read alignment with Bowtie 2. *Nat Methods*, 9(4), 357-359. <https://doi.org/10.1038/nmeth.1923>
- Lasko, L. M., Jakob, C. G., Edalji, R. P., Qiu, W., Montgomery, D., Digiammarino, E. L., Hansen, T. M., Risi, R. M., Frey, R., Manaves, V., Shaw, B., Algire, M., Hessler, P., Lam, L. T., Uziel, T., Faivre, E., Ferguson, D., Buchanan, F. G., Martin, R. L., Torrent, M., Chiang, G. G., Karukurichi, K., Langston, J. W., Weinert, B. T., Choudhary, C., de Vries, P., Van Drie, J. H., McElligott, D., Kesicki, E., Marmorstein, R., Sun, C., Cole, P. A., Rosenberg, S. H., Michaelides, M. R., Lai, A., & Bromberg, K. D. (2017). Discovery of a selective catalytic p300/CBP inhibitor that targets lineage-specific tumours. *Nature*, 550(7674), 128-132. <https://doi.org/10.1038/nature24028>
- Lewis, J. D., Meehan, R. R., Henzel, W. J., Maurer-Fogy, I., Jeppesen, P., Klein, F., & Bird, A. (1992). Purification, sequence, and cellular localization of a novel chromosomal protein that binds to methylated DNA. *Cell*, 69(6), 905-914. [https://doi.org/10.1016/0092-8674\(92\)90610-o](https://doi.org/10.1016/0092-8674(92)90610-o)
- Li, F., Chen, Q., Xue, H., Zhang, L., Wang, K., & Shen, F. (2020). LncRNA MNX1-AS1 promotes progression of intrahepatic cholangiocarcinoma through the MNX1/Hippo axis. *Cell Death Dis*, 11(10), 894. <https://doi.org/10.1038/s41419-020-03029-0>
- Li, H., Hu, F., Gale, R. P., Sekeres, M. A., & Liang, Y. (2022). Myelodysplastic syndromes. *Nat Rev Dis Primers*, 8(1), 74. <https://doi.org/10.1038/s41572-022-00402-5>
- Li, J. K., Liu, H., Zhang, H. W., Li, J., & Liang, Z. T. (2023). A Positive Feedback Loop of E2F4-Mediated Activation of MNX1 Regulates Tumour Progression in Colorectal Cancer. *J Cancer*, 14(14), 2739-2750. <https://doi.org/10.7150/jca.86718>
- Li, Z., Wang, Y., Liu, S., Li, W., Wang, Z., Jia, Z., Zhu, Z., & Bao, Y. (2022). MiR-200a-3p promotes gastric cancer progression by targeting DLC-1. *J Mol Histol*, 53(1), 39-49. <https://doi.org/10.1007/s10735-021-10037-7>
- Li, Z., Zhao, P., & Xia, Q. (2019). Epigenetic Methylations on N6-Adenine and N6-Adenosine with the same Input but Different Output. *Int J Mol Sci*, 20(12). <https://doi.org/10.3390/ijms20122931>
- Loven, J., Hoke, H. A., Lin, C. Y., Lau, A., Orlando, D. A., Vakoc, C. R., Bradner, J. E., Lee, T. I., & Young, R. A. (2013). Selective inhibition of tumor oncogenes by disruption of super-enhancers. *Cell*, 153(2), 320-334. <https://doi.org/10.1016/j.cell.2013.03.036>

- Lu, J., Guo, Y., Yin, J., Chen, J., Wang, Y., Wang, G. G., & Song, J. (2024). Structure-guided functional suppression of AML-associated DNMT3A hotspot mutations. *Nat Commun*, *15*(1), 3111. <https://doi.org/10.1038/s41467-024-47398-y>
- Lu, J., Tan, T., Zhu, L., Dong, H., & Xian, R. (2020). Hypomethylation Causes MIR21 Overexpression in Tumors. *Mol Ther Oncolytics*, *18*, 47-57. <https://doi.org/10.1016/j.omto.2020.05.011>
- Luo, H., Wang, F., Zha, J., Li, H., Yan, B., Du, Q., Yang, F., Sobh, A., Vulpe, C., Drusbosky, L., Cogle, C., Chepelev, I., Xu, B., Nimer, S. D., Licht, J., Qiu, Y., Chen, B., Xu, M., & Huang, S. (2018). CTCF boundary remodels chromatin domain and drives aberrant HOX gene transcription in acute myeloid leukemia. *Blood*, *132*(8), 837-848. <https://doi.org/10.1182/blood-2017-11-814319>
- Lupianez, D. G., Kraft, K., Heinrich, V., Krawitz, P., Brancati, F., Klopocki, E., Horn, D., Kayserili, H., Opitz, J. M., Laxova, R., Santos-Simarro, F., Gilbert-Dussardier, B., Wittler, L., Borschiwer, M., Haas, S. A., Osterwalder, M., Franke, M., Timmermann, B., Hecht, J., Spielmann, M., Visel, A., & Mundlos, S. (2015). Disruptions of topological chromatin domains cause pathogenic rewiring of gene-enhancer interactions. *Cell*, *161*(5), 1012-1025. <https://doi.org/10.1016/j.cell.2015.04.004>
- Ma, L., Wang, J., Zhang, Y., Fang, F., Ling, J., Chu, X., Zhang, Z., Tao, Y., Li, X., Tian, Y., Li, Z., Sang, X., Zhang, K., Lu, L., Wan, X., Chen, Y., Yu, J., Zhuo, R., Wu, S., Lu, J., Pan, J., & Hu, S. (2022). BRD4 PROTAC degrader MZ1 exerts anticancer effects in acute myeloid leukemia by targeting c-Myc and ANP32B genes. *Cancer Biol Ther*, *23*(1), 1-15. <https://doi.org/10.1080/15384047.2022.2125748>
- Maeshima, K., Kaizu, K., Tamura, S., Nozaki, T., Kokubo, T., & Takahashi, K. (2015). The physical size of transcription factors is key to transcriptional regulation in chromatin domains. *J Phys Condens Matter*, *27*(6), 064116. <https://doi.org/10.1088/0953-8984/27/6/064116>
- Mahmood, N., Arakelian, A., Cheishvili, D., Szyf, M., & Rabbani, S. A. (2020). S-adenosylmethionine in combination with decitabine shows enhanced anti-cancer effects in repressing breast cancer growth and metastasis. *J Cell Mol Med*, *24*(18), 10322-10337. <https://doi.org/10.1111/jcmm.15642>
- Mancarella, D., Ellinghaus, H., Sigismondo, G., Veselinov, O., Kuhn, A., Goyal, A., Hartmann, M., Fellenberg, J., Krijgsveld, J., Plass, C., Popanda, O., Schmezer, P., & Bakr, A. (2024). Deposition of onco-histone H3.3-G34W leads to DNA repair deficiency and activates cGAS/STING-mediated immune responses. *Int J Cancer*, *154*(12), 2106-2120. <https://doi.org/10.1002/ijc.34883>
- Mann, Z., Sengar, M., Verma, Y. K., Rajalingam, R., & Raghav, P. K. (2022). Hematopoietic Stem Cell Factors: Their Functional Role in Self-Renewal and Clinical Aspects. *Front Cell Dev Biol*, *10*, 664261. <https://doi.org/10.3389/fcell.2022.664261>
- Mao, Y., & Jiang, P. (2023). The crisscross between p53 and metabolism in cancer. *Acta Biochim Biophys Sin (Shanghai)*, *55*(6), 914-922. <https://doi.org/10.3724/abbs.2023109>

- Marnell, C. S., Bick, A., & Natarajan, P. (2021). Clonal hematopoiesis of indeterminate potential (CHIP): Linking somatic mutations, hematopoiesis, chronic inflammation and cardiovascular disease. *J Mol Cell Cardiol*, *161*, 98-105. <https://doi.org/10.1016/j.yjmcc.2021.07.004>
- Mattes, J., Yang, M., & Foster, P. S. (2007). Regulation of microRNA by antagonists: a new class of pharmacological antagonists for the specific regulation of gene function? *Am J Respir Cell Mol Biol*, *36*(1), 8-12. <https://doi.org/10.1165/rcmb.2006-0227TR>
- McGeary, S. E., Lin, K. S., Shi, C. Y., Pham, T. M., Bisaria, N., Kelley, G. M., & Bartel, D. P. (2019). The biochemical basis of microRNA targeting efficacy. *Science*, *366*(6472). <https://doi.org/10.1126/science.aav1741>
- Meyer, S. C., & Levine, R. L. (2014). Translational implications of somatic genomics in acute myeloid leukaemia. *Lancet Oncol*, *15*(9), e382-394. [https://doi.org/10.1016/S1470-2045\(14\)70008-7](https://doi.org/10.1016/S1470-2045(14)70008-7)
- Michaloglou, C., Vredeveld, L. C., Soengas, M. S., Denoyelle, C., Kuilman, T., van der Horst, C. M., Majoor, D. M., Shay, J. W., Mooi, W. J., & Peeper, D. S. (2005). BRAFE600-associated senescence-like cell cycle arrest of human naevi. *Nature*, *436*(7051), 720-724. <https://doi.org/10.1038/nature03890>
- Millan-Zambrano, G., Burton, A., Bannister, A. J., & Schneider, R. (2022). Histone post-translational modifications - cause and consequence of genome function. *Nat Rev Genet*, *23*(9), 563-580. <https://doi.org/10.1038/s41576-022-00468-7>
- Miranda, M., Noordermeer, D., & Moindrot, B. (2022). Detection of Allele-Specific 3D Chromatin Interactions Using High-Resolution In-Nucleus 4C-seq. *Methods Mol Biol*, *2532*, 15-33. https://doi.org/10.1007/978-1-0716-2497-5_2
- Mohamed Jiffry, M. Z., Kloss, R., Ahmed-Khan, M., Carmona-Pires, F., Okam, N., Weeraddana, P., Dharmaratna, D., Dandwani, M., & Moin, K. (2023). A review of treatment options employed in relapsed/refractory AML. *Hematology*, *28*(1), 2196482. <https://doi.org/10.1080/16078454.2023.2196482>
- Mohanta, T. K., Mishra, A. K., & Al-Harrasi, A. (2021). The 3D Genome: From Structure to Function. *Int J Mol Sci*, *22*(21). <https://doi.org/10.3390/ijms222111585>
- Monteagudo-Sanchez, A., Noordermeer, D., & Greenberg, M. V. C. (2024). The impact of DNA methylation on CTCF-mediated 3D genome organization. *Nat Struct Mol Biol*, *31*(3), 404-412. <https://doi.org/10.1038/s41594-024-01241-6>
- Montefiori, L. E., Bendig, S., Gu, Z., Chen, X., Polonen, P., Ma, X., Murison, A., Zeng, A., Garcia-Prat, L., Dickerson, K., Iacobucci, I., Abdelhamed, S., Hiltenbrand, R., Mead, P. E., Mehr, C. M., Xu, B., Cheng, Z., Chang, T. C., Westover, T., Ma, J., Stengel, A., Kimura, S., Qu, C., Valentine, M. B., Rashkovan, M., Luger, S., Litzow, M. R., Rowe, J. M., den Boer, M. L., Wang, V., Yin, J., Kornblau, S. M., Hunger, S. P., Loh, M. L., Pui, C. H., Yang, W., Crews, K. R., Roberts, K. G., Yang, J. J., Relling, M. V., Evans, W. E., Stock, W., Paietta, E. M., Ferrando, A. A., Zhang, J., Kern, W., Haferlach, T., Wu, G., Dick, J. E., Klco, J. M., Haferlach, C., & Mullighan, C. G. (2021). Enhancer Hijacking Drives Oncogenic

- BCL11B Expression in Lineage-Ambiguous Stem Cell Leukemia. *Cancer Discov*, 11(11), 2846-2867. <https://doi.org/10.1158/2159-8290.CD-21-0145>
- Moran, S., Arribas, C., & Esteller, M. (2016). Validation of a DNA methylation microarray for 850,000 CpG sites of the human genome enriched in enhancer sequences. *Epigenomics*, 8(3), 389-399. <https://doi.org/10.2217/epi.15.114>
- Mori, M., Kubota, Y., Durmaz, A., Gurnari, C., Goodings, C., Adema, V., Ponvilawan, B., Bahaj, W. S., Kewan, T., LaFramboise, T., Meggendorfer, M., Haferlach, C., Barnard, J., Wlodarski, M., Visconte, V., Haferlach, T., & Maciejewski, J. P. (2023). Genomics of deletion 7 and 7q in myeloid neoplasm: from pathogenic culprits to potential synthetic lethal therapeutic targets. *Leukemia*, 37(10), 2082-2093. <https://doi.org/10.1038/s41375-023-02003-x>
- Morris-Blanco, K. C., Chokkalla, A. K., Arruri, V., Jeong, S., Probelsky, S. M., & Vemuganti, R. (2022). Epigenetic mechanisms and potential therapeutic targets in stroke. *J Cereb Blood Flow Metab*, 42(11), 2000-2016. <https://doi.org/10.1177/0271678X221116192>
- Moyle, R. L., Carvalhais, L. C., Pretorius, L. S., Nowak, E., Subramaniam, G., Dalton-Morgan, J., & Schenk, P. M. (2017). An Optimized Transient Dual Luciferase Assay for Quantifying MicroRNA Directed Repression of Targeted Sequences. *Front Plant Sci*, 8, 1631. <https://doi.org/10.3389/fpls.2017.01631>
- Mu, C., Wang, T., Wang, X., Tian, H., & Liu, Y. (2016). Identification of microRNAs regulating Hlxb9 gene expression during the induction of insulin-producing cells. *Cell Biol Int*, 40(5), 515-523. <https://doi.org/10.1002/cbin.10586>
- Mujahed, H., Miliara, S., Neddermeyer, A., Bengtzen, S., Nilsson, C., Deneberg, S., Cordeddu, L., Ekwall, K., Lennartsson, A., & Lehmann, S. (2020). AML displays increased CTCF occupancy associated with aberrant gene expression and transcription factor binding. *Blood*, 136(3), 339-352. <https://doi.org/10.1182/blood.2019002326>
- Mulet-Lazaro, R., & Delwel, R. (2023). From Genotype to Phenotype: How Enhancers Control Gene Expression and Cell Identity in Hematopoiesis. *Hemasphere*, 7(11), e969. <https://doi.org/10.1097/HS9.0000000000000969>
- Mulet-Lazaro, R., & Delwel, R. (2024). Oncogenic Enhancers in Leukemia. *Blood Cancer Discov*, OF1-OF15. <https://doi.org/10.1158/2643-3230.BCD-23-0211>
- Mulet-Lazaro, R., van Herk, S., Erpelinck, C., Bindels, E., Sanders, M. A., Vermeulen, C., Renkens, I., Valk, P., Melnick, A. M., de Ridder, J., Rehli, M., Gebhard, C., Delwel, R., & Wouters, B. J. (2021). Allele-specific expression of GATA2 due to epigenetic dysregulation in CEBPA double-mutant AML. *Blood*, 138(2), 160-177. <https://doi.org/10.1182/blood.2020009244>
- Muller, F., Scherer, M., Assenov, Y., Lutsik, P., Walter, J., Lengauer, T., & Bock, C. (2019). RnBeads 2.0: comprehensive analysis of DNA methylation data. *Genome Biol*, 20(1), 55. <https://doi.org/10.1186/s13059-019-1664-9>
- Nagel, S. (2021). NKL-Code in Normal and Aberrant Hematopoiesis. *Cancers (Basel)*, 13(8). <https://doi.org/10.3390/cancers13081961>

- Nagel, S., Kaufmann, M., Scherr, M., Drexler, H. G., & MacLeod, R. A. (2005). Activation of HLXB9 by juxtaposition with MYB via formation of t(6;7)(q23;q36) in an AML-M4 cell line (GDM-1). *Genes Chromosomes Cancer*, 42(2), 170-178. <https://doi.org/10.1002/gcc.20113>
- Nemeth, K., Bayraktar, R., Ferracin, M., & Calin, G. A. (2024). Non-coding RNAs in disease: from mechanisms to therapeutics. *Nat Rev Genet*, 25(3), 211-232. <https://doi.org/10.1038/s41576-023-00662-1>
- Nicolaides, N. C., Gualdi, R., Casadevall, C., Manzella, L., & Calabretta, B. (1991). Positive autoregulation of c-myb expression via Myb binding sites in the 5' flanking region of the human c-myb gene. *Mol Cell Biol*, 11(12), 6166-6176. <https://doi.org/10.1128/mcb.11.12.6166-6176.1991>
- Nilsson, T., Waraky, A., Ostlund, A., Li, S., Staffas, A., Asp, J., Fogelstrand, L., Abrahamsson, J., & Palmqvist, L. (2022). An induced pluripotent stem cell t(7;12)(q36;p13) acute myeloid leukemia model shows high expression of MNX1 and a block in differentiation of the erythroid and megakaryocytic lineages. *Int J Cancer*, 151(5), 770-782. <https://doi.org/10.1002/ijc.34122>
- Ning, X., Shi, Z., Liu, X., Zhang, A., Han, L., Jiang, K., Kang, C., & Zhang, Q. (2015). DNMT1 and EZH2 mediated methylation silences the microRNA-200b/a/429 gene and promotes tumor progression. *Cancer Lett*, 359(2), 198-205. <https://doi.org/10.1016/j.canlet.2015.01.005>
- Noguera-Castells, A., Garcia-Prieto, C. A., Alvarez-Errico, D., & Esteller, M. (2023). Validation of the new EPIC DNA methylation microarray (900K EPIC v2) for high-throughput profiling of the human DNA methylome. *Epigenetics*, 18(1), 2185742. <https://doi.org/10.1080/15592294.2023.2185742>
- Ogawa, S. (2019). Genetics of MDS. *Blood*, 133(10), 1049-1059. <https://doi.org/10.1182/blood-2018-10-844621>
- Okhovat, M., VanCampen, J., Nevonen, K. A., Harshman, L., Li, W., Layman, C. E., Ward, S., Herrera, J., Wells, J., Sheng, R. R., Mao, Y., Ndjamen, B., Lima, A. C., Vigh-Conrad, K. A., Stendahl, A. M., Yang, R., Fedorov, L., Matthews, I. R., Easow, S. A., Chan, D. K., Jan, T. A., Eichler, E. E., Rugonyi, S., Conrad, D. F., Ahituv, N., & Carbone, L. (2023). TAD evolutionary and functional characterization reveals diversity in mammalian TAD boundary properties and function. *Nat Commun*, 14(1), 8111. <https://doi.org/10.1038/s41467-023-43841-8>
- Oliveto, S., Mancino, M., Manfrini, N., & Biffo, S. (2017). Role of microRNAs in translation regulation and cancer. *World J Biol Chem*, 8(1), 45-56. <https://doi.org/10.4331/wjbc.v8.i1.45>
- Ottoma, S., Mulet-Lazaro, R., Erpelinck-Verschueren, C., van Herk, S., Havermans, M., Arricibita Varea, A., Vermeulen, M., Beverloo, H. B., Groschel, S., Haferlach, T., Haferlach, C., B, J. W., Bindels, E., Smeenk, L., & Delwel, R. (2021). The leukemic oncogene EVI1 hijacks

- a MYC super-enhancer by CTCF-facilitated loops. *Nat Commun*, 12(1), 5679. <https://doi.org/10.1038/s41467-021-25862-3>
- Pabinger, S., Ernst, K., Pulverer, W., Kallmeyer, R., Valdes, A. M., Metrustry, S., Katic, D., Nuzzo, A., Kriegner, A., Vierlinger, K., & Weinhaeusel, A. (2016). Analysis and Visualization Tool for Targeted Amplicon Bisulfite Sequencing on Ion Torrent Sequencers. *PLoS One*, 11(7), e0160227. <https://doi.org/10.1371/journal.pone.0160227>
- Pachano, T., Sanchez-Gaya, V., Ealo, T., Mariner-Fauli, M., Bleckwehl, T., Asenjo, H. G., Respuela, P., Cruz-Molina, S., Munoz-San Martin, M., Haro, E., van, I. W. F. J., Landeira, D., & Rada-Iglesias, A. (2021). Orphan CpG islands amplify poised enhancer regulatory activity and determine target gene responsiveness. *Nat Genet*, 53(7), 1036-1049. <https://doi.org/10.1038/s41588-021-00888-x>
- Pang, Y., Liu, J., Li, X., Xiao, G., Wang, H., Yang, G., Li, Y., Tang, S. C., Qin, S., Du, N., Zhang, H., Liu, D., Sun, X., & Ren, H. (2018). MYC and DNMT3A-mediated DNA methylation represses microRNA-200b in triple negative breast cancer. *J Cell Mol Med*, 22(12), 6262-6274. <https://doi.org/10.1111/jcmm.13916>
- Pappalardi, M. B., Keenan, K., Cockerill, M., Kellner, W. A., Stowell, A., Sherk, C., Wong, K., Pathuri, S., Briand, J., Steidel, M., Chapman, P., Groy, A., Wiseman, A. K., McHugh, C. F., Campobasso, N., Graves, A. P., Fairweather, E., Werner, T., Raoof, A., Butlin, R. J., Rueda, L., Horton, J. R., Fosbenner, D. T., Zhang, C., Handler, J. L., Muliaditan, M., Mebrahtu, M., Jaworski, J. P., McNulty, D. E., Burt, C., Eberl, H. C., Taylor, A. N., Ho, T., Merrihew, S., Foley, S. W., Rutkowska, A., Li, M., Romeril, S. P., Goldberg, K., Zhang, X., Kershaw, C. S., Bantscheff, M., Jurewicz, A. J., Minthorn, E., Grandi, P., Patel, M., Benowitz, A. B., Mohammad, H. P., Gilmartin, A. G., Prinjha, R. K., Ogilvie, D., Carpenter, C., Heerding, D., Baylin, S. B., Jones, P. A., Cheng, X., King, B. W., Luengo, J. I., Jordan, A. M., Waddell, I., Kruger, R. G., & McCabe, M. T. (2021). Discovery of a first-in-class reversible DNMT1-selective inhibitor with improved tolerability and efficacy in acute myeloid leukemia. *Nat Cancer*, 2(10), 1002-1017. <https://www.ncbi.nlm.nih.gov/pubmed/34790902>
- Pecot, C. V., Rupaimoole, R., Yang, D., Akbani, R., Ivan, C., Lu, C., Wu, S., Han, H. D., Shah, M. Y., Rodriguez-Aguayo, C., Bottsford-Miller, J., Liu, Y., Kim, S. B., Unruh, A., Gonzalez-Villasana, V., Huang, L., Zand, B., Moreno-Smith, M., Mangala, L. S., Taylor, M., Dalton, H. J., Sehgal, V., Wen, Y., Kang, Y., Baggerly, K. A., Lee, J. S., Ram, P. T., Ravoori, M. K., Kundra, V., Zhang, X., Ali-Fehmi, R., Gonzalez-Angulo, A. M., Massion, P. P., Calin, G. A., Lopez-Berestein, G., Zhang, W., & Sood, A. K. (2013). Tumour angiogenesis regulation by the miR-200 family. *Nat Commun*, 4, 2427. <https://doi.org/10.1038/ncomms3427>
- Pelcovits, A., & Niroula, R. (2020). Acute Myeloid Leukemia: A Review. *R I Med J* (2013), 103(3), 38-40. <https://www.ncbi.nlm.nih.gov/pubmed/32236160>
- Peng, Y., & Croce, C. M. (2016). The role of MicroRNAs in human cancer. *Signal Transduct Target Ther*, 1, 15004. <https://doi.org/10.1038/sigtrans.2015.4>

- Pollyea, D. A., Altman, J. K., Assi, R., Bixby, D., Fathi, A. T., Foran, J. M., Gojo, I., Hall, A. C., Jonas, B. A., Kishtagari, A., Lancet, J., Maness, L., Mangan, J., Mannis, G., Marcucci, G., Mims, A., Moriarty, K., Mustafa Ali, M., Neff, J., Nejati, R., Olin, R., Percival, M. E., Perl, A., Przespolewski, A., Rao, D., Ravandi, F., Shallis, R., Shami, P. J., Stein, E., Stone, R. M., Sweet, K., Thota, S., Uy, G., Vachhani, P., Cassara, C. J., Freedman-Cass, D. A., & Stehman, K. (2023). Acute Myeloid Leukemia, Version 3.2023, NCCN Clinical Practice Guidelines in Oncology. *J Natl Compr Canc Netw*, 21(5), 503-513. <https://doi.org/10.6004/jnccn.2023.0025>
- Popovic, D., Vucic, D., & Dikic, I. (2014). Ubiquitination in disease pathogenesis and treatment. *Nat Med*, 20(11), 1242-1253. <https://doi.org/10.1038/nm.3739>
- Ragusa, D., Ciciro, Y., Federico, C., Saccone, S., Bruno, F., Saeedi, R., Sisu, C., Pina, C., Sala, A., & Tosi, S. (2022). Engineered model of t(7;12)(q36;p13) AML recapitulates patient-specific features and gene expression profiles. *Oncogenesis*, 11(1), 50. <https://doi.org/10.1038/s41389-022-00426-2>
- Ragusa, D., Dijkhuis, L., Pina, C., & Tosi, S. (2023). Mechanisms associated with t(7;12) acute myeloid leukaemia: from genetics to potential treatment targets. *Biosci Rep*, 43(1). <https://doi.org/10.1042/BSR20220489>
- Ragusa, D., Tosi, S., & Sisu, C. (2022). Pan-Cancer Analysis Identifies MNX1 and Associated Antisense Transcripts as Biomarkers for Cancer. *Cells*, 11(22). <https://doi.org/10.3390/cells11223577>
- Rani, V., & Sengar, R. S. (2022). Biogenesis and mechanisms of microRNA-mediated gene regulation. *Biotechnol Bioeng*, 119(3), 685-692. <https://doi.org/10.1002/bit.28029>
- Rasmussen, K. D., & Helin, K. (2016). Role of TET enzymes in DNA methylation, development, and cancer. *Genes Dev*, 30(7), 733-750. <https://doi.org/10.1101/gad.276568.115>
- Ravi, R. K., Walton, K., & Khosroheidari, M. (2018). MiSeq: A Next Generation Sequencing Platform for Genomic Analysis. *Methods Mol Biol*, 1706, 223-232. https://doi.org/10.1007/978-1-4939-7471-9_12
- Ray, M. K., Wiskow, O., King, M. J., Ismail, N., Ergun, A., Wang, Y., Plys, A. J., Davis, C. P., Kathrein, K., Sadreyev, R., Borowsky, M. L., Eggan, K., Zon, L., Galloway, J. L., & Kingston, R. E. (2016). CAT7 and cat7l Long Non-coding RNAs Tune Polycomb Repressive Complex 1 Function during Human and Zebrafish Development. *J Biol Chem*, 291(37), 19558-19572. <https://doi.org/10.1074/jbc.M116.730853>
- Riffo-Campos, A. L., Riquelme, I., & Brebi-Mieville, P. (2016). Tools for Sequence-Based miRNA Target Prediction: What to Choose? *Int J Mol Sci*, 17(12). <https://doi.org/10.3390/ijms17121987>
- Roberts, A. W. (2020). Therapeutic development and current uses of BCL-2 inhibition. *Hematology Am Soc Hematol Educ Program*, 2020(1), 1-9. <https://doi.org/10.1182/hematology.2020000154>
- Roman-Gomez, J., Jimenez-Velasco, A., Castillejo, J. A., Agirre, X., Barrios, M., Navarro, G., Molina, F. J., Calasanz, M. J., Prosper, F., Heiniger, A., & Torres, A. (2004). Promoter

- hypermethylation of cancer-related genes: a strong independent prognostic factor in acute lymphoblastic leukemia. *Blood*, 104(8), 2492-2498. <https://doi.org/10.1182/blood-2004-03-0954>
- Rupaimoole, R., & Slack, F. J. (2017). MicroRNA therapeutics: towards a new era for the management of cancer and other diseases. *Nat Rev Drug Discov*, 16(3), 203-222. <https://doi.org/10.1038/nrd.2016.246>
- Sadras, T., Kok, C. H., Perugini, M., Ramshaw, H. S., & D'Andrea, R. J. (2017). miR-155 as a potential target of IL-3 signaling in primary AML cells. *Leuk Res*, 57, 57-59. <https://doi.org/10.1016/j.leukres.2017.02.010>
- Sarda, S., Das, A., Vinson, C., & Hannenhalli, S. (2017). Distal CpG islands can serve as alternative promoters to transcribe genes with silenced proximal promoters. *Genome Res*, 27(4), 553-566. <https://doi.org/10.1101/gr.212050.116>
- Scheller, M., Ludwig, A. K., Gollner, S., Rohde, C., Kramer, S., Stable, S., Janssen, M., Muller, J. A., He, L., Baumer, N., Arnold, C., Gerss, J., Schonung, M., Thiede, C., Niederwieser, C., Niederwieser, D., Serve, H., Berdel, W. E., Thiem, U., Hemmerling, I., Leuschner, F., Plass, C., Schlesner, M., Zaugg, J., Milsom, M. D., Trumpp, A., Pabst, C., Lipka, D. B., & Muller-Tidow, C. (2021). Hotspot DNMT3A mutations in clonal hematopoiesis and acute myeloid leukemia sensitize cells to azacytidine via viral mimicry response. *Nat Cancer*, 2(5), 527-544. <https://doi.org/10.1038/s43018-021-00213-9>
- Schmutz, M., Zucknick, M., Schlenk, R. F., Mertens, D., Benner, A., Weichenhan, D., Mucke, O., Dohner, K., Plass, C., Bullinger, L., & Claus, R. (2023). Predictive value of DNA methylation patterns in AML patients treated with an azacytidine containing induction regimen. *Clin Epigenetics*, 15(1), 171. <https://doi.org/10.1186/s13148-023-01580-z>
- Schoofs, T., & Muller-Tidow, C. (2011). DNA methylation as a pathogenic event and as a therapeutic target in AML. *Cancer Treat Rev*, 37 Suppl 1, S13-18. <https://doi.org/10.1016/j.ctrv.2011.04.013>
- Seelan, R. S., Mukhopadhyay, P., Pisano, M. M., & Greene, R. M. (2018). Effects of 5-Aza-2'-deoxycytidine (decitabine) on gene expression. *Drug Metab Rev*, 50(2), 193-207. <https://doi.org/10.1080/03602532.2018.1437446>
- Serrano, M., Lin, A. W., McCurrach, M. E., Beach, D., & Lowe, S. W. (1997). Oncogenic ras provokes premature cell senescence associated with accumulation of p53 and p16INK4a. *Cell*, 88(5), 593-602. [https://doi.org/10.1016/s0092-8674\(00\)81902-9](https://doi.org/10.1016/s0092-8674(00)81902-9)
- Seyhan, A. A. (2024). Trials and Tribulations of MicroRNA Therapeutics. *Int J Mol Sci*, 25(3). <https://doi.org/10.3390/ijms25031469>
- Shabashvili, D. E., Feng, Y., Kaur, P., Venugopal, K., & Guryanova, O. A. (2022). Combination strategies to promote sensitivity to cytarabine-induced replication stress in acute myeloid leukemia with and without DNMT3A mutations. *Exp Hematol*, 110, 20-27. <https://doi.org/10.1016/j.exphem.2022.03.008>

- Shallis, R. M., Wang, R., Davidoff, A., Ma, X., & Zeidan, A. M. (2019). Epidemiology of acute myeloid leukemia: Recent progress and enduring challenges. *Blood Rev*, *36*, 70-87. <https://doi.org/10.1016/j.blre.2019.04.005>
- Shang, R., Lee, S., Senavirathne, G., & Lai, E. C. (2023). microRNAs in action: biogenesis, function and regulation. *Nat Rev Genet*, *24*(12), 816-833. <https://doi.org/10.1038/s41576-023-00611-y>
- Sharifnia, T., Wawer, M. J., Chen, T., Huang, Q. Y., Weir, B. A., Sizemore, A., Lawlor, M. A., Goodale, A., Cowley, G. S., Vazquez, F., Ott, C. J., Francis, J. M., Sassi, S., Cogswell, P., Sheppard, H. E., Zhang, T., Gray, N. S., Clarke, P. A., Blagg, J., Workman, P., Sommer, J., Hornicek, F., Root, D. E., Hahn, W. C., Bradner, J. E., Wong, K. K., Clemons, P. A., Lin, C. Y., Kotz, J. D., & Schreiber, S. L. (2019). Small-molecule targeting of brachyury transcription factor addiction in chordoma. *Nat Med*, *25*(2), 292-300. <https://doi.org/10.1038/s41591-018-0312-3>
- Sheng, X., Xia, Z., Yang, H., & Hu, R. (2024). The ubiquitin codes in cellular stress responses. *Protein Cell*, *15*(3), 157-190. <https://doi.org/10.1093/procel/pwad045>
- Shimamoto, T., Ohyashiki, J. H., & Ohyashiki, K. (2005). Methylation of p15(INK4b) and E-cadherin genes is independently correlated with poor prognosis in acute myeloid leukemia. *Leuk Res*, *29*(6), 653-659. <https://doi.org/10.1016/j.leukres.2004.11.014>
- Shimony, S., Stahl, M., & Stone, R. M. (2023). Acute myeloid leukemia: 2023 update on diagnosis, risk-stratification, and management. *Am J Hematol*, *98*(3), 502-526. <https://doi.org/10.1002/ajh.26822>
- Short, N. J., Daver, N., Dinardo, C. D., Kadia, T., Nasr, L. F., Macaron, W., Yilmaz, M., Borthakur, G., Montalban-Bravo, G., Garcia-Manero, G., Issa, G. C., Chien, K. S., Jabbour, E., Nasnas, C., Huang, X., Qiao, W., Matthews, J., Stojanik, C. J., Patel, K. P., Abramova, R., Thankachan, J., Konopleva, M., Kantarjian, H., & Ravandi, F. (2024). Azacitidine, Venetoclax, and Gilteritinib in Newly Diagnosed and Relapsed or Refractory FLT3-Mutated AML. *J Clin Oncol*, *42*(13), 1499-1508. <https://doi.org/10.1200/JCO.23.01911>
- Si, J., Bumber, Y. A., Shu, J., Qin, T., Ahmed, S., He, R., Jelinek, J., & Issa, J. P. (2010). Chromatin remodeling is required for gene reactivation after decitabine-mediated DNA hypomethylation. *Cancer Res*, *70*(17), 6968-6977. <https://doi.org/10.1158/0008-5472.CAN-09-4474>
- Simoncova, K., Janotka, L., Kavcova, H., Sulova, Z., Breier, A., & Messingerova, L. (2022). Different mechanisms of drug resistance to hypomethylating agents in the treatment of myelodysplastic syndromes and acute myeloid leukemia. *Drug Resist Updat*, *61*, 100805. <https://doi.org/10.1016/j.drug.2022.100805>
- Skvortsova, K., Iovino, N., & Bogdanovic, O. (2018). Functions and mechanisms of epigenetic inheritance in animals. *Nat Rev Mol Cell Biol*, *19*(12), 774-790. <https://doi.org/10.1038/s41580-018-0074-2>
- Smeenk, L., Ottema, S., Mulet-Lazaro, R., Ebert, A., Havermans, M., Varea, A. A., Fellner, M., Pastoors, D., van Herk, S., Erpelinck-Verschueren, C., Grob, T., Hoogenboezem, R. M.,

- Kavelaars, F. G., Matson, D. R., Bresnick, E. H., Bindels, E. M., Kentsis, A., Zuber, J., & Delwel, R. (2021). Selective Requirement of MYB for Oncogenic Hyperactivation of a Translocated Enhancer in Leukemia. *Cancer Discov*, *11*(11), 2868-2883. <https://doi.org/10.1158/2159-8290.CD-20-1793>
- Smith, Z. D., & Meissner, A. (2013). DNA methylation: roles in mammalian development. *Nat Rev Genet*, *14*(3), 204-220. <https://doi.org/10.1038/nrg3354>
- Sollier, E., Heilmann, J., Gerhauser, C., Scherer, M., Plass, C., & Lutsik, P. (2024). Figeno: multi-region genomic figures with long-read support. *Bioinformatics*, *40*(6). <https://doi.org/10.1093/bioinformatics/btae354>
- Sollier, E., Riedel, A., Toprak, U. H., Wierzbinska, J. A., Weichenhan, D., Schmid, J. P., Hakobyan, M., Touzart, A., Jahn, E., Vick, B., Brown-Burke, F., Kelly, K., Kelekci, S., Pejkovska, A., Goyal, A., Bähr, M., Breuer, K., Chen, M.-J. M., Llamazares-Prada, M., Hartmann, M., Schönung, M., Correia, N., Trumpp, A., Abdullah, Y., Klingmüller, U., Mughal, S. S., Brors, B., Westermann, F., Schlesner, M., Vosberg, S., Herold, T., Greif, P. A., Pfeifer, D., Lübbert, M., Fischer, T., Heidel, F. H., Gebhard, C., Walter, W., Haferlach, T., Eisfeld, A.-K., Mrózek, K., Nicolet, D., Bullinger, L., Smeenk, L., Erpelinck, C., Mulet-Lazaro, R., Delwel, R., Ernst, A., Scherer, M., Lutsik, P., Jeremias, I., Döhner, K., Döhner, H., Lipka, D. B., & Plass, C. (2024). Pyjacker identifies enhancer hijacking events in acute myeloid leukemia including *MNX1* activation via deletion 7q. *bioRxiv*, 2024.2009.2011.611224. <https://doi.org/10.1101/2024.09.11.611224>
- Song, S. J., Poliseno, L., Song, M. S., Ala, U., Webster, K., Ng, C., Beringer, G., Brikbak, N. J., Yuan, X., Cantley, L. C., Richardson, A. L., & Pandolfi, P. P. (2013). MicroRNA-antagonism regulates breast cancer stemness and metastasis via TET-family-dependent chromatin remodeling. *Cell*, *154*(2), 311-324. <https://doi.org/10.1016/j.cell.2013.06.026>
- Spruijt, C. G., & Vermeulen, M. (2014). DNA methylation: old dog, new tricks? *Nat Struct Mol Biol*, *21*(11), 949-954. <https://doi.org/10.1038/nsmb.2910>
- Srivastava, P., Paluch, B. E., Matsuzaki, J., James, S. R., Collamat-Lai, G., Blagitko-Dorfs, N., Ford, L. A., Naqash, R., Lubbert, M., Karpf, A. R., Nemeth, M. J., & Griffiths, E. A. (2016). Induction of cancer testis antigen expression in circulating acute myeloid leukemia blasts following hypomethylating agent monotherapy. *Oncotarget*, *7*(11), 12840-12856. <https://doi.org/10.18632/oncotarget.7326>
- Stich, M., Ganss, L., Puschhof, J., Prigge, E. S., Reuschenbach, M., Guitierrez, A., Vinokurova, S., & von Knebel Doeberitz, M. (2017). 5-aza-2'-deoxycytidine (DAC) treatment downregulates the HPV E6 and E7 oncogene expression and blocks neoplastic growth of HPV-associated cancer cells. *Oncotarget*, *8*(32), 52104-52117. <https://doi.org/10.18632/oncotarget.10631>
- Stomper, J., Rotondo, J. C., Greve, G., & Lubbert, M. (2021). Hypomethylating agents (HMA) for the treatment of acute myeloid leukemia and myelodysplastic syndromes: mechanisms of resistance and novel HMA-based therapies. *Leukemia*, *35*(7), 1873-1889. <https://doi.org/10.1038/s41375-021-01218-0>

- Sun, H., Li, M., Li, Y., Zheng, N., Li, J., Li, X., Liu, Y., Ji, Q., Zhou, L., Su, J., Huang, W., Liu, Z., Liu, P., & Zou, L. (2024). Gastrodin Improves the Activity of the Ubiquitin-Proteasome System and the Autophagy-Lysosome Pathway to Degrade Mutant Huntingtin. *Int J Mol Sci*, 25(14). <https://doi.org/10.3390/ijms25147709>
- Svobodova, E., Kubikova, J., & Svoboda, P. (2016). Production of small RNAs by mammalian Dicer. *Pflugers Arch*, 468(6), 1089-1102. <https://doi.org/10.1007/s00424-016-1817-6>
- Szabo, Q., Bantignies, F., & Cavalli, G. (2019). Principles of genome folding into topologically associating domains. *Sci Adv*, 5(4), eaaw1668. <https://doi.org/10.1126/sciadv.aaw1668>
- Tanaka, A., Nishimura, K., Saika, W., Kon, A., Koike, Y., Tatsumi, H., Takeda, J., Nomura, M., Zang, W., Nakayama, M., Matsuda, M., Yamazaki, H., Fukumoto, M., Ito, H., Hayashi, Y., Kitamura, T., Kawamoto, H., Takaori-Kondo, A., Koseki, H., Ogawa, S., & Inoue, D. (2023). SETBP1 is dispensable for normal and malignant hematopoiesis. *Leukemia*, 37(9), 1802-1811. <https://doi.org/10.1038/s41375-023-01970-5>
- Tanaka, T., Arai, M., Wu, S., Kanda, T., Miyauchi, H., Imazeki, F., Matsubara, H., & Yokosuka, O. (2011). Epigenetic silencing of microRNA-373 plays an important role in regulating cell proliferation in colon cancer. *Oncol Rep*, 26(5), 1329-1335. <https://doi.org/10.3892/or.2011.1401>
- Taryma-Lesniak, O., Kjeldsen, T. E., Hansen, L. L., & Wojdacz, T. K. (2022). Influence of Unequal Amplification of Methylated and Non-Methylated Template on Performance of Pyrosequencing. *Genes (Basel)*, 13(8). <https://doi.org/10.3390/genes13081418>
- Tay, Y., Zhang, J., Thomson, A. M., Lim, B., & Rigoutsos, I. (2008). MicroRNAs to Nanog, Oct4 and Sox2 coding regions modulate embryonic stem cell differentiation. *Nature*, 455(7216), 1124-1128. <https://doi.org/10.1038/nature07299>
- Teschendorff, A. E., Marabita, F., Lechner, M., Bartlett, T., Tegner, J., Gomez-Cabrero, D., & Beck, S. (2013). A beta-mixture quantile normalization method for correcting probe design bias in Illumina Infinium 450 k DNA methylation data. *Bioinformatics*, 29(2), 189-196. <https://doi.org/10.1093/bioinformatics/bts680>
- Thaler, J., Harrison, K., Sharma, K., Lettieri, K., Kehrl, J., & Pfaff, S. L. (1999). Active suppression of interneuron programs within developing motor neurons revealed by analysis of homeodomain factor HB9. *Neuron*, 23(4), 675-687. [https://doi.org/10.1016/s0896-6273\(01\)80027-1](https://doi.org/10.1016/s0896-6273(01)80027-1)
- Thomas, H. F., & Buecker, C. (2023). What is an enhancer? *Bioessays*, 45(10), e2300044. <https://doi.org/10.1002/bies.202300044>
- Treiber, T., Treiber, N., & Meister, G. (2019). Regulation of microRNA biogenesis and its crosstalk with other cellular pathways. *Nat Rev Mol Cell Biol*, 20(1), 5-20. <https://doi.org/10.1038/s41580-018-0059-1>
- Tronick, E., & Hunter, R. G. (2016). Waddington, Dynamic Systems, and Epigenetics. *Front Behav Neurosci*, 10, 107. <https://doi.org/10.3389/fnbeh.2016.00107>

- Trotman, J. B., Bracerros, K. C. A., Cherney, R. E., Murvin, M. M., & Calabrese, J. M. (2021). The control of polycomb repressive complexes by long noncoding RNAs. *Wiley Interdiscip Rev RNA*, 12(6), e1657. <https://doi.org/10.1002/wrna.1657>
- Tuorto, F., Liebers, R., Musch, T., Schaefer, M., Hofmann, S., Kellner, S., Frye, M., Helm, M., Stoecklin, G., & Lyko, F. (2012). RNA cytosine methylation by Dnmt2 and NSun2 promotes tRNA stability and protein synthesis. *Nat Struct Mol Biol*, 19(9), 900-905. <https://doi.org/10.1038/nsmb.2357>
- Venugopal, S., Mascarenhas, J., & Steensma, D. P. (2021). Loss of 5q in myeloid malignancies - A gain in understanding of biological and clinical consequences. *Blood Rev*, 46, 100735. <https://doi.org/10.1016/j.blre.2020.100735>
- Wachter, F., & Pikman, Y. (2024). Pathophysiology of Acute Myeloid Leukemia. *Acta Haematol*, 147(2), 229-246. <https://doi.org/10.1159/000536152>
- Waclawiczek, A., Leppa, A. M., Renders, S., Stumpf, K., Reyneri, C., Betz, B., Janssen, M., Shahswar, R., Donato, E., Karpova, D., Thiel, V., Unglaub, J. M., Grabowski, S., Gryzik, S., Vierbaum, L., Schlenk, R. F., Rollig, C., Hundemer, M., Pabst, C., Heuser, M., Raffel, S., Muller-Tidow, C., Sauer, T., & Trumpp, A. (2023). Combinatorial BCL2 Family Expression in Acute Myeloid Leukemia Stem Cells Predicts Clinical Response to Azacitidine/Venetoclax. *Cancer Discov*, 13(6), 1408-1427. <https://doi.org/10.1158/2159-8290.CD-22-0939>
- Waddington, C. H. (1957). *The strategy of the genes; a discussion of some aspects of theoretical biology*. Allen & Unwin.
- Wagner, T., Priyanka, P., Micheletti, R., Friedman, M. J., Nair, S. J., Gamliel, A., Taylor, H., Song, X., Cho, M., Oh, S., Li, W., Han, J., Ohgi, K. A., Abrass, M., D'Antonio-Chronowska, A., D'Antonio, M., Hazuda, H., Duggirala, R., Blangero, J., Ding, S., Guzman, C., Frazer, K. A., Aggarwal, A. K., Zemljic-Harper, A. E., Rosenfeld, M. G., & Suh, Y. (2024). Recruitment of CTCF to the SIRT1 promoter after Oxidative Stress mediates Cardioprotective Transcription. *bioRxiv*. <https://doi.org/10.1101/2024.05.17.594600>
- Wang, J., Huang, T. Y., Hou, Y., Bartom, E., Lu, X., Shilatifard, A., Yue, F., & Saratsis, A. (2021). Epigenomic landscape and 3D genome structure in pediatric high-grade glioma. *Sci Adv*, 7(23). <https://doi.org/10.1126/sciadv.abg4126>
- Wang, M., Kong, W., He, B., Li, Z., Song, H., Shi, P., & Wang, J. (2018). Vitamin D and the promoter methylation of its metabolic pathway genes in association with the risk and prognosis of tuberculosis. *Clin Epigenetics*, 10(1), 118. <https://doi.org/10.1186/s13148-018-0552-6>
- Wang, Q., Gu, L., Adey, A., Radlwimmer, B., Wang, W., Hovestadt, V., Bahr, M., Wolf, S., Shendure, J., Eils, R., Plass, C., & Weichenhan, D. (2013). Tagmentation-based whole-genome bisulfite sequencing. *Nat Protoc*, 8(10), 2022-2032. <https://doi.org/10.1038/nprot.2013.118>

- Wang, X., Wang, Z., Huang, R., Lu, Z., Chen, X., & Huang, D. (2022). UPP1 Promotes Lung Adenocarcinoma Progression through Epigenetic Regulation of Glycolysis. *Aging Dis*, *13*(5), 1488-1503. <https://doi.org/10.14336/AD.2022.0218>
- Wang, Y., Wang, F., Wang, R., Zhao, P., & Xia, Q. (2015). 2A self-cleaving peptide-based multi-gene expression system in the silkworm *Bombyx mori*. *Sci Rep*, *5*, 16273. <https://doi.org/10.1038/srep16273>
- Wang, Y., Zhou, F., Li, M., Zhang, Y., Li, N., & Shao, L. (2022). MiR-34a-5p promotes hepatic gluconeogenesis by suppressing SIRT1 expression. *Exp Cell Res*, *420*(1), 113336. <https://doi.org/10.1016/j.yexcr.2022.113336>
- Waraky, A., Ostlund, A., Nilsson, T., Weichenhan, D., Lutsik, P., Bahr, M., Hey, J., Tunali, G., Adamsson, J., Jacobsson, S., Morsy, M. H. A., Li, S., Fogelstrand, L., Plass, C., & Palmqvist, L. (2024). Aberrant MNX1 expression associated with t(7;12)(q36;p13) pediatric acute myeloid leukemia induces the disease through altering histone methylation. *Haematologica*, *109*(3), 725-739. <https://doi.org/10.3324/haematol.2022.282255>
- Weichenhan, D., Lipka, D. B., Lutsik, P., Goyal, A., & Plass, C. (2022). Epigenomic technologies for precision oncology. *Semin Cancer Biol*, *84*, 60-68. <https://doi.org/10.1016/j.semcancer.2020.08.004>
- Weichenhan, D., Riedel, A., Meinen, C., Basic, A., Toth, R., Bahr, M., Lutsik, P., Hey, J., Sollier, E., Toprak, U. H., Kelekci, S., Lin, Y. Y., Hakobyan, M., Touzart, A., Goyal, A., Wierzbinska, J. A., Schlesner, M., Westermann, F., Lipka, D. B., & Plass, C. (2023). Translocation t(6;7) in AML-M4 cell line GDM-1 results in MNX1 activation through enhancer-hijacking. *Leukemia*, *37*(5), 1147-1150. <https://doi.org/10.1038/s41375-023-01865-5>
- Weichenhan, D., Riedel, A., Sollier, E., Toprak, U. H., Hey, J., Breuer, K. H., Wierzbinska, J. A., Touzart, A., Lutsik, P., Bahr, M., Ostlund, A., Nilsson, T., Jacobsson, S., Waraky, A., Behrens, Y. L., Gohring, G., Schlegelberger, B., Steinek, C., Harz, H., Leonhardt, H., Dolnik, A., Reinhardt, D., Bullinger, L., Palmqvist, L., Lipka, D. B., & Plass, C. (2024). Altered enhancer-promoter interaction leads to MNX1 expression in pediatric acute myeloid leukemia with t(7;12)(q36;p13). *Blood Adv*. <https://doi.org/10.1182/bloodadvances.2023012161>
- Weichenhan, D., Wang, Q., Adey, A., Wolf, S., Shendure, J., Eils, R., & Plass, C. (2018). Tagmentation-Based Library Preparation for Low DNA Input Whole Genome Bisulfite Sequencing. *Methods Mol Biol*, *1708*, 105-122. https://doi.org/10.1007/978-1-4939-7481-8_6
- Weinberg, O. K., Porwit, A., Orazi, A., Hasserjian, R. P., Foucar, K., Duncavage, E. J., & Arber, D. A. (2023). The International Consensus Classification of acute myeloid leukemia. *Virchows Arch*, *482*(1), 27-37. <https://doi.org/10.1007/s00428-022-03430-4>
- Wen, L., Xie, B., Li, H., Huang, J., Shi, Y., Tao, Y., & Chen, Y. (2024). EP300 through upregulating the expression of vimentin to promote the progression of chordoma. *Neurosurg Focus*, *56*(5), E17. <https://doi.org/10.3171/2024.2.FOCUS244>

- Wiklund, E. D., Bramsen, J. B., Hulf, T., Dyrskjot, L., Ramanathan, R., Hansen, T. B., Villadsen, S. B., Gao, S., Ostenfeld, M. S., Borre, M., Peter, M. E., Orntoft, T. F., Kjems, J., & Clark, S. J. (2011). Coordinated epigenetic repression of the miR-200 family and miR-205 in invasive bladder cancer. *Int J Cancer*, *128*(6), 1327-1334. <https://doi.org/10.1002/ijc.25461>
- Wu, J., Yue, C., Xu, W., Li, H., Zhu, J., & Li, L. (2023). MNX1 facilitates the malignant progress of lung adenocarcinoma through transcriptionally upregulating CCDC34. *Oncol Lett*, *26*(2), 325. <https://doi.org/10.3892/ol.2023.13911>
- Wu, X., & Zhang, Y. (2017). TET-mediated active DNA demethylation: mechanism, function and beyond. *Nat Rev Genet*, *18*(9), 517-534. <https://doi.org/10.1038/nrg.2017.33>
- Xiao, L., Parolia, A., Qiao, Y., Bawa, P., Eyunni, S., Mannan, R., Carson, S. E., Chang, Y., Wang, X., Zhang, Y., Vo, J. N., Kregel, S., Simko, S. A., Delekta, A. D., Jaber, M., Zheng, H., Apel, I. J., McMurry, L., Su, F., Wang, R., Zelenka-Wang, S., Sasmal, S., Khare, L., Mukherjee, S., Abbineni, C., Aithal, K., Bhakta, M. S., Ghurye, J., Cao, X., Navone, N. M., Nesvizhskii, A. I., Mehra, R., Vaishampayan, U., Blanchette, M., Wang, Y., Samajdar, S., Ramachandra, M., & Chinnaiyan, A. M. (2022). Targeting SWI/SNF ATPases in enhancer-addicted prostate cancer. *Nature*, *601*(7893), 434-439. <https://doi.org/10.1038/s41586-021-04246-z>
- Xu, J., Song, F., Lyu, H., Kobayashi, M., Zhang, B., Zhao, Z., Hou, Y., Wang, X., Luan, Y., Jia, B., Stasiak, L., Wong, J. H., Wang, Q., Jin, Q., Jin, Q., Fu, Y., Yang, H., Hardison, R. C., Dovat, S., Plataniias, L. C., Diao, Y., Yang, Y., Yamada, T., Viny, A. D., Levine, R. L., Claxton, D., Broach, J. R., Zheng, H., & Yue, F. (2022). Subtype-specific 3D genome alteration in acute myeloid leukaemia. *Nature*, *611*(7935), 387-398. <https://doi.org/10.1038/s41586-022-05365-x>
- Yamamoto, K., Yakushijin, K., Sanada, Y., Kawamoto, S., Matsuoka, H., & Minami, H. (2015). Coexistent t(8;21)(q22;q22) Translocation and 5q Deletion in Acute Myeloid Leukemia. *J Clin Exp Hematop*, *55*(3), 181-185. <https://doi.org/10.3960/jslrt.55.181>
- Yamato, G., Kawai, T., Shiba, N., Ikeda, J., Hara, Y., Ohki, K., Tsujimoto, S. I., Kaburagi, T., Yoshida, K., Shiraishi, Y., Miyano, S., Kiyokawa, N., Tomizawa, D., Shimada, A., Sotomatsu, M., Arakawa, H., Adachi, S., Taga, T., Horibe, K., Ogawa, S., Hata, K., & Hayashi, Y. (2022). Genome-wide DNA methylation analysis in pediatric acute myeloid leukemia. *Blood Adv*, *6*(11), 3207-3219. <https://doi.org/10.1182/bloodadvances.2021005381>
- Yang, A. S., Estecio, M. R., Doshi, K., Kondo, Y., Tajara, E. H., & Issa, J. P. (2004). A simple method for estimating global DNA methylation using bisulfite PCR of repetitive DNA elements. *Nucleic Acids Res*, *32*(3), e38. <https://doi.org/10.1093/nar/gnh032>
- Yang, J. J., Park, T. S., & Wan, T. S. (2017). Recurrent Cytogenetic Abnormalities in Acute Myeloid Leukemia. *Methods Mol Biol*, *1541*, 223-245. https://doi.org/10.1007/978-1-4939-6703-2_19

- Yang, X., & Wang, J. (2018). Precision therapy for acute myeloid leukemia. *J Hematol Oncol*, *11*(1), 3. <https://doi.org/10.1186/s13045-017-0543-7>
- Yu, S. J., Hu, J. Y., Kuang, X. Y., Luo, J. M., Hou, Y. F., Di, G. H., Wu, J., Shen, Z. Z., Song, H. Y., & Shao, Z. M. (2013). MicroRNA-200a promotes anoikis resistance and metastasis by targeting YAP1 in human breast cancer. *Clin Cancer Res*, *19*(6), 1389-1399. <https://doi.org/10.1158/1078-0432.CCR-12-1959>
- Zang, Y., Tai, Y., Wan, B., & Jia, X. (2016). miR-200a-3p promotes the proliferation of human esophageal cancer cells by post-transcriptionally regulating cytoplasmic collapsin response mediator protein-1. *Int J Mol Med*, *38*(5), 1558-1564. <https://doi.org/10.3892/ijmm.2016.2758>
- Zhang, Y., Chang, K., Ogunlade, B., Herndon, L., Tadesse, L. F., Kirane, A. R., & Dionne, J. A. (2024). From Genotype to Phenotype: Raman Spectroscopy and Machine Learning for Label-Free Single-Cell Analysis. *ACS Nano*. <https://doi.org/10.1021/acsnano.4c04282>
- Zhang, Y., Sun, Z., Jia, J., Du, T., Zhang, N., Tang, Y., Fang, Y., & Fang, D. (2021). Overview of Histone Modification. *Adv Exp Med Biol*, *1283*, 1-16. https://doi.org/10.1007/978-981-15-8104-5_1
- Zhao, L. L., Xiang, Y., Wang, J. X., Shen, C., Liu, H., Zong, Q. B., Zhang, H. M., Li, J. P., Wang, C., Sun, F., & Liao, X. H. (2024). The effect of LNCRNA SHANK3 on the malignant development of gastric cancer cells by regulating the miR-4530/MNX1. *Transl Oncol*, *46*, 102000. <https://doi.org/10.1016/j.tranon.2024.102000>
- Zhong, G., Zhao, W., Li, Y., Jin, G., Zeng, W., Yu, C., Zhou, J., & Yu, L. (2022). MAGEA1 and hTERT Peptide Treatment Improves the Potency of The Dendritic Cell- Cytotoxic T Lymphocytes (DC-CTL) Immunotherapy in DAC Treated Acute Myeloid Leukemia. *J Cancer*, *13*(4), 1252-1260. <https://doi.org/10.7150/jca.66501>
- Zhou, J. D., Zhang, L. C., Zhang, T. J., Gu, Y., Wu, D. H., Zhang, W., Ma, J. C., Wen, X. M., Guo, H., Lin, J., & Qian, J. (2018). Dysregulation of miR-200s clusters as potential prognostic biomarkers in acute myeloid leukemia. *J Transl Med*, *16*(1), 135. <https://doi.org/10.1186/s12967-018-1494-7>
- Zhou, J. D., Zhang, T. J., Xu, Z. J., Deng, Z. Q., Gu, Y., Ma, J. C., Wen, X. M., Leng, J. Y., Lin, J., Chen, S. N., & Qian, J. (2020). Genome-wide methylation sequencing identifies progression-related epigenetic drivers in myelodysplastic syndromes. *Cell Death Dis*, *11*(11), 997. <https://doi.org/10.1038/s41419-020-03213-2>
- Zhou, L., Yao, Q., Li, H., & Chen, J. (2021). Targeting BRD9 by I-BRD9 efficiently inhibits growth of acute myeloid leukemia cells. *Transl Cancer Res*, *10*(7), 3364-3372. <https://doi.org/10.21037/tcr-21-42>
- Zhou, R., Mo, W., Wang, S., Zhou, W., Chen, X., & Pan, S. (2019). miR-141-3p and TRAF5 Network Contributes to the Progression of T-Cell Acute Lymphoblastic Leukemia. *Cell Transplant*, *28*(1_suppl), 59S-65S. <https://doi.org/10.1177/0963689719887370>

- Zhou, W., Triche, T. J., Jr., Laird, P. W., & Shen, H. (2018). SeSAmE: reducing artifactual detection of DNA methylation by Infinium BeadChips in genomic deletions. *Nucleic Acids Res*, 46(20), e123. <https://doi.org/10.1093/nar/gky691>
- Zhu, J., Woods, D., McMahon, M., & Bishop, J. M. (1998). Senescence of human fibroblasts induced by oncogenic Raf. *Genes Dev*, 12(19), 2997-3007. <https://doi.org/10.1101/gad.12.19.2997>

9. Poster Presentations and Publications

9.1. Publications

Kelekci, S. Kelly K. Goyal, A., Wehrwein, N., Riedel, A., Weichenhan, D., Scherer, M., Michels, B., Körner, C. Orzella, I., Hakobyan, M., Bähr, M., Everatt, E., Hey, J., Dunford, J., Lipka, D., Lutsik, P., Oppermann, U., Plass, C. (**in preparation**), Epigenetic compound screening reveals hypomethylation-mediated reduction of *MNX1* expression

Schönefeld, A., Zanetti, C., Schmitt, E., Woods, K., Westerback, A., Shah, V., Rühle, F., **Kelekci, S.**, Thevissen, S., Schäffer, A., Sasca, D., Kindler, T., Theobald, M., Akgoz-Feuerstein, C., Gerhäuser, C., Lutsik, P., Hecker, J., Götze, K., Platzbecker, U., Plass, C., Medyouf, H. Guezzuez, B., (**in preparation**), Dual DNMT1/G9A inhibition resores myelo-monocytic differentiation and induces IFN response in NPM1-mutant Acute Myeloid Leukemia

Sollier, E., Riedel, A., Toprak, U. H., Wierzbinska, J. A., Weichenhan, D., Schmid, J. P., Hakobyan, M., Touzart, A., Jahn, E., Vick, B., Brown-Burke, F., Kelly, K., **Kelekci, S.**, Pejkovska, A., Goyal, A., Bähr, M., Breuer, K., Chen, M.-J. M., Llamazares-Prada, M., Hartmann, M., Schönung, M., Correia, N., Trumpp, A., Abdullah, Y., Klingmüller, U., Mughal, S. S., Brors, B., Westermann, F., Schlesner, M., Vosberg, S., Herold, T., Greif, P. A., Pfeifer, D., Lübbert, M., Fischer, T., Heidel, F. H., Gebhard, C., Walter, W., Haferlach, T., Eisfeld, A.-K., Mrózek, K., Nicolet, D., Bullinger, L., Smeenk, L., Erpelinck, C., Mulet-Lazaro, R., Delwel, R., Ernst, A., Scherer, M., Lutsik, P., Jeremias, I., Döhner, K., Döhner, H., Lipka, D. B., & Plass, C. (2024). Pyjacker identifies enhancer hijacking events in acute myeloid leukemia including *MNX1* activation via deletion 7q. *bioRxiv*, 2024.2009.2011.611224. <https://doi.org/10.1101/2024.09.11.611224>

Bakr, A., Corte, G. D.*, Veselinov, O.*, **Kelekci, S.***, Chen, M.*, Lin, Y., Sigismondo, G., Iacovone, M., Cross, A., Syed, R., Jeong, Y., Sollier, E., Liu, C., Lutsik, P., Krijgsveld, J., Weichenhan, D., Plass, C., Popanda, P., Schmezer, P., (2024), ARID1A regulates DNA repair through chromatin organization and its deficiency triggers DNA damage-mediated anti-tumor immune response. *Nucleic Acids Research*, <https://doi.org/10.1093/nar/gkae233> (* co-shared second authorship)

Weichenhan, D., Riedel, A., Meinen, C., Basic, A., Toth, R., Bahr, M., Lutsik, P., Hey, J., Sollier, E., Toprak, U. H., **Kelekci, S.**, Lin, Y. Y., Hakobyan, M., Touzart, A., Goyal, A., Wierzbinska, J. A., Schlesner, M., Westermann, F., Lipka, D. B., & Plass, C. (2023). Translocation t(6;7) in AML-M4 cell line GDM-1 results in MNX1 activation through enhancer-hijacking. *Leukemia*, 37(5), 1147-1150. <https://doi.org/10.1038/s41375-023-01865-5>

9.2. Poster presentations

Kelekci, S., Epigenetic Compound Screening in AML with *MNX1*-overexpression, Symposium on Stem Cells and Cancer, Heidelberg, Germany (2023)

Kelekci, S., Epigenetic Compound Screening in AML with *MNX1*-overexpression, DKFZ PhD poster presentations, Heidelberg, Germany (2023)

Kelekci, S., Epigenetic Compound Screening in AML with *MNX1*-overexpression, DKFZ PhD retreat, Löwenstein, Germany (**Awarded as the 3rd best poster**)

Kelekci, S., Epigenetic Compound Screening in AML with *MNX1*-overexpression, Spetses Summer School in Cancer Epigenetics-Principles, Applications and Single-Cell Resolution, Spetses, Greece (2022)

Kelekci, S., Epigenetic Compound Screening in AML with *MNX1*-overexpression, International PhD Student Cancer Conference, Heidelberg, Germany (2022)

10. Acknowledgements

First and foremost, I take great pride in conveying my gratitude to **Prof. Dr. Christoph Plass** for giving me the opportunity to join his division and for his insightful feedback on my abstracts, reports, manuscript, and thesis.

I am deeply grateful to my dissertation defense committee members, **Prof. Dr. Frank Lyko** and **Prof. Dr. Stephan Wiemann**, for their will to review my thesis.

I want to thank my thesis advisory committee (TAC) members, **Prof. Dr. Karsten Rippe** and **Prof. Dr. Carsten Müller Tidow**, for the excellent discussions in my TAC meetings that significantly improved the quality of my project.

With great appreciation, I express my gratitude to **Dr. Dieter Weichenhan** for his help with 4C, ACT-seq, and local deep bisulfite sequencing experiments, and especially for proofreading my thesis.

I am grateful to **Dr. Ashish Goyal**, whose constant willingness to help and support enabled me to overcome challenges throughout my project. I wish to follow his friendliness and scientific integrity in my future career.

My heartfelt thanks to **Katherine Kelly**, a colleague who supported me with her excellent analysis skills and motivated me on challenging days. I appreciate and will never forget her support via proofreading of my TAC reports, manuscript, and thesis.

Special thanks to **Dr. Ali Bakr** and **Dr. Mei-Ju May Chen** for enabling me to improve in bioinformatic fields, involving me in side projects, and collaborating on fantastic publication(s).

Another special mention must be made to **Elena Everatt**, my super-nice office mate, for all the fruitful scientific discussions and support.

I want to thank **Marion Bähr** for sharing her knowledge of state-of-the-art laboratory techniques.

I am honored to thank my incredible interns, **Irene Orzella** and **Nick Wehrwein**, for their contributions to my project and for learning how to teach science with them.

I will always be grateful to my Master's supervisor, **Prof. Dr. Tamer Önder**, for inspiring me to find joy in science, being an incredible mentor, and believing in my potential. He shared the Ph.D. program at DKFZ with me, allowing me to secure my current position.

I want to thank the 'Heidelberg'in Gülleri,' my friends whom I got to know during my Ph.D. at DKFZ: **Aysu Başak Kök**, **Pelin Ünal**, **Ecem Kaplan**, and **Boğaç Aybey**, for their friendship, amazing travels, and memories throughout my PhD.

I want to thank my lifelong friends, **Kübra Çelikbaş-Yılmaz** and **Ceren Çelebi**, for their infinite support and constant companionship.

I am eternally grateful to my boyfriend, **Marko Mandic**, for his endless support, always listening to me, and encouragement. His positive attitude, the songs he shared with me, and his unconditional love were my most significant source of strength.

Last but not least, I would like to express my immense gratitude to my family, **Miyeser Kelekçi** and **Özge Kelekçi**, for their invaluable role in my personal and professional development and for their unwavering support and encouragement no matter how far apart we live. Sizi çok ama çok seviyorum ve hep seveceğim.

